International
Progress Report

IPR-02-40

Äspö Hard Rock Laboratory

Äspö HRL Task Force on numerical modelling

Task 5. Coupling geochemistry and transport

D.Billaux
B. Paris
ITASCA Consultants, France

February 2001

Svensk Kärnbränslehantering AB
Swedish Nuclear Fuel
and Waste Management Co
Box 5864
SE-102 40 Stockholm Sweden
Tel +46 8 459 84 00
Fax +46 8 661 57 19

Äspö Hard Rock Laboratory

Report no.	No.
IPR-02-40	F65K
Author	Date
Billaux, Paris	01-02-01
Checked by	Date
H. Benabderrhamane	01-02-01
Approved	Date
Christer Svemar	02-11-19

Äspö Hard Rock Laboratory

Äspö HRL Task Force on numerical modelling

Task 5. Coupling geochemistry and transport

D.Billaux

B. Paris

ITASCA Consultants, France

February 2001

Keywords: Groundwater flow, solute transport, coupled hydrogeochemistry, Äspö, Task 5

ITASCA Consultants , s. a.	Nature du document : **Rapport Final**	Identification ANDRA : **C RP 0 ITA 00.010/D** Identification ITASCA : **00.010D**

« Åspö HRL Task Force on Numerical Modeling »

Task 5: Coupling geochemistry and transport

Référence Commande : **011472SHG** **du 24.06.1999**	Index du document : **D**	Date du document: **Février 2001**
Nom et visa Rédacteur : **D. BILLAUX** **B. PARIS**	Nom et visa Vérificateur : **D. BILLAUX** **B. PARIS**	Nom et visa Approbateur : **D. BILLAUX**

Archivage Itasca : \\Itasca\COMMUN\Rapports_et_plus\Rapports\2000\aspo_chem\00-010d.doc

Summary

Objective

The ANDRA/Itasca team participated in Task 5 for the purpose of gaining experience on modeling for a real site, and a first limited approach to coupling of transport and geochemistry. The issues of interest were:

- How can geochemistry help to improve the reliability of the hydrogeological modeling?
- What kind of complexities are added by looking at geochemistry and hydrogeology at the same time?

Approach - Modeling choices

After a model was constructed, it was first calibrated based upon water flow computations only. The model was then recalibrated using geochemical data. This is a discrete fracture model, with channelized flow in fractures. We consider Darcy's flow, with no density effect. The 21 fracture zones (Hydraulic Conductor Domains) as given in the data set are taken into account, whereas rock outside fracture zones is not modeled. The fracture zones are represented as planes, bounded either by the model boundaries or by planar boundaries as specified in the database. In each fracture plane, flow and transport occur along "channel pipes", i.e. a regular grid of one-dimensional elements. The grid has channels intersecting each other in four directions ("squares + diagonals" grid), at 45° angles.

Transmissivity, width, and storage coefficient are constant for each feature, except at the top boundary under the Baltic, where a "skin factor" is used. The transmissivity values are initialized from the data set, then changed during calibration phase. The specific storage is used as given when data are available (NE-1, NNW-1, NNW-2), and computed from the correlation in TR 97-06 for all other fracture zones. The boundary conditions are:

- Constant flux under land, and constant head (with skin factor) under sea at the top surface;
- Constant head on vertical faces;
- No flux on the bottom face.

The hydraulic calibration is performed by imposing the flow rates in the tunnel and trying to reproduce the available drawdown histories in boreholes. The calibration parameters are the transmissivities in fracture zones.

Conservative transport is modeled by advective / dispersive particle transport, with spreading due to both longitudinal dispersion in channels and to complete mixing at channel intersections. For end-member simulation, the initial mixing ratios in each channel are interpolated from the cubic-grid interpolation at the start of the period, as provided in the database. These mixing ratios are maintained constant on vertical boundaries throughout the simulation. For the top boundary, we use pure meteoric water under land and pure Baltic water under sea.

Mixing ratios at the control points are then used to calibrate the skin factor at the bottom of the Baltic Sea. The final skin factor we use is 100, i.e. we add at the bottom of the sea, above each fracture zone, a 10m-thick layer with a transmissivity equal to 1/100 of the mean fracture zone transmissivity.

Overall, the final model after calibration is relatively close to the initial one. Fracture zone NE2's transmissivity needed a 100-fold increase. This may mean there is another unknown conductor in its vicinity. Otherwise, only NNW1 (divided by 10) and NNW3 (multiplied by 10) had to be modified significantly.

Modeling results

Sensitivity studies were performed by doing simulations with modified parameters, testing:

- The effect of the chosen discretization (grid size from 40m to 80m, with either square grids or “four directions” grids.
- Fracture zone hydraulic conductivities (calibration procedure - both “bulk conductivities and skin factor under Baltic sea).
- Fracture zone specific storage (from no storage to ten time the chosen one).
- Longitudinal dispersivity (tenfold increase).

The simulation results had a very small sensitivity to discretization. The hydraulic conductivities used had a high influence on flow patterns, whereas specific storage was not very influential, with relatively fast piezometric response to the tunnel advance. Similarly, dispersion in the model was dominated by the mixing at intersections, so that the longitudinal dispersivity had little effect.

The simulations tend to overestimate the amount of Baltic water arriving at the Control Points, despite the skin factor we use at the bottom of the Baltic Sea. Note that for simulations performed after hydraulic calibration only, the overestimation is much larger.

Coupling with geochemistry

Fully coupled reactive transport was simulated on a part of the model domain only. We did not use the endmembers provided by the Task Force, but directly dealt with chemical species. For some species, concentrations had to be derived from endmember mixing ratios and endmember compositions.

The simulated geochemical processes included solution complexation, precipitation / dissolution of minerals and gas dissolution (CO_2) for those of the nodes opened to the atmosphere.

The simulations performed show some interesting potential features about coupling transport with geochemistry. For example, in the context of the Äspö island, it appears that variable water salinity influences the aqueous solution ionic strength and consequently the “apparent” chemical reaction constants.

Conclusions

Using flow results only to calibrate the transmissivities of the Hydraulic Conductor Domains proved to yield non-unique results. However, by looking at chemical transport, we were able to calibrate the flow parameters in a better way, by adding more constraints to the calibration process. Overall uncertainties remain quite large. Specifically, the interpolation of the initial chemical compositions we used is not satisfactory, and the influence of the not-well-known fixed-concentration lateral boundary conditions has a large impact on the final results.

Reactive transport results show that, even in zones where geochemistry is considered as simple and of little importance (e.g. in the absence of significant redox or surface reactions), transport of chemical species might in fact be affected by mineral precipitation / dissolution, therefore constraining the hydrogeological modeling.

SAMMANFATTNING

Mål

ANDRA/Itaska-teamet deltog i Task 5 i syfte att få erfarenhet om modellering av en verklig plats samt en första, begränsad kunskap om tillvägagångssättet vid koppling av transport och geokemi. De intressanta frågorna är:

- Hur kan geokemi bidra till en ökad trovärdighet hos hydrogeologisk modellering?
- Vilka grader av komplexitet kommer till om man integrerar geokemi och hydrogeologi?

Tillämpning - modellval

Efter det att en modell konstruerats kalibrerades den först mot enbart flödesmodellering. Modellen kalibrerades sedan pånytt mot geokemiska data. Den använda modellen är en diskret sprickmodell med kanalflöde i sprickor. Vi har antagit Darcyflöde utan densitetseffekt. Hänsyn tas till 21sprickzoner (hydraulisk flödesdomäner) i enlighet med givna data, medan berg utanför respektive sprickzon ej modelleras. Sprickzonerna representeras som plan, omgiven av antingen modellens yttre ränder eller planens ränder så som de specificeras i databasen. I varje sprickplan sker flöde och transport längs ”kanaler”, dvs. i ett regelbundet mönster av endimensionella element. I mönstret korsar kanaler varandra i fyra riktningar (mönster med ”fyrkanter och diagonaler”) i 45 graders vinkel.

Transmissivitet, bredd och magasinskoefficient är konstanter för vare struktur förutom i övre randen under Östersjön, där en ”skinnfaktor” används. Transmissivitetsdata initieras från datamängden och ändras sedan under kalibreringsfasen. Den specifika magasinskoefficienten används när data är tillgängliga (NE-1, NNW-1, NNW-2) och datorhanterade utifrån sambanden i TR 97-06 för alla andra zoner. Randvillkoren är:

- Konstant flöde under markytan och konstant tryck under havsytan (med skinnfaktor) vid den övre ytans gräns
- Konstant tryck längs den vertikala ytan
- Inget flöde vid den undre gränsen

Den hydrauliska kalibreringen görs genom att ansätta flödesmängderna in till tunneln och reproducera de tillgängliga, historiska nivåerna i borrhålen. Kalibreringsparametrarna är transmissiviteter i sprickzoner.

Icke-sorberande transport modelleras som advektiv/dispersiv partikeltransport med spridning orsakad av såväl longitudinell dispersion i kanaler som fullständig blandning i kanalkorsningar. För simulering av ursprungsvattnen interpoleras den ursprungliga blandningskvoten i varje kanal från interpoleringen av kubikmönster i början av perioden, i enlighet med data i databasen. Blandningskvoter hålls konstanta längs vertikala ränder under hela simuleringen. För den övre randen använder vi uteslutande meteoriskt vatten under land och enbart Östersjövatten under havet.

Blandningskvoter i kontrollpunkter används sedan för att kalibrera skinnfaktorn i botten på Östersjön. Den slutliga skinnfaktorn vi använder är 100, vilket är liktydigt med att vi på botten av havet, ovanför sprickzonen lägger till en 10 m tjock zon med en transmissivitet som motsvarar 1/100 av medelvärdet hos den genomsnittliga transmissiviteten i sprickzonerna.

På det hela taget är den slutliga modellen efter kalibrering relativt oförändrad jämfört med den ursprungliga. Sprickzon NE2s transmissivitet krävde en 100-faldig ökning. Detta kan betyda att det finns en annan, okänd ledare i närheten. I övrigt behövdes bara NNW1 (divideras med 10) och NNW3 (multipliceras med10) modifieras i någon större omfattning.

Modelleringsresultat

Känslighetsstudier gjordes genom simuleringar med modifierade parametrar, testande:

- Effekten av det valda diskretiseringen (gridstorlek från 40 till 80 m med antingen fyrkantiga grid eller ”fyrvägs”-grid)
- Hydraulisk konduktivitet i sprickzoner (kalibreringsprocedur: både ”bulk”-konduktivitet och skinnzonfaktor under Östersjön)
- Specifik magasinskoefficient hos sprickzoner (från ingen specifik kapacitet alls till tio gånger den valda)
- Longitudinell dispersivitet (tiofaldig ökning)

Simuleringarnas resultat hade liten känslighet för diskretiseringen. De använda hydrauliska konduktiviteterna hade en stor betydelse för flödes mönstret, medan specifika magasinskoefficienten inte hade något speciellt inflytande vid relativt snabb piezometrisk reaktion på tunnelframdrift. Dispersion dominerades i modellen av blandning i korsningar medan den longitudinella dispersionen hade liten påverkan.

Simuleringarna tenderar att överskatta mängden Östersjövatten, som kommer till kontrollpunkterna, trots att vi använt en skinnfaktor längs bottnen av Östersjön. Observera att for simuleringar som gjorts efter hydraulisk kalibrering är överskattningen mycket högre.

Koppling med geokemi

En fullt kopplad, reaktiv transport simulerades bara i en del av modelldomänen. Vi använde inte ursprungvattnen som gavs av Task Force, utan hanterade kemiska ämnen direkt. För vissa ämnen behövde koncentrationer räknas fram med hjälp av ursprungsvattnens blandningskvot och sammansättning.

De simulerade geokemiska processerna inkluderade lösningskomplexering, utfällning/upplösning av mineraler och gaser (CO_2) för de noder som står öppna mot atmosfären.

De gjorda simuleringarna pekar ut några intressanta potentiella egenskaper om koppling mellan transport och geokemi. I samband med Äspö ö, t. ex., verkar det som om en variabel salthalt i vattnet påverkar jonstyrkan i vattenlösningen och följaktligen den ”uppenbara” kemireaktionens konstanter.

Slutsatser

Användning av enbart flödesresultat för kalibrering av transmissiviteter hos hydrauliska ledares domäner (Hydraulic Conductor Domain – HCD) tenderar att producera icke-unika resultat. Men, genom att studera kemisk transport har vi möjlighet att kalibrera flödesparametrarna på ett bättre sätt, genom att lägga till fler begränsningar i kalibreringsprocessen. Övergripande osäkerheter förblir ganska stora. Speciellt interpolering av den ursprungliga kemiska sammansättningen, som vi använt, är inte tillfredsställande, och påverkan från den dåligt kända fasta koncentrationens laterala randvillkor har en stor påverkan på slutresultatet.

Reaktiva transportresultat visar att, även om zonen där geokemi beaktas som enkel och av ringa betydelse (t ex utan signifikanta redox- eller ytreaktioner), kan transport av kemiska ämnen påverkas av mineralers utfällning/upplösning, och härigenom begränsa den hydrogeologiska modelleringen.

Table of Contents

List of Figures

List of Tables

1 INTRODUCTION

This report describes the participation of the ANDRA/Itasca team to Task 5 of the ÄSPÖ Task Force on Modeling of Groundwater Flow and Transport of Solutes, during the period August 1999 to May 2000. Task 5 was initiated in 1997 with the aim to compare and eventually integrate hydrogeology and hydro chemistry models at the scale of the Äspö site. It was hoped that the combination of two largely different approaches to site characterization and modeling would yield a better overall understanding of the transport pathways through the site. To achieve this objective, the project teams were asked to perform calibrated modeling of the effect of constructing the access drift and the circular tunnel of the Äspö Hard Rock Laboratory.

The specific aim of the ANDRA/Itasca team in this exercise was to gain experience on the modeling of a real site. Also, it was intended to check on the main aspects of the coupling between solute transport and geochemistry. In the approach we follow, the hydrogeological model is clearly the basis for the work, and reactive geochemistry is added to it. Therefore, the issues we wished to address through this work can be defined as the following:

How can geochemistry help to improve the reliability of hydrogeological modeling?

What kind of complexities is added by looking at geochemistry and hydrogeology at the same time?

This work is carried out in several phases: after defining the conceptual model and its geometry, we first perform a hydraulic calibration, then a transport calibration, which involves recalibration of the flow model. On one part of the model (upstream from one of the "Control Points" defined by the Task Force), we then experiment a coupled active geochemistry – solute transport approach. Note that references to Data Deliveries follow the numbering used in the Modeling Questionnaire for task 5.

2 CALIBRATION

The Äspö site is situated off the southeastern coast of Sweden, in the Baltic Sea. It is a granite island surrounded by shallow waters that separate it from the mainland and several other islands (Figure 2-1). The area we model is a two kilometers by two kilometers region, that encompasses most of the island, plus some of the surrounding sea branches and islands The thickness of the model is one kilometer.

2.1 Conceptual and structural model

Our conceptual model is based on the observation that most flow and transport in this region can be explained by looking at large fractured zones. These features, called "Hydraulic Conductor Domains" (or "HCD") according to the terminology used by the Äspö Laboratory, dominate the site-scale response to large draw downs such as the effect of the drift. Therefore, we consider only these main conductors, and disregard the "background fractures" in the rest of our work. The model is thus of the "discrete fractures" type. The HCDs' geometry is deterministic, as given in the data delivered by the Task Force (Data Delivery 2e). So this model is **not** a stochastic model in the usual sense, i.e. a fracture mesh obtained by generating pseudo-random fractures according to given statistical properties. Figure 2-2 shows the trace (top 50 m) of the HCDs in the model, as well as the topography of the site as entered from Data Delivery 5b. Figure 2-3 shows the relative geometry of the 21 zones represented within the model, as well as the tunnel and the outline of the Äspö Island for reference. Note that the HCDs are either "infinite" in extent, in which case they completely cross the volume of interest (for example HCD NE-1), or are polygonal, with limits either directly in the rock or at their intersection with other HCDs (for example HCD NE-2). Table 2-1 is a summary of these geometrical properties, together with flow properties input values. We also indicate the "zone number" we assign to each HCD in our model. Table 2-2 describes the virtual planes used to specify HCD limits when they do not correspond to other HCD's.

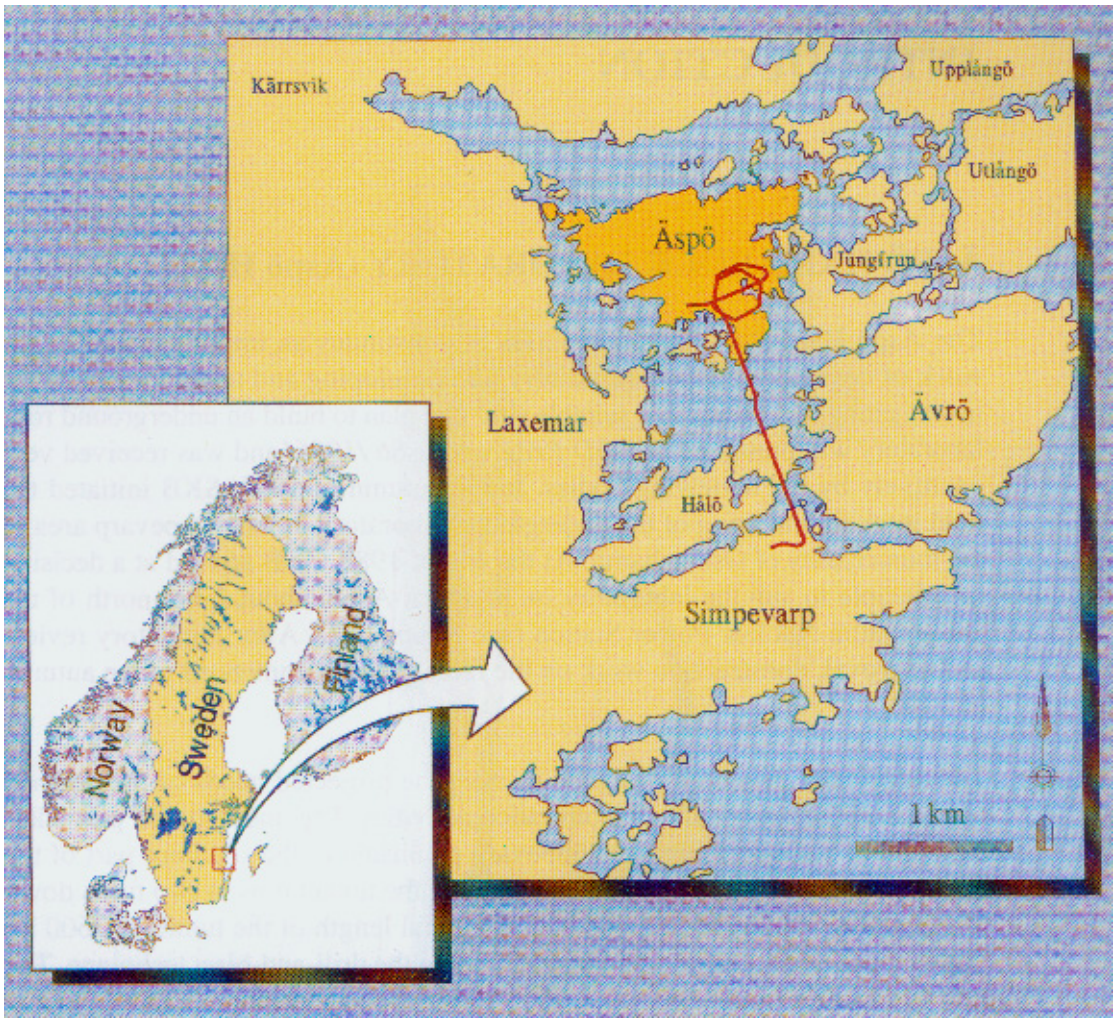

Figure 2-1: *the Äspö area (after SKB TR 97-06)*

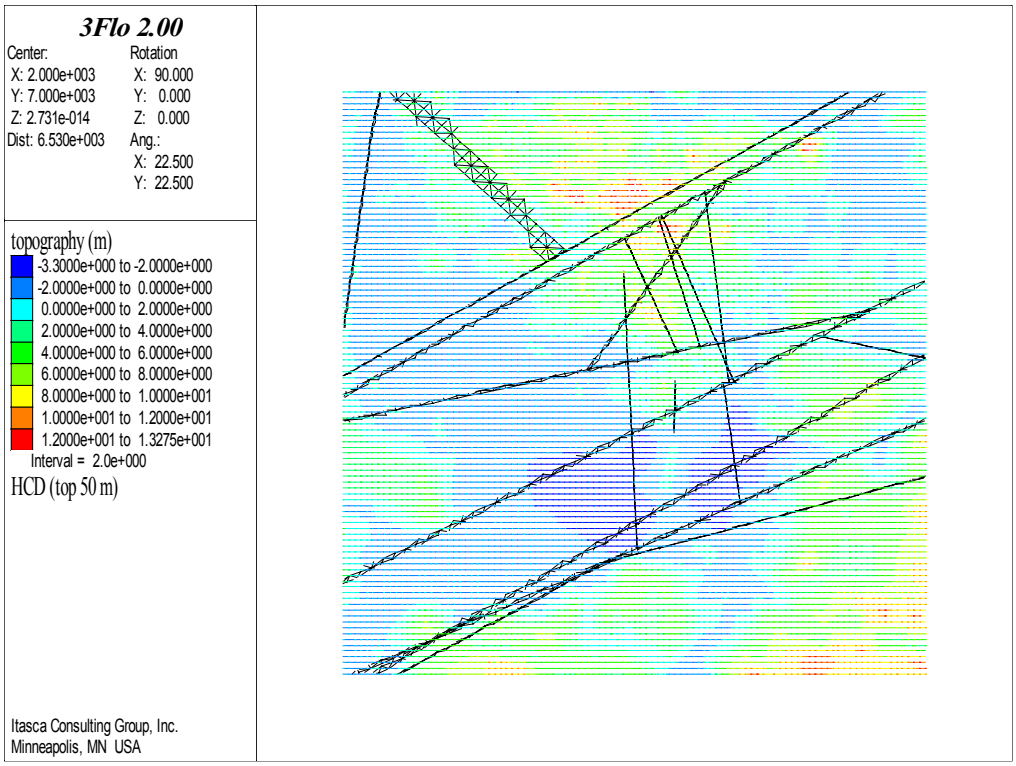

Figure 2-2: *outline of the Hydraulic Conductors, and surface topography*

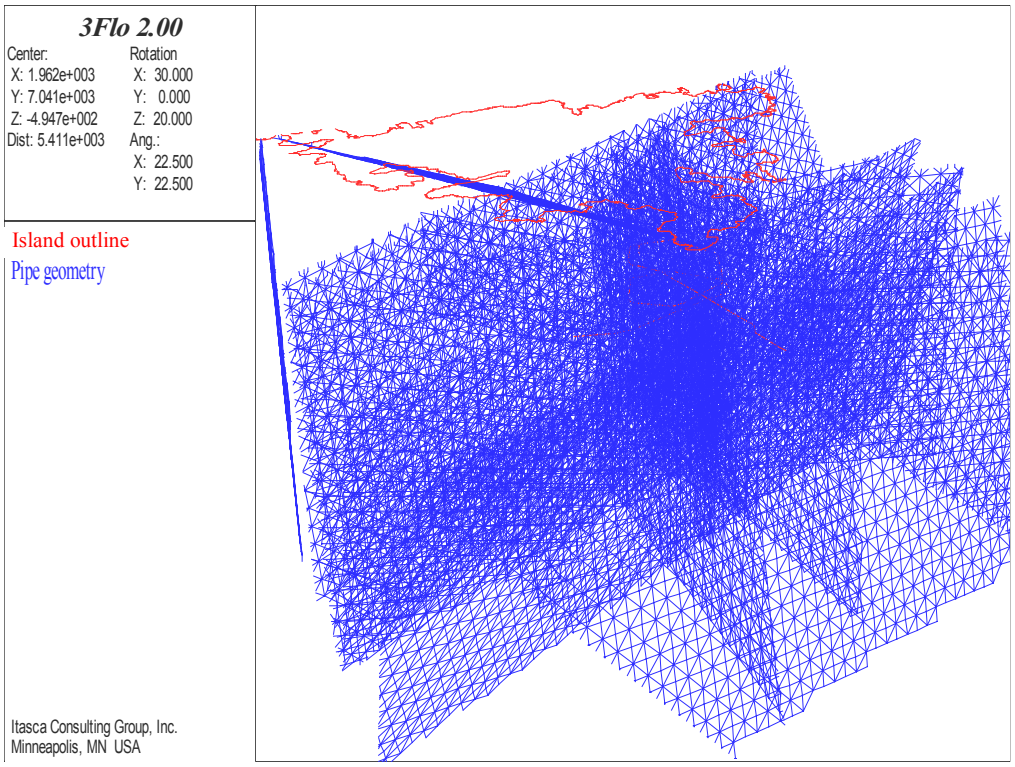

Figure 2-3: *the 21 zones in the model. View from top-South-West. Perspective view: varying scale, given by Äspö Island.*

Table 2-1: Hydraulic Conductor Domains - Geometrical and flow properties

Zone name	Zone number	Transmissivity *(m^2/s)*	Thickness *(m)*	Specific Storage Coefficient	Linked to	Stops at
EW-1N	1	1.5e-6	30.		EW-1S	
EW-1S	2	2.2e-5	30.			
EW-3	3	2.4e-5	15.			NE-1
EW-7	4	6.8e-5	10.			NE-4N
NE-1	5	3.e-4	30.	2.6e-6		
NE-2	6	4.1e-7	5.			EW-1S NE-1 EW-3
NE-3	7	2.9e-4	50.			
NE-4N	8	3.e-5	40.			
NE-4S	9	3.e-5	40.			NE-4N
NW-1	10	1.7e-7	10.			EW-1N
NNW-1	11	1.1e-5	20.	5.e-6		EW-3 EW-1S
NNW-2	12	5.6e-5	20.	2.e-6		NE-1 EW-1S
NNW-3	13	2.e-5	20.			F2 F3
NNW-4	14	1.5e-4	10.			NE-1 EW-1S
NNW-5	15	2.e-6	20.			NE-4N F1
NNW-6	16	1.4e-5	20.			EW-7 NE-4N NE-1
NNW-7	17	4.8e-6	20.			EW-3 EW-1S
NNW-8	18	1.e-5	20.			EW-1N A1 A2
SFZ11	19	3.6e-6	20.			NE-1
SFZ14a	20	3.6e-6	20.			SFZ14b
SFZ14b	21	3.6e-6	20.			SFZ14a

Table 2-2: virtual planes used for specifying Hydraulic Conductor Domains limits

Plane name	Plane number	Normal vector (Äspö frame of reference)			Reference point (Äspö coordinates)		
		x	y	z	x	y	z
A1	22	0.	0.	1.	2000.	7000.	-300.
A2	23	0.	0.	1.	2000.	7000.	-700.
F1	24	0.	-1.	0.	2000.	7394.1	-500.
F2	25	0.	-1.	0.	2000.	7025.4	-500.
F3	26	0.	-1.	0.	2000.	6812.9	-500.

We consider the Hydraulic Conductor Domains as planes. However, within each HCD, flow is not homogeneous. In fact, these are zones, with a thickness up to 50m, were the rock is more densely fractured and therefore allows better flow path connections. We represent this by using on each plane a connected network of channels (see Figure 2-3). To these regular grids are added channels representing HCD intersections as preferential pathways (Figure 2-4). Note that for flow computations, using channels instead of classical two-dimensional elements has very little influence, since an exact equivalence can be written between the two types of representations, as long as the channel mesh density is high enough. However, this is not true any more for transport computations. Also, adding the HCD intersections preferential pathways may have an influence on both flow and transport responses. Since we have no direct knowledge of the pathway geometries within HCD planes, we experiment two types of arrangements (i.e. simple square grid, or "square plus diagonals", as shown in Figure 2-3). Flow results for the two arrangements are the same, and in fact, for the model we consider, the transport behavior is not altered in a significant manner.

In the model as described above, there is no possibility of a link between the north and the south of the volume under study, since HCDs EW-1N and EW-1S do not intersect, and are not crossed by any other conductor. In fact (as mentioned in report TR97-06), even though the thick EW1 zone conducts water mostly along its sides, represented by HCDs EW-1N and EW-1S, there is some hydraulic communication between the "north" and "south" sides of EW-1, as can be readily concluded from the tunnel advance responses in the region north of EW-1N, although the tunnel never crosses it. We reproduce this possibility by adding channel links between the two HCDs (Figure 2-5).

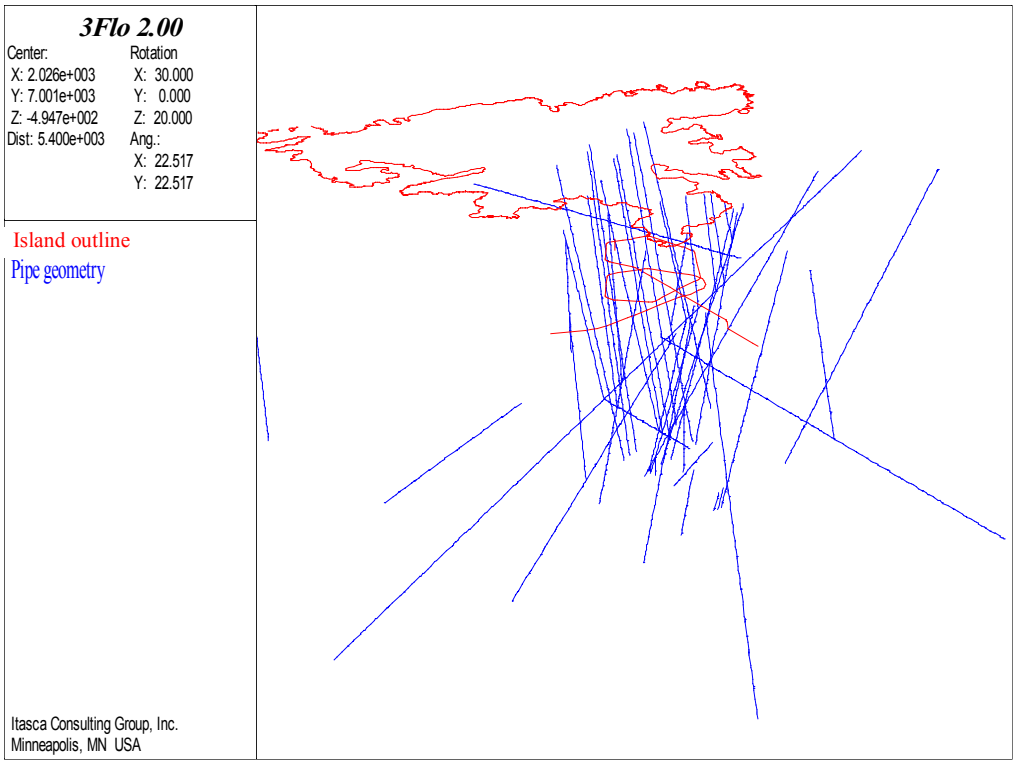

Figure 2-4: *HCD intersections. View from top-South-West*
Perspective view: varying scale, given by Äspö Island.

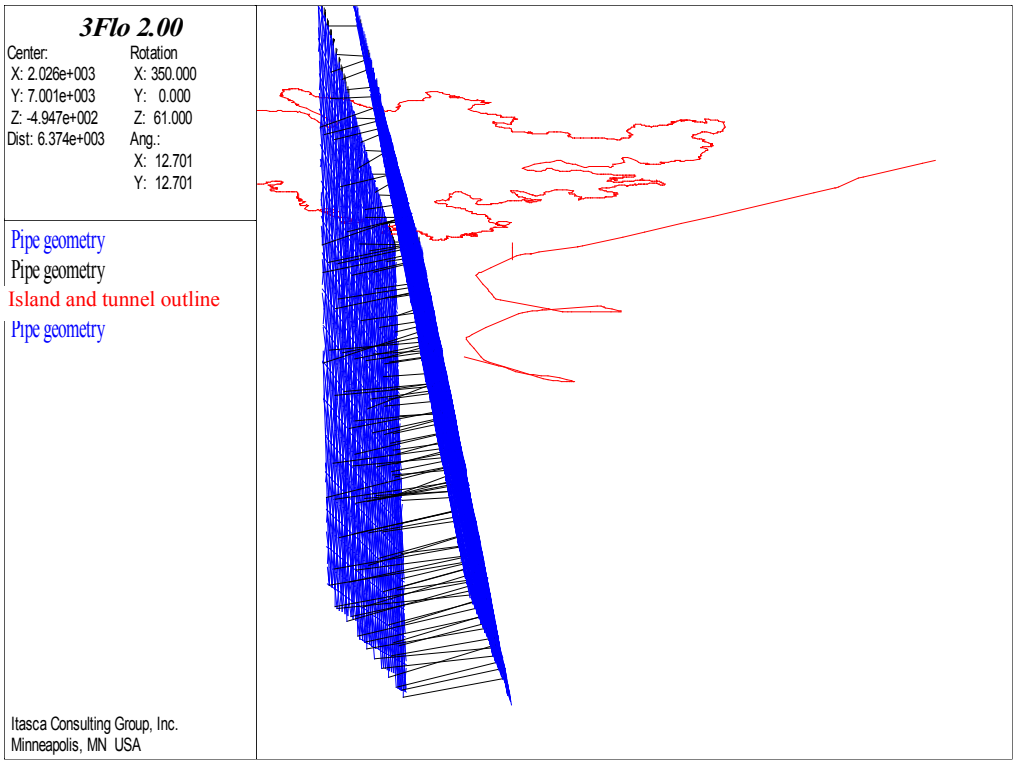

Figure 2-5: *links between HCDs EW-1N and EW-1S. View from bottom-West Perspective view: varying scale, given by Äspö Island.*

2.2 Simulation of the tunnel advance

The tunnel construction can be seen as the progressive extension of a "channel" with an infinite conductivity, and a fixed atmospheric pressure. However, since the surroundings of the tunnel were heavily grouted when flowing features where encountered, a large skin effect can be expected where it crosses the main HCDs. This skin effect is unknown. On the other hand, we know, for 18 weirs at intervals along the tunnel, the flow rates coming into the tunnel every month (Data Delivery 9a). By using these flow rates directly, we can "bypass" the unknown skin effect and apply the right boundary condition to our model. The simulation of the tunnel advance thus goes as follows:

1. Compute tunnel intersection with next HCD. Tunnel geometry is taken from Data Delivery 2c1;

2. Compute time of arrival at the detected intersection (from tunnel advance given in Data Delivery 2b1);

3. Compute corresponding number of time steps, taking into account geometrical time step increase factor, maximum initial time step and maximum final step;

4. Compute flow until the time of arrival at the detected intersection;

5. Add the "infinite" (in fact, 1000 times any conductivity in the network) conductivity pipe representing the length of tunnel down to the intersection;

6. Connect the new HCD to the tunnel. The 1D tunnel channel is not likely to cross the 1D channels on the HCD. Therefore, one small pipe is needed in the plane of the HCD, in order to connect the closest node on this HCD and the node at the tunnel location.

During the whole process, check if a weir was encountered before the HCD intersection. If yes, "activate" this weir: a node is placed at this location and is declared as an "imposed flux" boundary. At each time step afterwards, the code will check flux values at this weir from a monthly table and will interpolate the boundary condition.

Table 2-3 shows the tunnel intersections as encountered in the model (Note that the shaft is treated in the same way as the tunnel).

Table 2-3: tunnel and Shaft intersections

Coordinates (m)			Tunnel or Shaft Abscissa	Intersection	Date
x	y	z	(m)	Type	
Tunnel					
2162.8	6337.6	-94.6	682.0	weir 01	14/05/1991
2150.3	6435.3	-106.9	780.4	HCD EW-7	27/06/1991
2147.1	6459.9	-110.4	805.3	HCD NE-4N	30/07/1991
2149.8	6637.6	-135.8	987.0	HCD NE-3	28/10/1991
2144.8	6680.1	-141.8	1030.0	weir 02	25/11/1991
2117.8	6880.3	-170.1	1232.0	weir 03	13/02/1992
2109.2	6944.6	-179.2	1296.9	HCD NE-1	21/04/1992
2099.2	7019.1	-189.7	1372.0	weir 04	28/06/1992
2093.2	7063.5	-196.0	1416.9	HCD EW-3	12/08/1992
2042.4	7219.7	-219.4	1584.0	weir 05	09/09/1992
2034.7	7233.3	-221.5	1599.6	HCD NE-2	14/09/1992
2061.0	7338.8	-233.2	1711.9	HCD NNW-7	21/10/1992
2073.4	7369.6	-237.6	1745.0	weir 06	02/11/1992
2137.4	7403.0	-246.8	1821.5	HCD NNW-1	18/11/1992
2166.5	7411.4	-251.1	1851.7	HCD NNW-2	02/12/1992
2174.5	7413.7	-252.2	1860.1	HCD NE-2	03/12/1992
2196.5	7420.0	-255.4	1883.0	weir 07	09/12/1992
2304.6	7350.7	-273.0	2021.3	HCD NNW-4	19/01/1993
2309.6	7345.9	-274.0	2028.0	weir 08	20/01/1993
2317.0	7261.9	-285.2	2121.6	HCD NNW-4	17/02/1993
2303.4	7207.2	-293.1	2178.0	weir 09	08/03/1993
2271.7	7171.2	-298.8	2231.2	HCD NNW-2	23/03/1993
2217.4	7155.6	-306.7	2287.6	HCD NNW-1	31/03/1993
2161.2	7139.5	-314.9	2346.1	HCD NNW-7	14/04/1993
2150.7	7136.5	-316.4	2357.0	weir 10	17/04/1993
2045.6	7204.4	-333.5	2491.5	HCD NE-2	10/05/1993
2042.0	7207.9	-334.2	2496.0	weir 11	11/05/1993
2066.3	7351.9	-351.1	2653.8	HCD NNW-7	20/11/1993
2083.1	7393.9	-357.4	2699.0	weir 12	02/12/1993
2129.7	7426.8	-366.0	2760.6	HCD NNW-1	28/12/1993
2156.3	7434.5	-369.9	2788.4	HCD NNW-2	11/01/1994

Coordinates (m)			Tunnel or Shaft Abscissa	Intersection	Date
2205.9	7448.8	-377.1	2840.0	weir 13	19/01/1994
2240.0	7452.7	-382.1	2875.3	HCD NE-2	25/01/1994
2305.9	7423.6	-392.2	2947.4	HCD NNW-4	09/02/1994
2348.4	7404.6	-398.7	2994.0	weir 14	15/02/1994
2321.5	7318.1	-417.7	3138.8	HCD NNW-4	18/03/1994
2282.0	7311.0	-418.8	3179.0	weir 15	12/04/1994
2215.6	7299.2	-427.5	3246.4	HCD NNW-2	05/07/1994
2173.4	7291.6	-433.7	3289.3	HCD NNW-1	14/07/1994
2134.2	7284.6	-439.5	3329.1	HCD NE-2	25/07/1994
2108.4	7280.0	-443.3	3355.3	HCD NNW-7	28/07/1994
2038.8	7267.6	-449.9	3426.0	weir 16	10/08/1994
1969.3	7263.0	-449.2	3495.9	HCD NNW-5	26/08/1994
Shaft					
2075.0	7299.0	-186.7	186.7	HCD NNW-7	30/01/1993
2075.0	7299.0	-195.6	195.6	HCD NE-2	04/02/1993
2075.0	7299.0	-220.0	220.0	weir 18	19/02/1993

2.3 The numerical model

The resulting model of the Äspö site is made of 35,000 to 50,000 conducting pipes, depending on the pipe mesh density on the HCDs. The simple Darcy 1D flow equation in the pipes is solved by a finite element method, using implicit finite differences in time. Density variations are not taken into account.

2.3.1 Properties

Properties are considered as variable from one HCD to another. However, we consider that all pipe elements within any given HCD have the same properties.

The transmissivities of the 21 HCDs are the ones given in Table 2-1. They are taken from Data Delivery 2e. They are then adjusted during the "flow-only" calibration phase. Note that these transmissivities ***T*** are not directly used for the pipe elements in the model: they are translated into channel conductivities ***C***, using the following equation:

$$C = T * \frac{gs}{shapef}$$

Where:

gs is the grid size (length of the square edges), and
shapef is a shape factor, with a value of "1" for the simple square grid, and of "$1+\sqrt{2}$" for the "squares plus diagonals" grid (two superimposed square grids, with relative spacings 1 and $\sqrt{2}$).

It can easily be verified that the above values yield flow properties equivalent to those of a continuum with transmissivity ***T***.
For the pipe elements representing HCD intersections, we take the maximum of the conductivities computed from the two HCD transmissivities. The link pipe elements between HCDs EW-1N and EW-1S are given conductivities yielding an approximate "equivalent cross-permeability" equal to one thirtieth of the permeability of EW-1N.

The pipe sections ***ps*** are computed from HCD thickness ***th*** (Data Delivery 2e) and porosity ***n***. Porosities are computed using the correlation with HCD transmissivities given in report TR97-06:

$$n=34.87*(\frac{T}{th})^{0.753}$$

We then can write:

$$ps=\frac{th*n*gs}{2*shapef},$$

with the same notations as above.

Finally, storage coefficients ***Ss*** are used as given when data are available (i.e. for HCDs NE-1, NNW-1, NNW-2, Table 2-1), and are computed from the correlation given in report TR97-06 otherwise:

$$Ss = 0.00922 * T^{0.785}$$

2.3.2 Boundaries

The model uses Äspö coordinates. In this frame of reference, its boundaries are at: x = 1000 m and 3000 m, y = 6000 m and 8000 m, and z = -1000 m and 0 m. The initial heads are set to 0 across the entire model. Heads are then fixed on all vertical boundaries. The bottom boundary is considered as impermeable, while the top boundary is treated in more detail. From the topography of the island and its surrounding (provided in Data Delivery 5b), we check for each node at the top boundary if it is inland or under the sea bottom. The two groups of nodes are then dealt with separately.

Each sea-bottom node is fitted with an extra pipe, with a low conductivity, representing the skin effect that may exist due to the deposition of sediments on the floor of the Baltic See. The head at the other end of the "skin effect" pipe is then fixed to 0. We use a "skin factor" defining the ratio between "skin-effect" pipes and regular "HCD-pipes". This ratio may be applied uniformly, producing a layer of material on the sea floor with a permeability depending on the HCD it is "protecting". We call this case the "proportional skin case". It may otherwise be applied globally, to compute one uniform pipe conductivity, which does not depend on the HCD the pipe is connecting to the sea floor. In this case, the uniform conductivity is defined by multiplying the mean conductivity of all sea-floor pipes by the skin factor. We call this case the "uniform skin case". Figure 2-6 is a view of the "skin effect" pipes. The skin factor is a fitting parameter.

For inland nodes, we reproduce the recharge by simply imposing a flow to each node. The total land area in the model is computed from the topographic data (Data Delivery 5b). The imposed flow at each land node is then taken as the total inflow (land area times recharge) divided by the number of nodes. We can take into account, in a crude fashion, the fact that the recharge will depend on the piezometric level, by the following simple relaxation procedure: at each time step, if the head at a land node goes above 2.5m, the recharge at the node is multiplied by a factor 0.95. If on the contrary the head goes below 0.0m, the recharge at the node is multiplied by a factor 1.05, up to a maximum of four times the initial recharge. Figure 2-7 shows the pipes attached to land nodes.

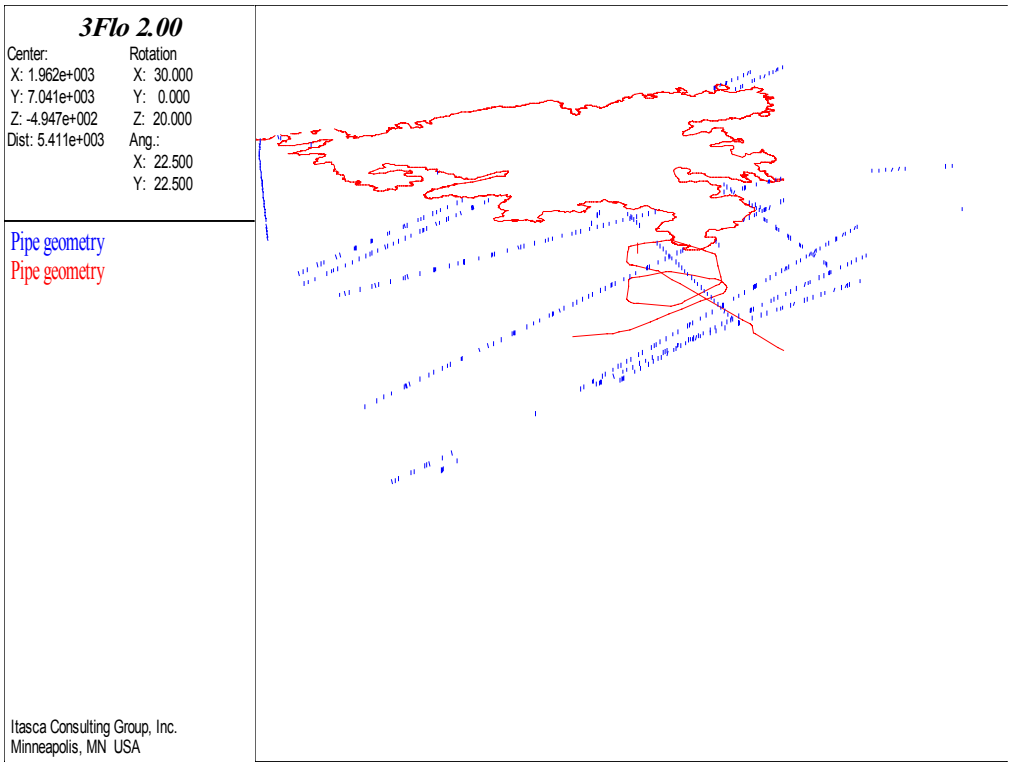

Figure 2-6: *boundary conditions at the top of the model: "skin-effect" pipes under sea Perspective view: varying scale, given by Äspö Island.*

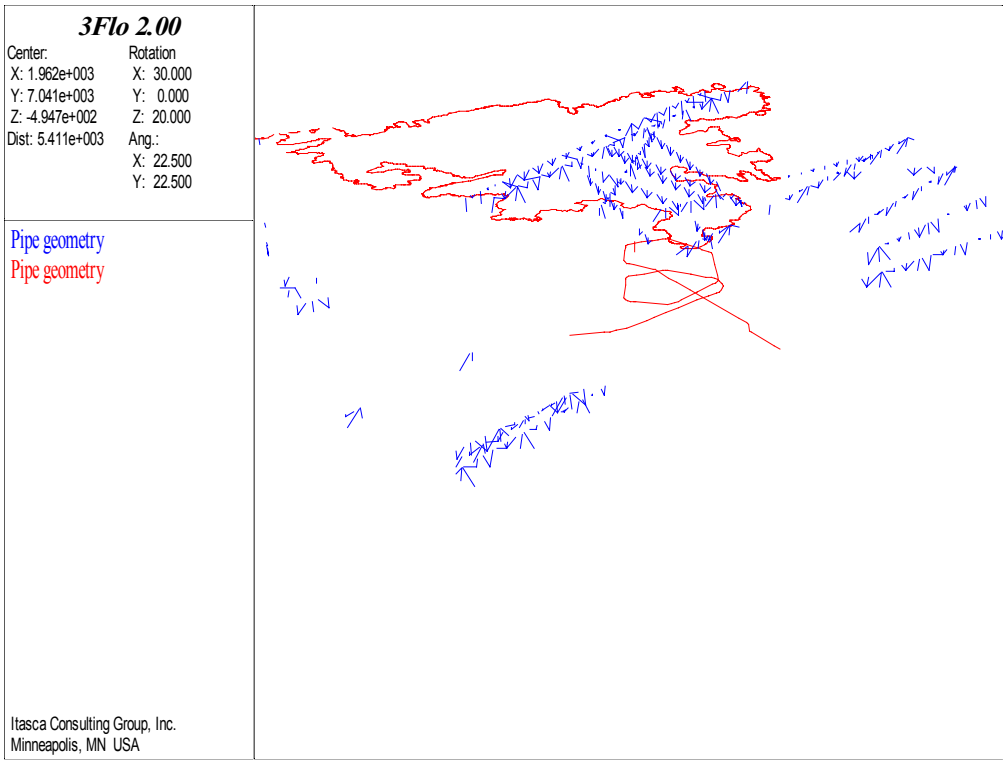

Figure 2-7: *boundary conditions at the top of the model: "imposed flux" land surface nodes Perspective view: varying scale, given by Äspö Island.*

2.4 Calibration

The flow calibration is performed by trial and error, with the objective to reproduce as precisely as possible the piezometric response measured in boreholes when the drift was excavated. The borehole geometries, for boreholes KAS02, KAS03, KAS04, KAS05, KAS06, KAS07, KAS08, KAS09, KAS12, KAS14, are taken from Data Delivery 3e, and shown in Figure 2-8. The area around the tunnel spiral is relatively well sampled. Intersections between all specified borehole sections and the HCD as defined above are then computed. Table 2-4 shows all the boreholes – HCD intersections obtained in the model. For each borehole section concerned, we store its monthly measured piezometric history from Data Delivery 3b. The history of hydraulic head in the node closest to each intersection is then recorded during the simulation, and compared to the measured heads.

Note that two borehole sections, KAS02 (346-799) and KAS14 (0 –130), intersect two HCDs each. Since we do not explicitly model the short-circuit due to a borehole, this means we will get two different head histories for each of these two sections. If the borehole cuts the two HCDs close to their intersection, then the heads will only slightly differ. This is the case for borehole KAS14, section (0-130). However, if the borehole section is quite long, it can cut two HCDs quite far from their intersection, it this intersection exists. This is the case for borehole KAS02, for which we therefore will obtain quite different results in the two HCDs. In this case, we can only check that the measured head is between the heads computed in the two HCDs.

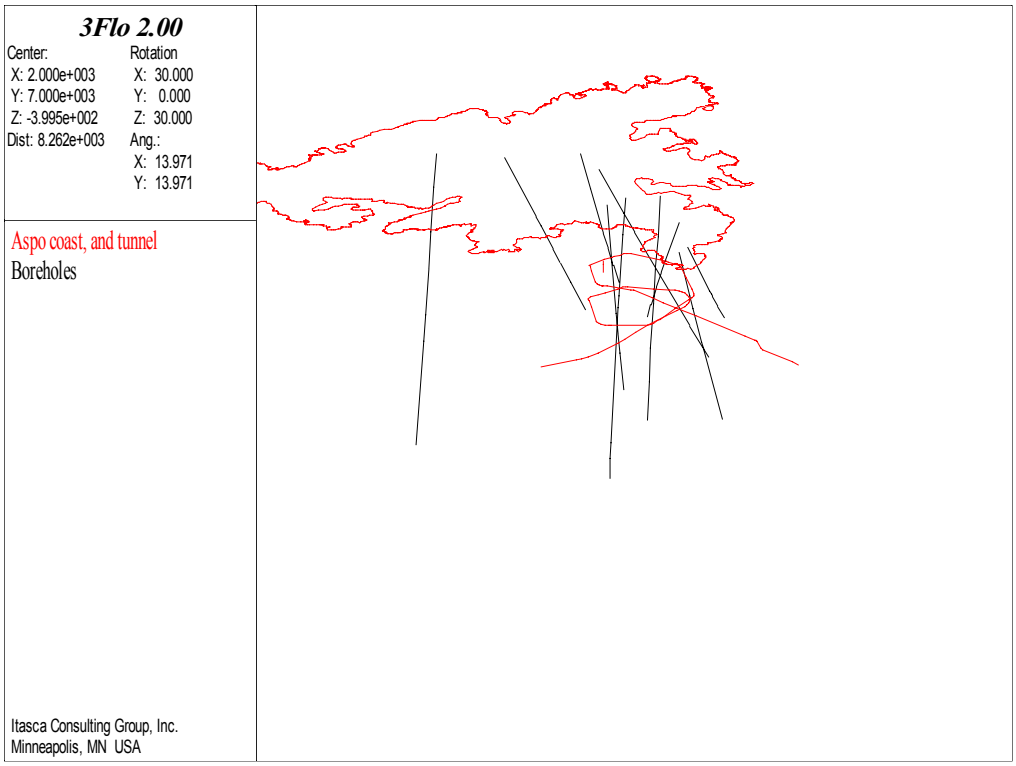

Figure 2-8: *borehole positions. View from top-West*
Perspective view: varying scale, given by Äspö Island.

A first set of calibration runs is performed, using a proportional skin. Table 2-5 summarizes the transmissivities modified by the fitting, while Figure 2-9 shows the calibration comparison between measured and computed head levels, and Figure 2-10 / Figure 2-11 show resulting hydraulic heads at the end of the simulation time. These results are obtained with a skin factor of 0.1. Note that on Figure 2-9 some curves for measured heads show strange results, with heads going up very fast (sections 0-185 and 332-392 in KAS04, and section 250-330 in KAS06). We checked that the corresponding numbers effectively exist in the Data Delivery, so we leave them on the figures. However, we do not take these seemingly spurious jumps into account.

The head variations we obtain show a good agreement with the measured values (note that "goodness of fit" should be appreciated taking into account the scale of head variations in each figure). The size of the draw down is in general well reproduced, and the time frames also conform. Note that the initial response of the model is in general flatter, with draw down starting only when the drift effectively cuts an HCD, while in reality, the effect of the tunnel if not great, can be seen from the start, because of the contribution of the "matrix". Essentially, the overall shape of the computed curve at a point depends on the geometry of the model (i.e. "when does the tunnel intersect the HCDs?), while the relative size of the draw downs depends on the transmissivities of the HCDs.

Table 2-4: borehole – HCD intersections

Borehole	Section	HCD intersected
Kas02	346-799	NE-2
Kas02	346-799	NNW-7
Kas03	107-252	NW-1
Kas03	377-532	NNW-8
Kas04	0-185	EW-1N
Kas04	332-392	EW-1S
Kas05	440-549	NE-2
Kas06	0-190	EW-3
Kas06	250-330	NNW-1
Kas06	391-430	NNW-2
Kas07	0-109	NNW-1
Kas07	191-290	NNW-7
Kas07	501-604	NE-1
Kas08	503-601	NE-1
Kas09	0-115	NE-1
Kas14	0-130	NE-1
Kas14	0-130	NNW-3

Table 2-5: proportional skin and fitted transmissivities

Zone name	Zone number	Initial Transmissivity (m^2/s)	Fitted Transmissivity (m^2/s)	Thickness (m)
EW-3	3	2.4e-5	3.6e-5	15.
NE-1	5	3.e-4	2.0e-4	30.
NE-2	6	4.1e-7	2.05e-5	5.
NNW-1	11	1.1e-5	1.1e-6	20.
NNW-2	12	5.6e-5	3.7e-5	20.

Figure 2-9: *proportional skin fit and calibrated head histories*

Black is measured, red is computed. Time in days after 01/10/1990

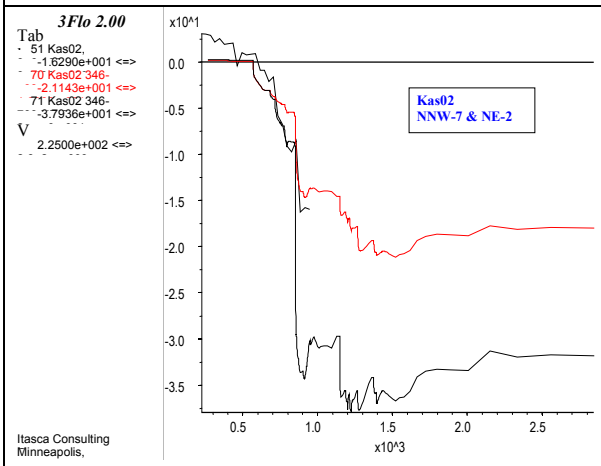

Kas02 section 346-799

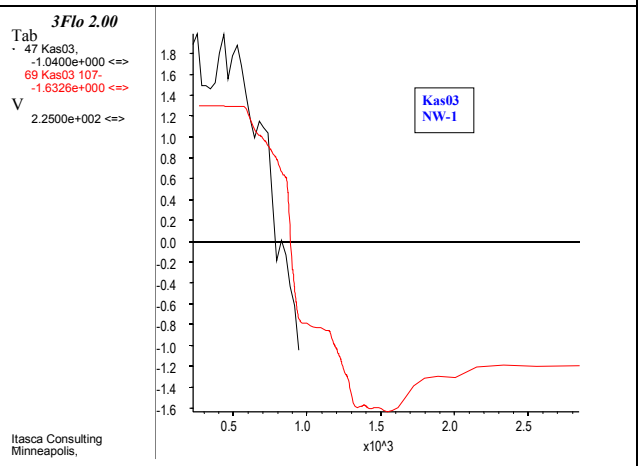

Kas03 section 107-252

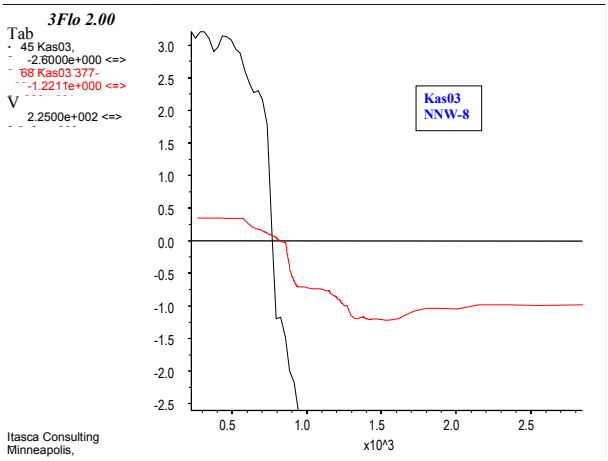

Kas03 section 377-532

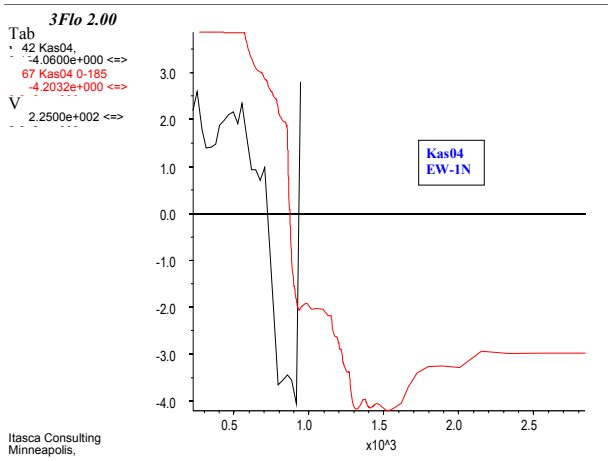

Kas04 section 0-185

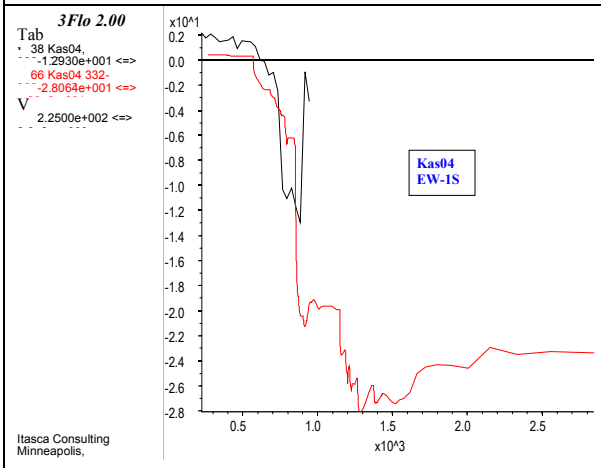

Kas04 section 332-392

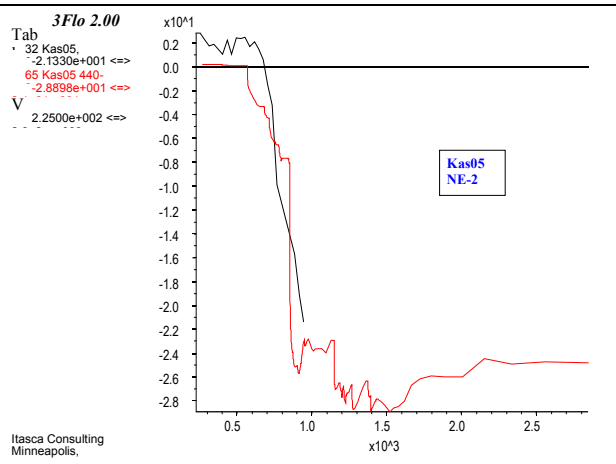

Kas05 section 440-549

Figure 2-9 (continued): *proportional skin fit and calibrated head histories*

Black is measured, red is computed. Time in days after 01/10/1990

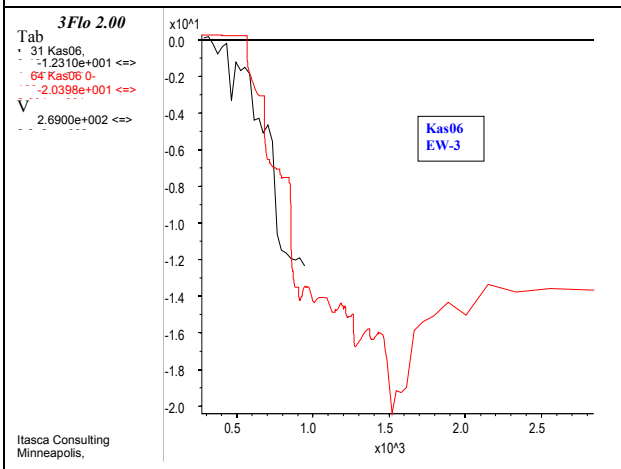

Kas06 section 0-190

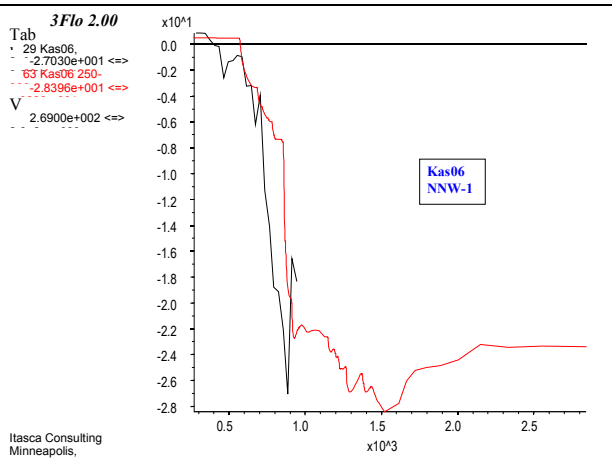

Kas06 section 250-330

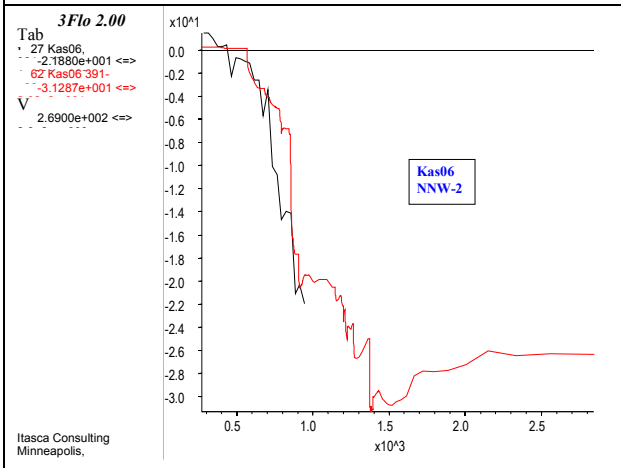

Kas06 section 391-430

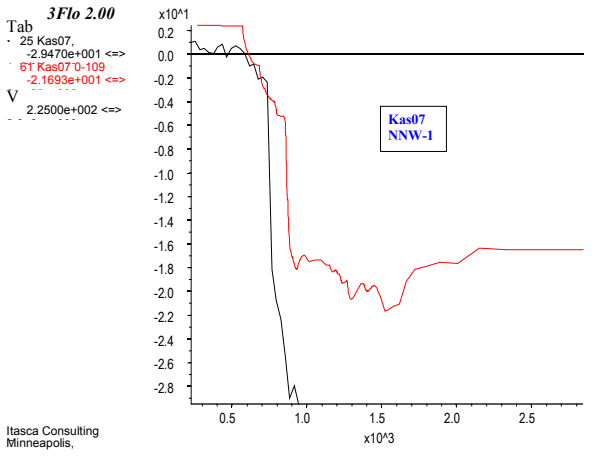

Kas07 section 0-109

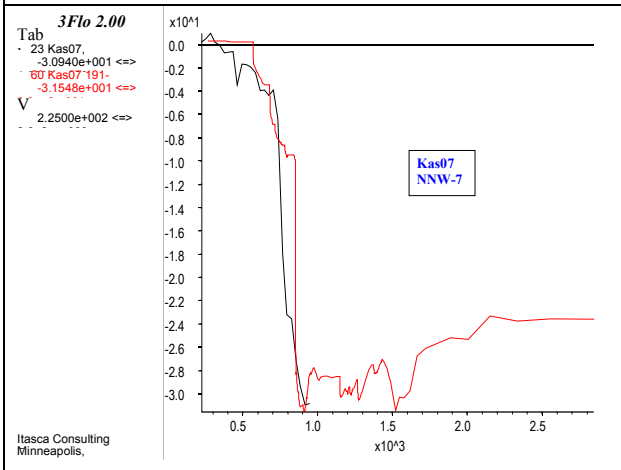

Kas07 section 191-290

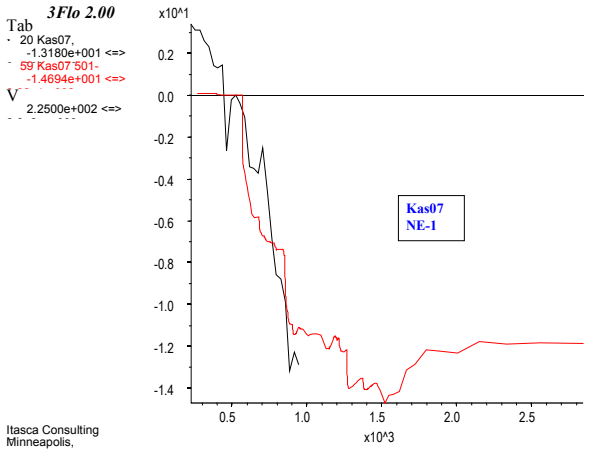

Kas07 section 501-604

Figure 2-9 (continued): *proportional skin fit and calibrated head histories*

Black is measured, red is computed. Time in days after 01/10/1990

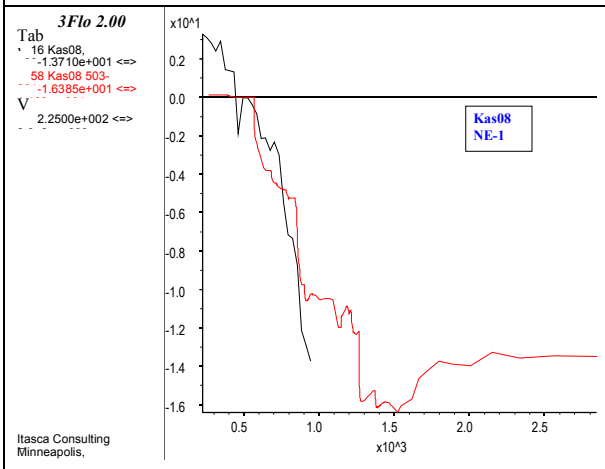

Kas08 section 503-601

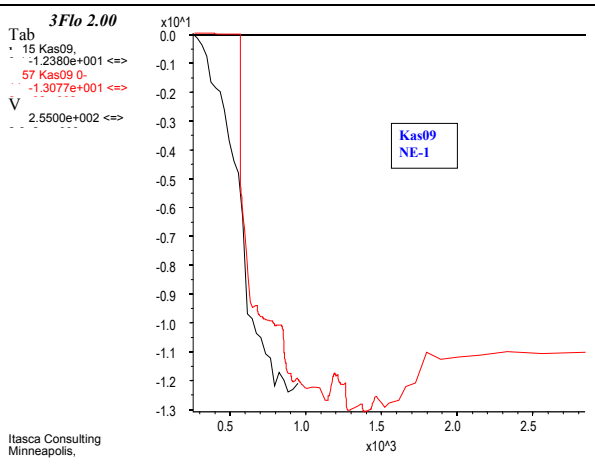

Kas09 section 0-115

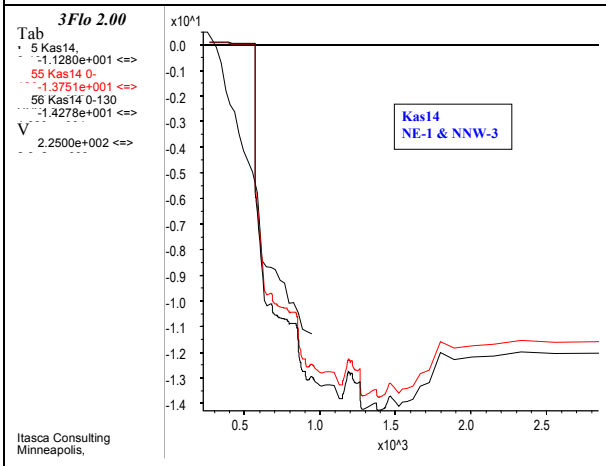

Kas14 section 0-130

Figure 2-10: *hydraulic head at end of simulation. NE and EW HCDs*

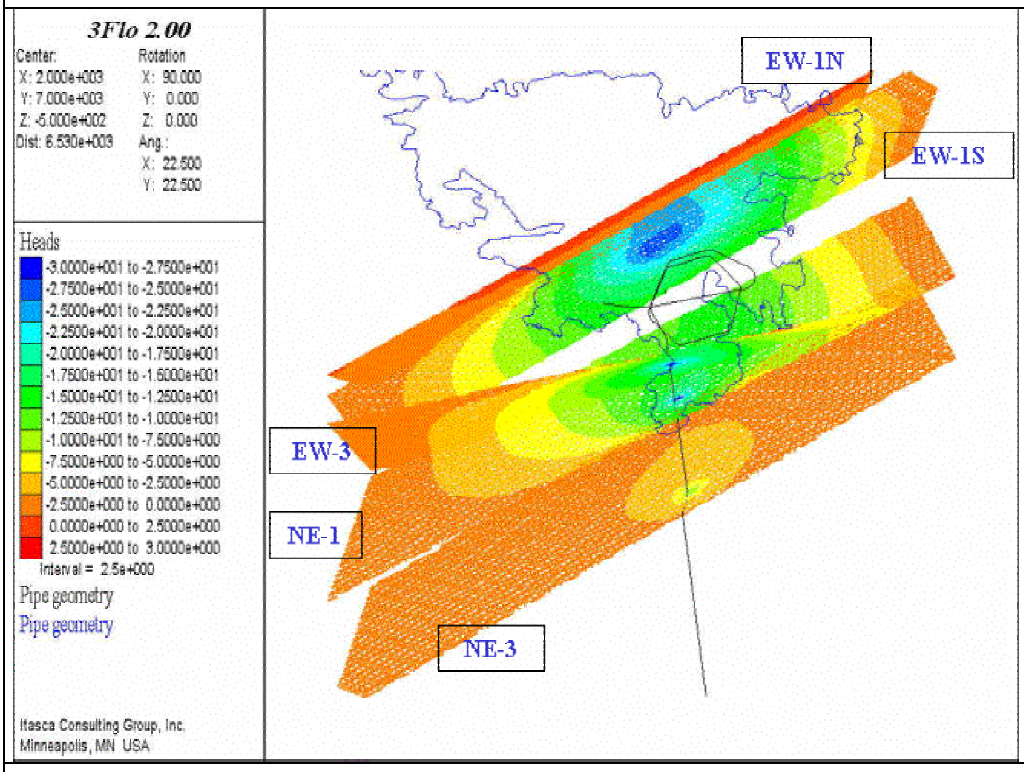

Figure 2-11: *hydraulic head at end of simulation. NE-2 and NNW HCDs*

Figure width : 750 m

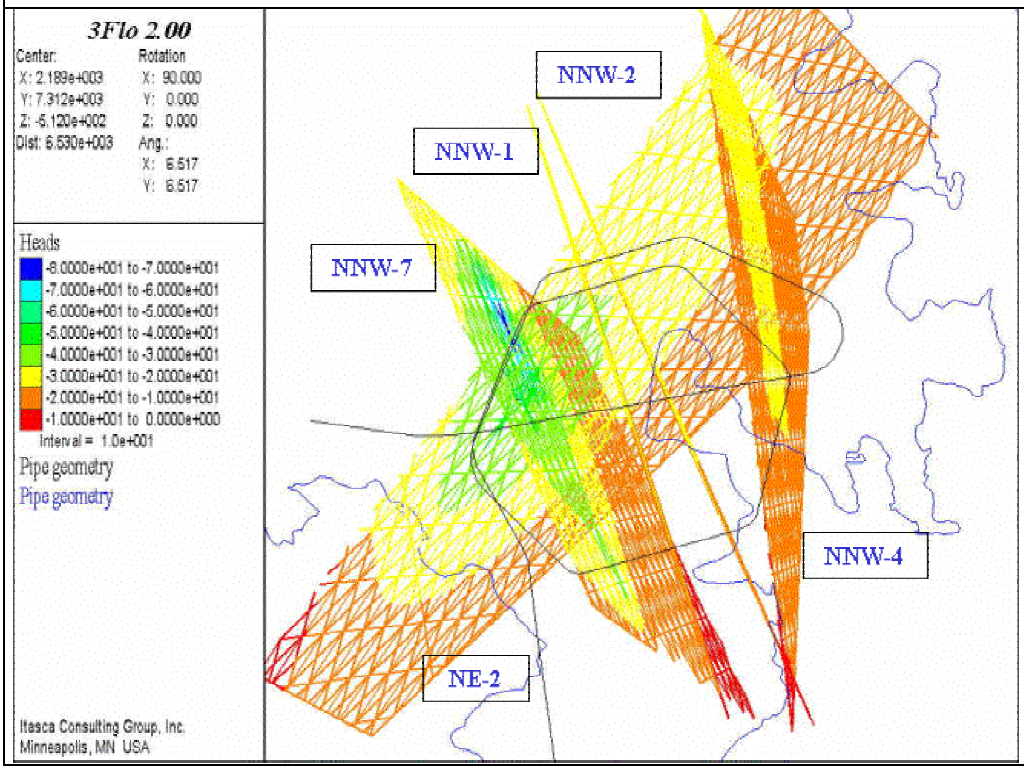

3 TRANSPORT CALIBRATION

We model the transport of non-reactive species, as well as of the four end-members specified by the Task Force. Solutes are carried along the pipe network by advection and longitudinal dispersion. Also, complete mixing at pipe intersections provides further dispersion of the solutes.

3.1 Numerical model: properties and boundary conditions

The longitudinal dispersivity is considered as constant throughout the model, and is taken from report TR97-06:

$$d=0.053*gs^{1.21},$$

where the dispersion scale is taken as the grid size ***gs*** (length of the square edges).

Boundary conditions are: no flux through the bottom boundary, and constant concentrations imposed through the vertical boundaries and the top boundary. The concentrations on the vertical boundaries are fixed at their initial values (Data Delivery 7d), while the concentrations at the top boundary are taken as pure Meteoric water under land and pure Baltic water under sea.

The solute transport is modeled by the Particle Tracking method, with multi-component, non-uniform particles. The model is initialized with particles in all pipes, depending on the starting concentrations, then particles are supplied at the boundaries according to computed flow rates and imposed concentrations. The number of particles in the model varies during the simulation, with an average of about 600,000.

We monitor tracer arrivals at several Control Points, as defined in Data Delivery 15. We take into account only Control Points number 2, 3, 4, 5, 8, and 11, which receive directly flows from HCDs: Control Point 2 at tunnel section 813m (HCD NE-4N), Control Point 3 at tunnel section 1300m (HCD NE-1), Control Point 4 at tunnel section 2021m (HCD NNW-4), Control Point 5 at tunnel section 2788m (HCD NNW-2), Control Point 8 at tunnel section 3138m (HCD NNW-4), and finally Control Point 11 in borehole KAS07, section (501-604), cutting HCD NE-1. The corresponding positions are shown in Fig. 3-1.

3.2 First calibration: skin effect

Figure 3-2 shows Chlorine concentrations at three control points while Figure 3-3 gives the four end-members (Baltic, Meteoric, Brine and Glacial waters) evolution with time. In all cases, we compute large ratios of Baltic waters, while meteoric water is underestimated : in our model, the communication between the Baltic sea and the part of flow network represented by the Control Points is too direct. For example, Control Point 2 is overwhelmed by Baltic water very early after the tunnel hits HCD NE-3 (28-10-1991 ; 380 days after start). However, simply reducing the overall skin factor is not acceptable, since it would yield too high heads below the island. So we reduce the influence of the Baltic sea on the main conductors by applying a uniform skin : the main conductors, responsible for most of the Baltic water inflow, should now be “isolated” by a layer less permeable than before.

We need to redo the flow calibration, in order to "compensate" for the differing skin factor. Table 3-1 shows the new fitted transmissivities (HCDs not mentioned keep their initial values) : the transmissivities we obtain are not far from the previously calibrated ones. We need to increase the transmissivities of some of the most conductive HCDs, compared to the previous calibration, since they are the ones for which the communication with Baltic is reduced the most by going from a proportional to a uniform skin factor. Among these, only HCD NNW-3 needs a significant (tenfold) increase. This zone, together with NE-1, governs the response in borehole Kas14, section 0-130 (see Figure 3-4 showing the head response). However, since the NE-1 transmissivity controls other head responses (Kas08-section 503-601 for example, see Figure 3-4), it is constrained by these other measurements, and only NNW-3 is made more conductive.

We do not touch the conductivity of the pipes enabling the communication between HCDs EW-1S and EW-1N. In fact, because they have low transmissivities, the zones north of EW-1N (including EW-1N itself), receive a higher permeability skin in the new model and see a larger influence of the sea. This explains the deterioration of the fit for the borehole sections north of this zone, in Kas03 and the top section of Kas04 (compare Figure 3-4 with Figure 2-9). For the remaining sections, the new calibration yields results very similar to the ones previously obtained.

Figure 3-5 and Figure 3-6 illustrate the new head field, using the same color scale as Figure 2-10 and Figure 2-11. The tunnel draw down is now much more widespread in NE-3, and is less marked in the NNW and EW HCDs. Figure 3-7 and Figure 3-8 show the results of the chlorine run, with high chlorine concentrations migrating from depth in HCD NE-1 (Figure 3-7), but competing with less chlorinated waters at the depth of Control Point CP3 (see Figure 3-8 : this yields the spiky part of the curve for Control Point CP3), then stabilizing to Baltic water – like concentrations.

This run shows mixed results: Baltic water ratios are decreased in Control points 3,4,5,11, but are still significantly higher than measures, and Control Point 2 is essentially not affected. In other words, the supposedly better representation of the Baltic sea skin effect reduces the error, but leaves it still quite large. We conjecture that the way we represent recharge by meteoric water on land (i.e. constant imposed flux) is likely to severely underestimate the amount of meteoric water provided by the boundary condition to the system, and therefore may explain the large values of Baltic water we experience in the model. So we decide to try to redo the simulations, representing the recharge over land in a more realistic way.

Table 3-1: uniform skin and fitted transmissivities

Zone name	Zone number	Initial Transmissivity (m^2/s)	Transmissivity, Proportional skin case (m^2/s)	Fitted Transmissivity (m^2/s)	Thickness (m)
EW-3	3	2.4e-5	3.6e-5	3.6e-5	15.
NE-1	5	3.e-4	2.0e-4	4.0e-4	30.
NE-2	6	4.1e-7	2.05e-5	4.1e-5	5.
NNW-1	11	1.1e-5	1.1e-6	1.1e-6	20.
NNW-2	12	5.6e-5	3.7e-5	3.7e-5	20.
NNW-3	13	2.e-5	2.e-5	2.e-4	20.

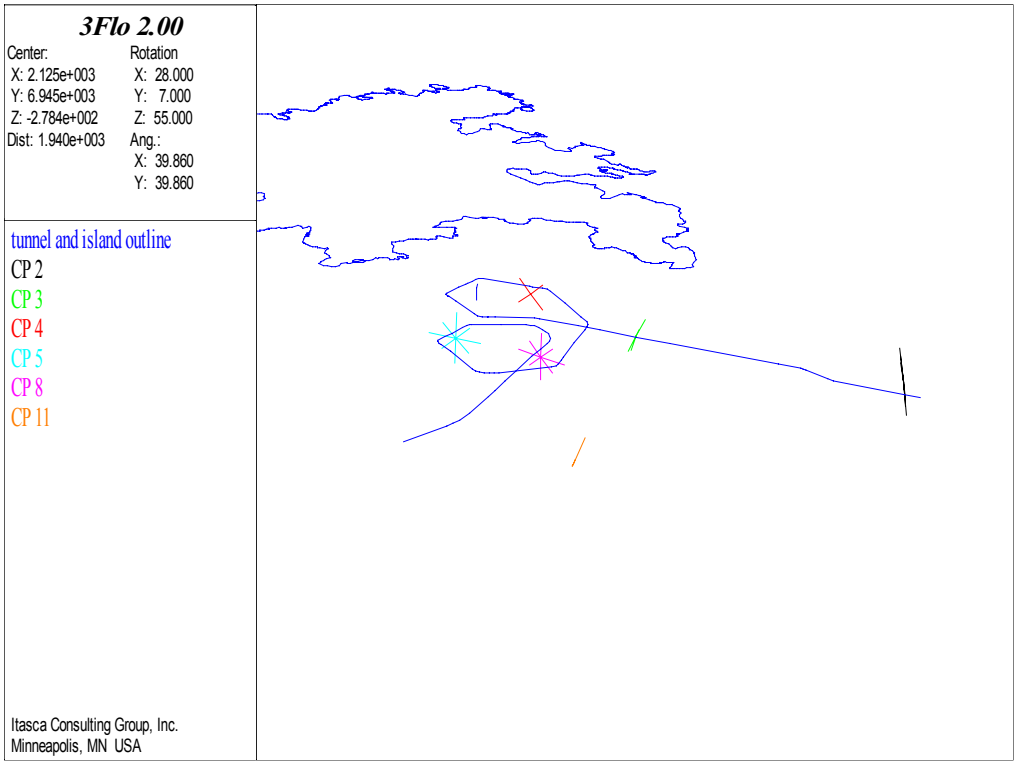

Figure 3-1: *control Points geometry. View from top-South-West*

Figure 3-2: *chlorine concentrations*

Time in days after 01/10/1990, concentration in mg/l

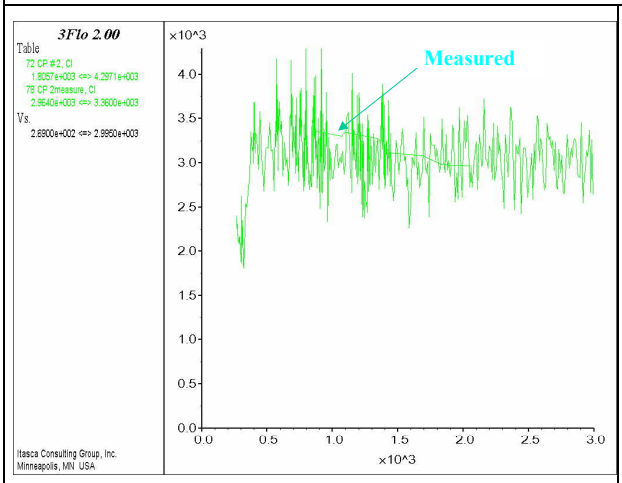

Control Point 2

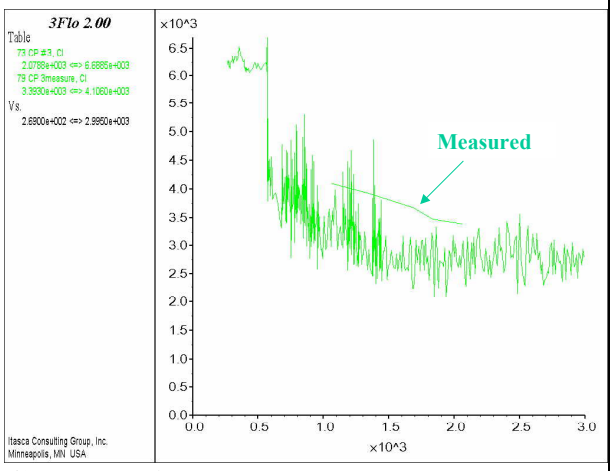

Control Point 3

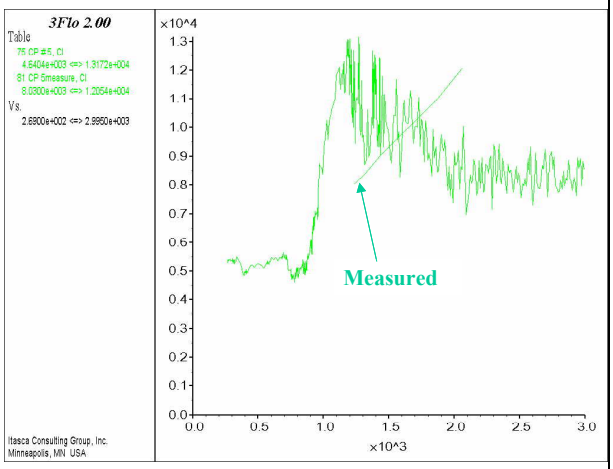

Control Point 5

Figure 3-3: *proportional skin fit and end-member evolution*

Time in days after 01/10/1990.

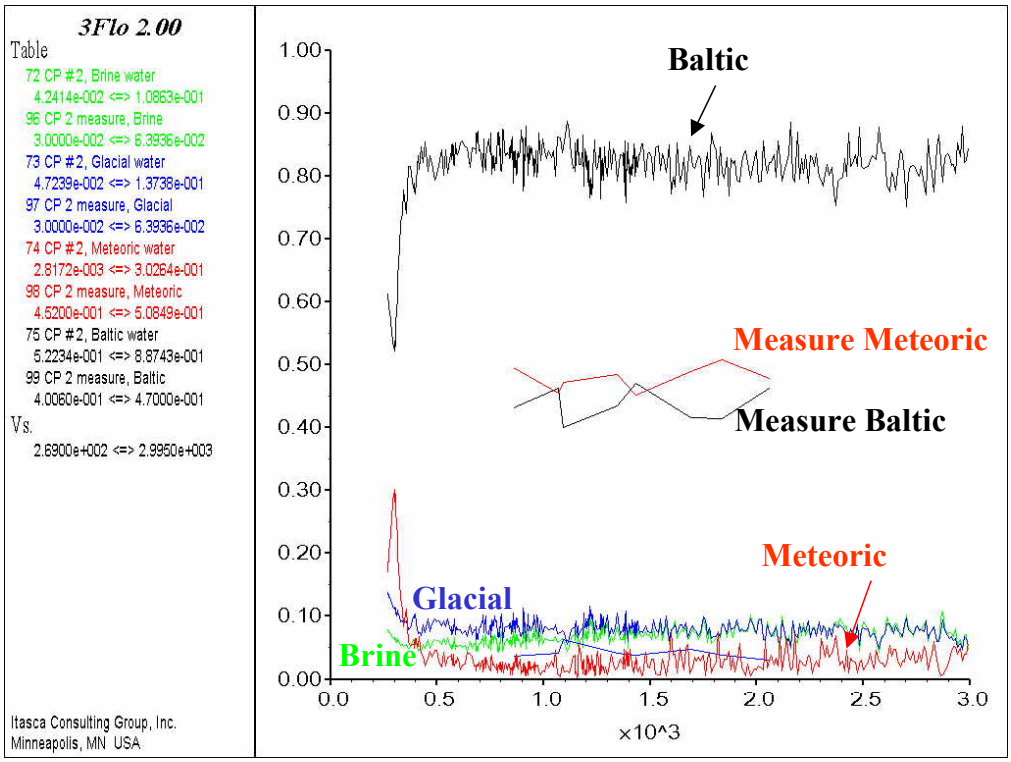

Control Point 2

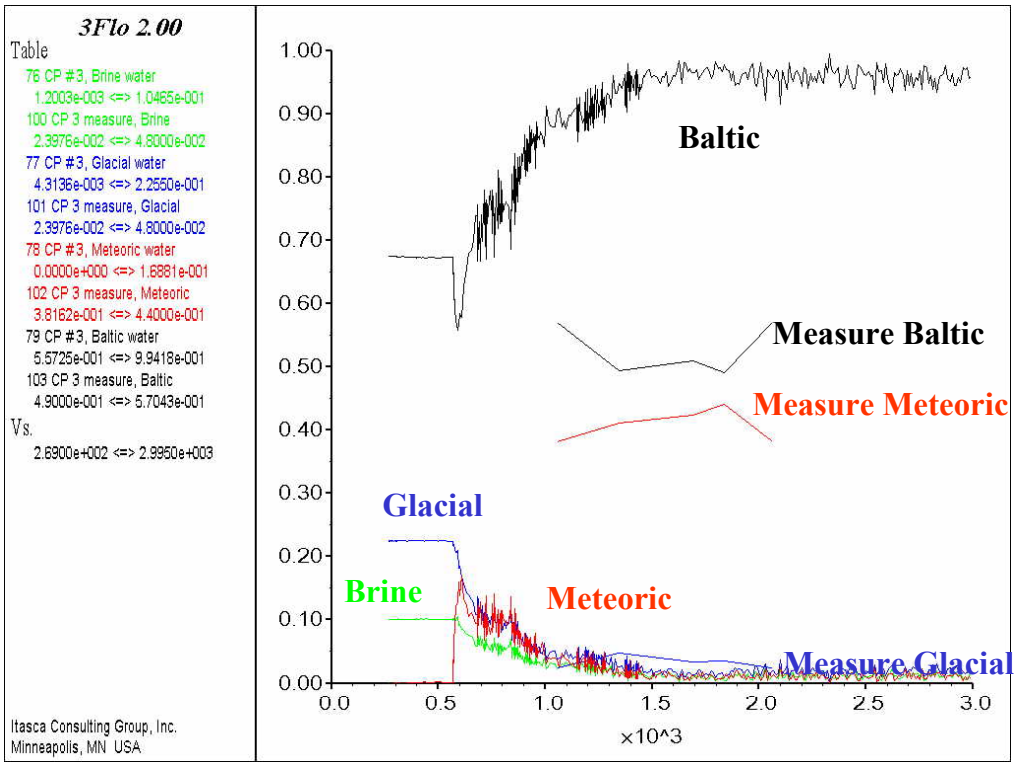

Control Point 3

Figure 3-3 (continued): *proportional skin fit and end-member evolution*

Time in days after 01/10/1990.

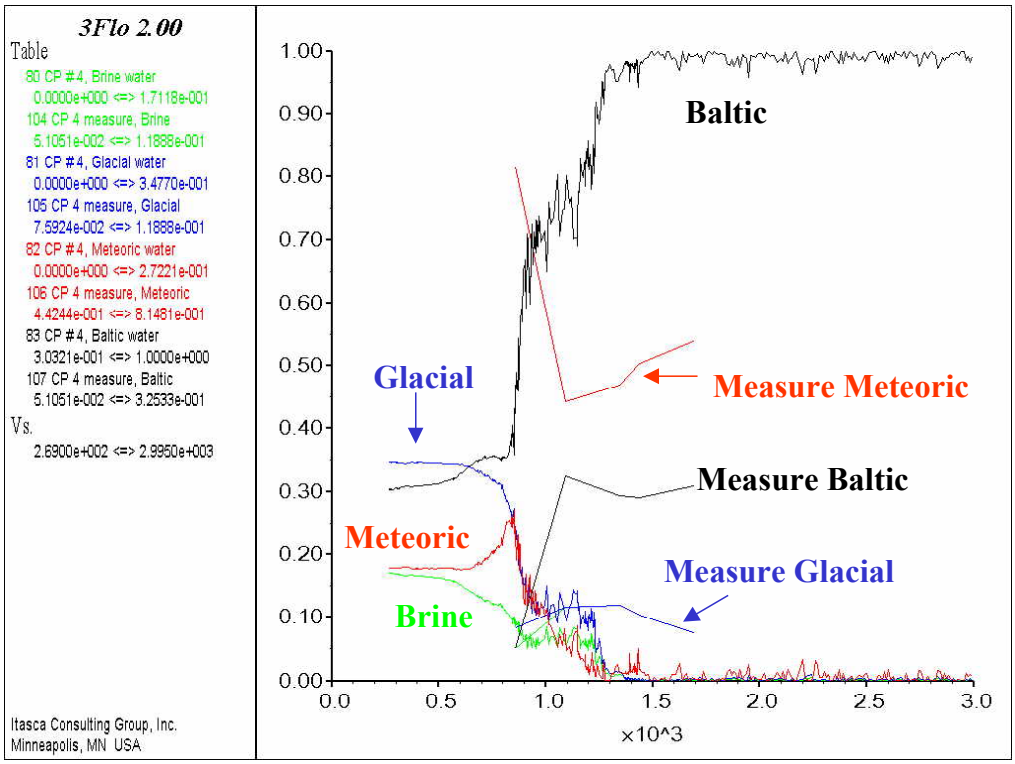

Control Point 4

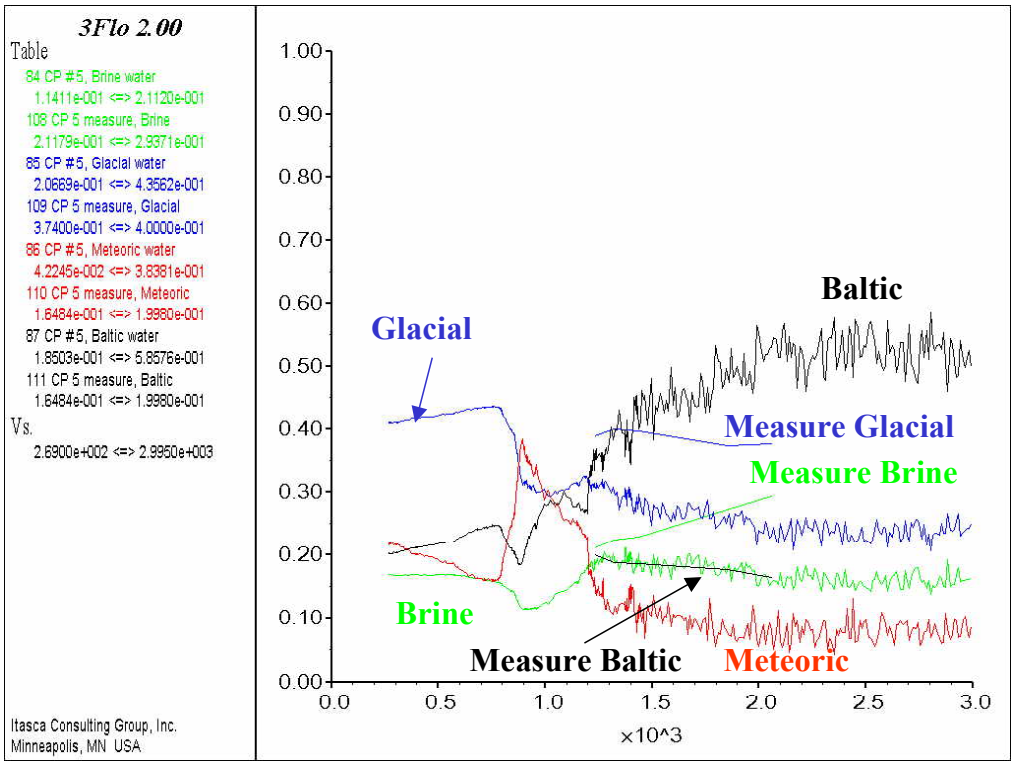

Control Point 5

Figure 3-3 (continued): *proportional skin fit and end-member evolution*

Time in days after 01/10/1990.

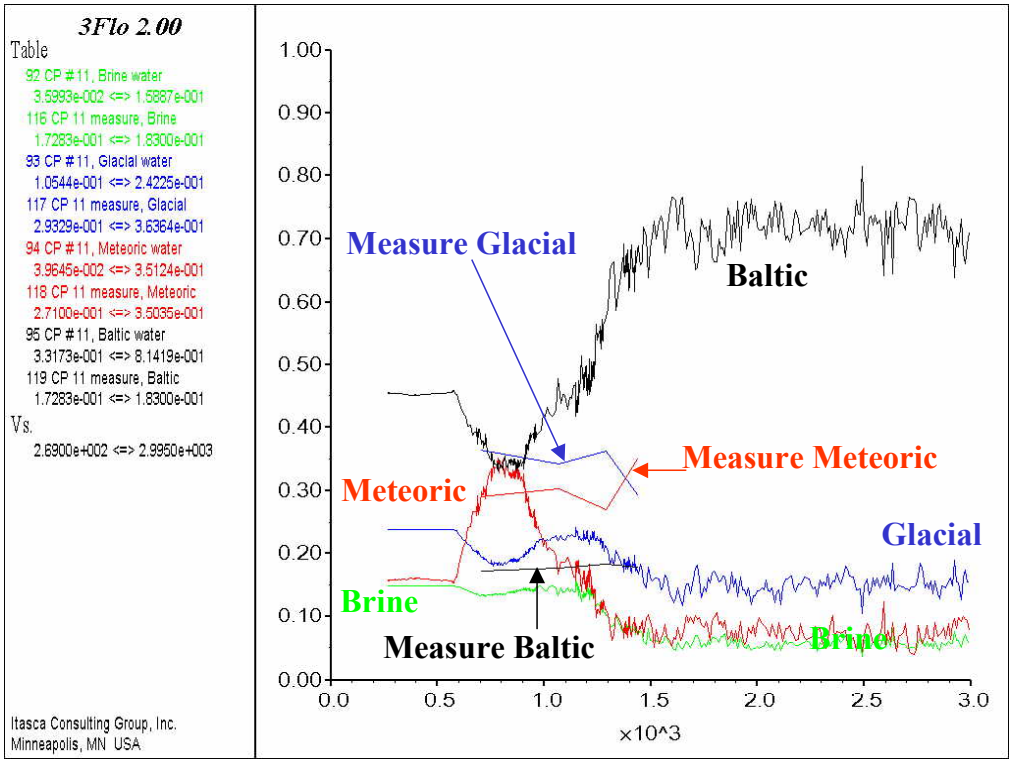

Control Point 11

Figure 3-4: *uniform skin fit and calibrated head histories*

Black is measured, red is computed. Time in days after 01/10/1990.

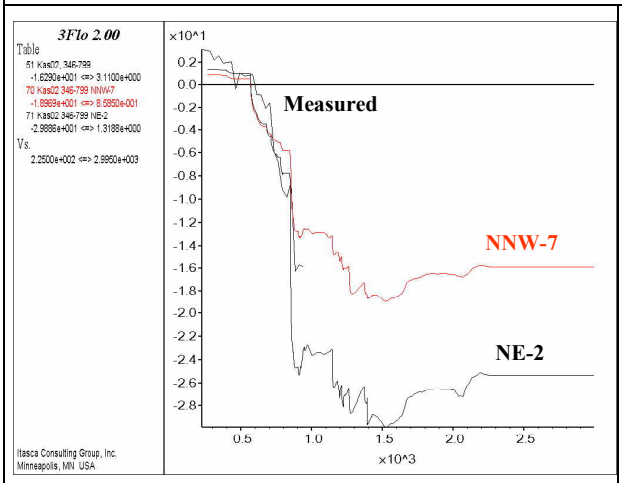

Kas02 section 346-799

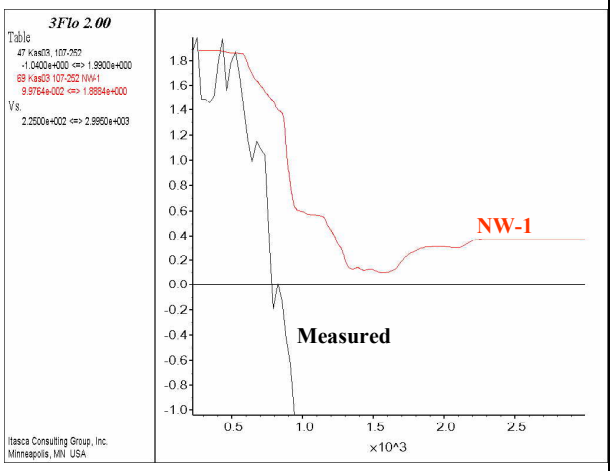

Kas03 section 107-252

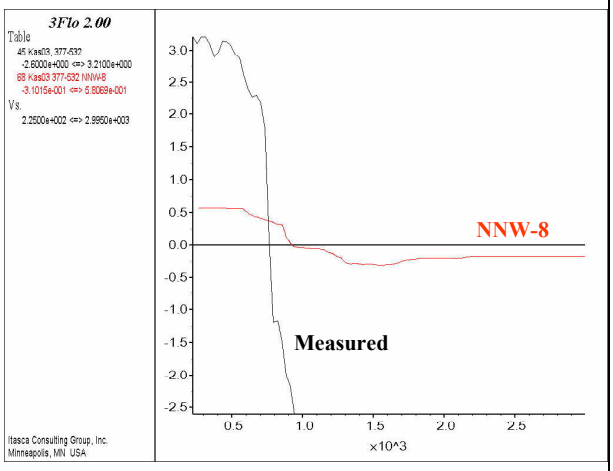

Kas03 section 377-532

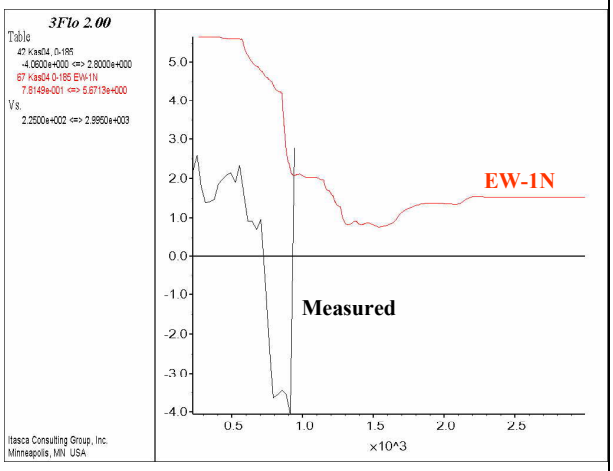

Kas04 section 0-185

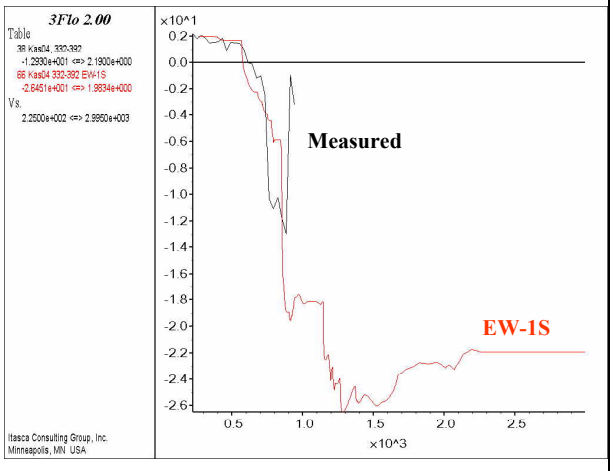

Kas04 section 332-392

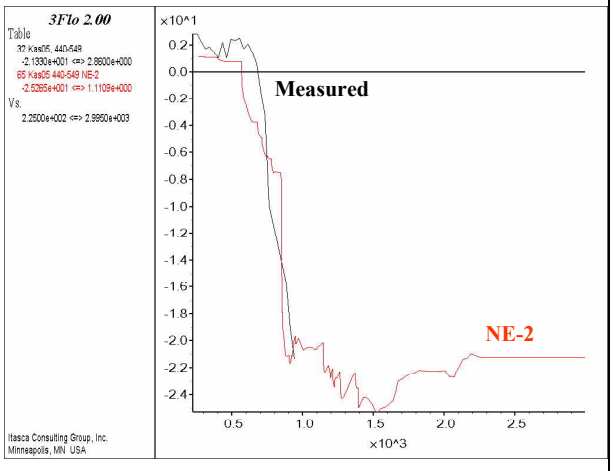

Kas05 section 440-549

Figure 3-4 (continued): *uniform skin fit and calibrated head histories*

Black is measured, red is computed. Time in days after 01/10/1990.

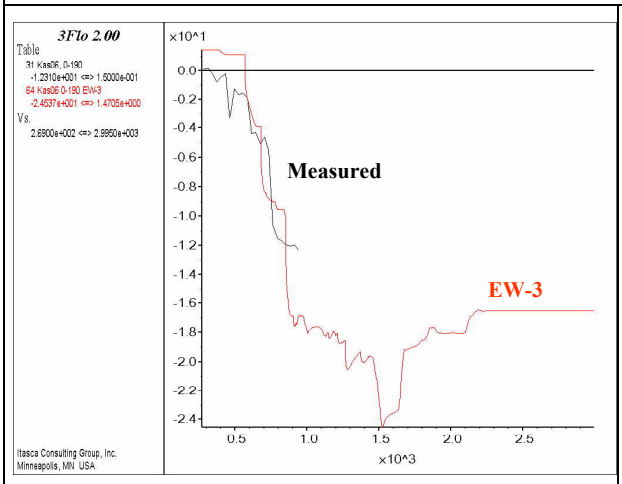

Kas06 section 0-190

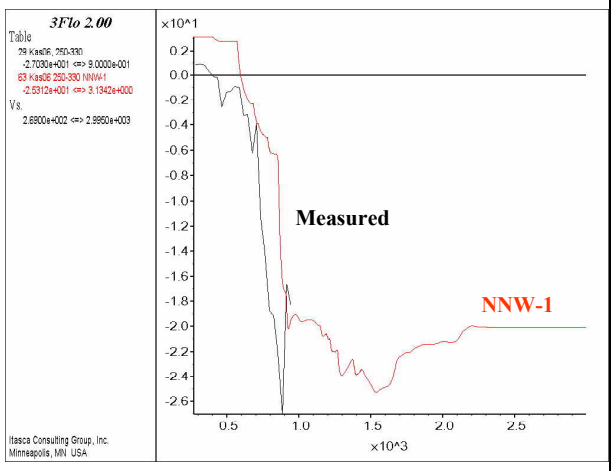

Kas06 section 250-330

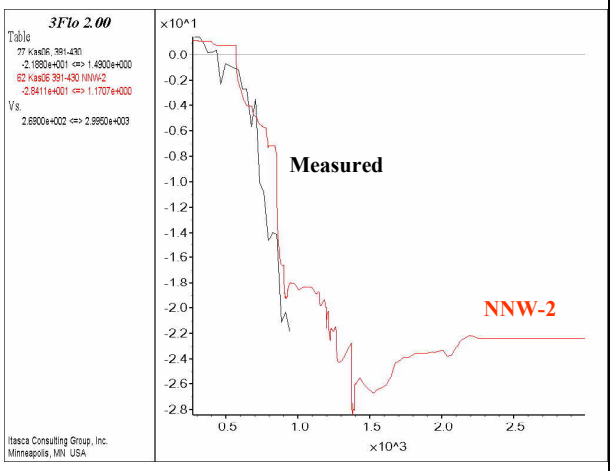

Kas06 section 391-430

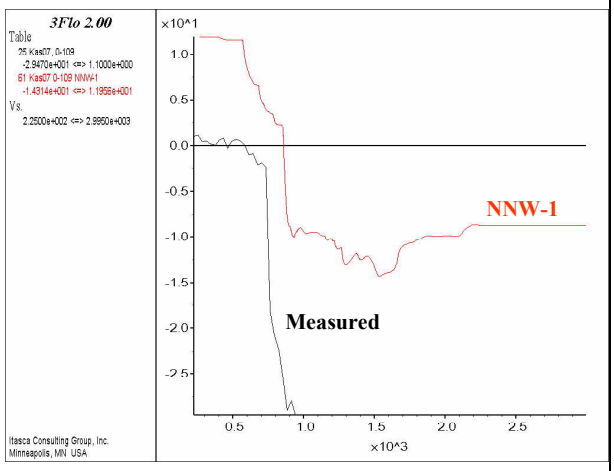

Kas07 section 0-109

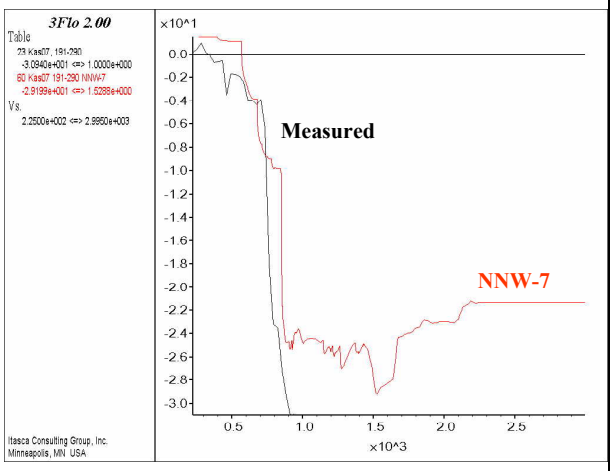

Kas07 section 191-290

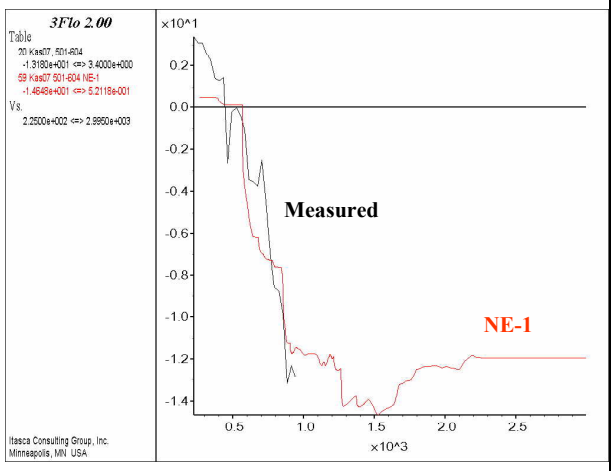

Kas07 section 501-604

Figure 3-4 (continued): *uniform skin fit and calibrated head histories*

Black is measured, red is computed. Time in days after 01/10/1990.

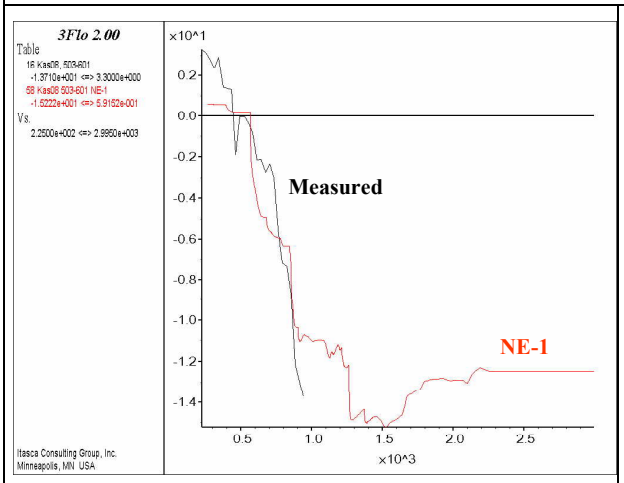

Kas08 section 503-601

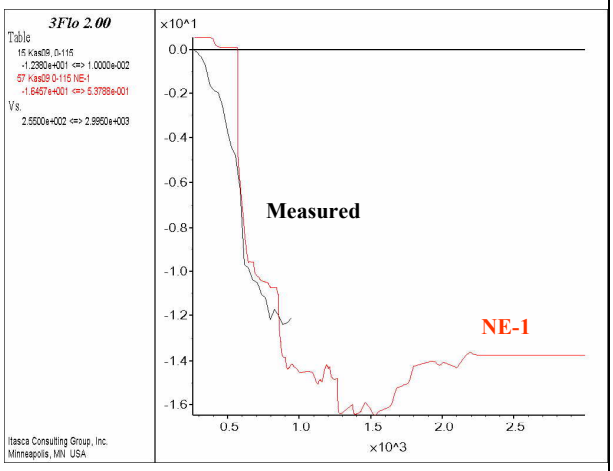

Kas09 section 0-115

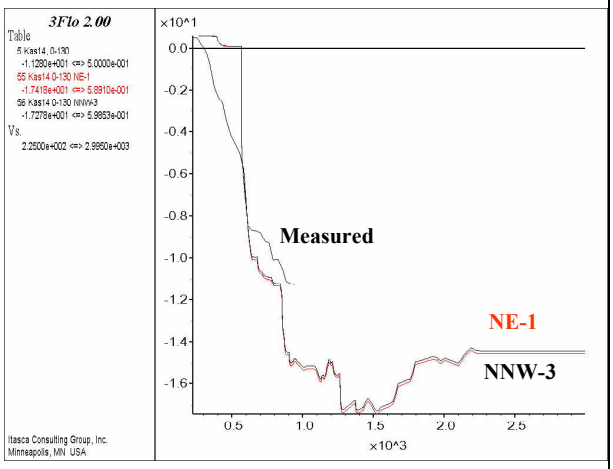

Kas14 section 0-130

Figure 3-5: *hydraulic head at end of simulation - NE and EW HCDs*

Varying scale, given by island outline

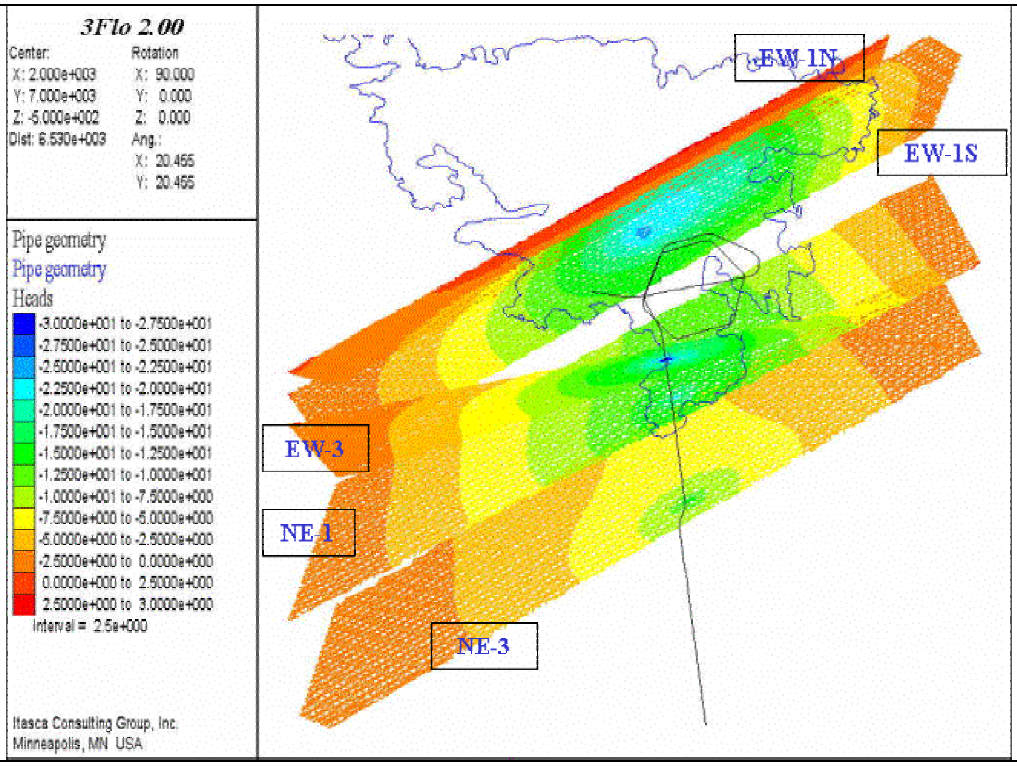

Figure 3-6: *hydraulic head at end of simulation - NE-2 and NNW HCDs*

Figure width : 750 m

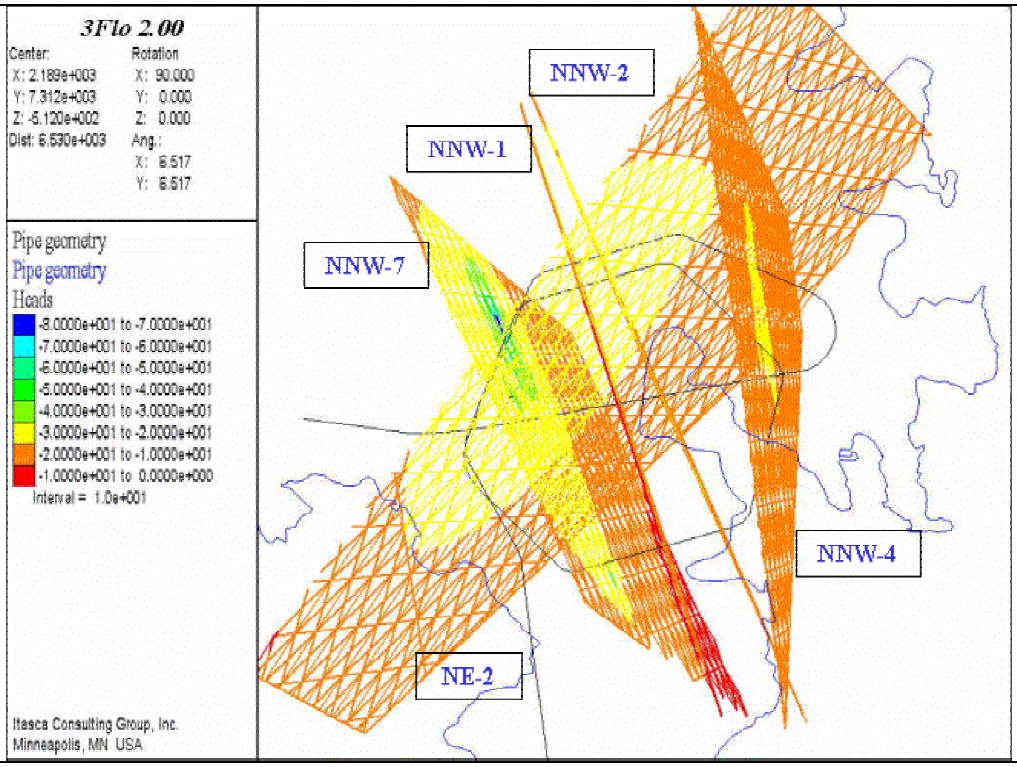

Figure 3-7: *chlorine concentrations in Zone NE-1, mg/l*

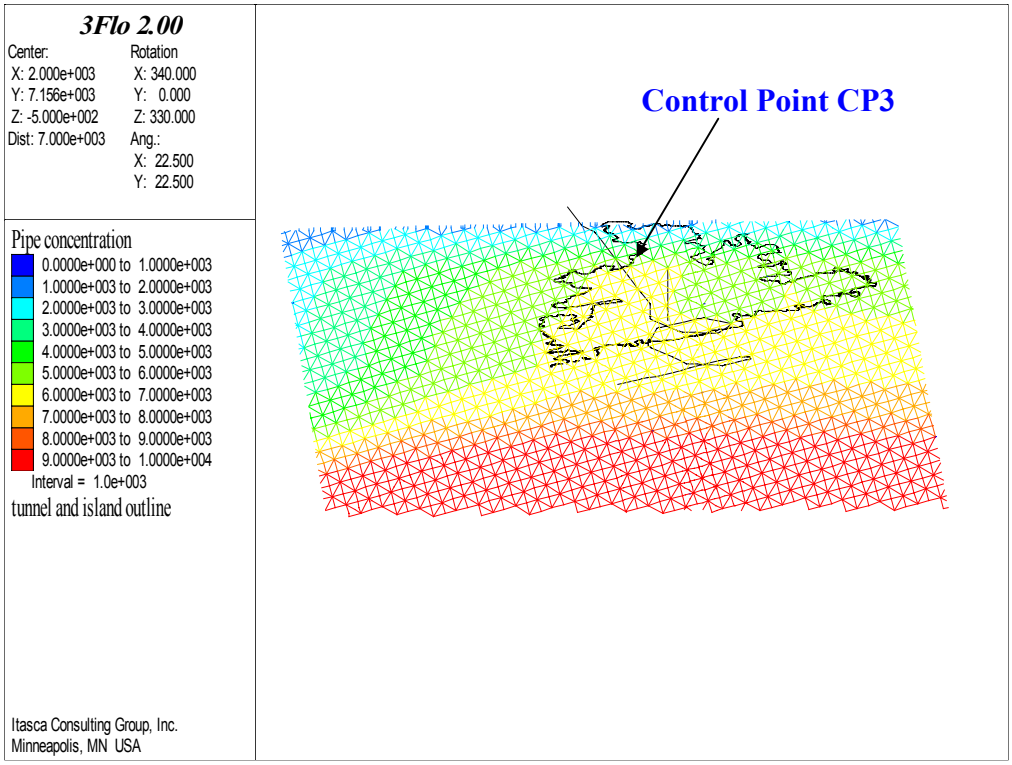

start of simulation

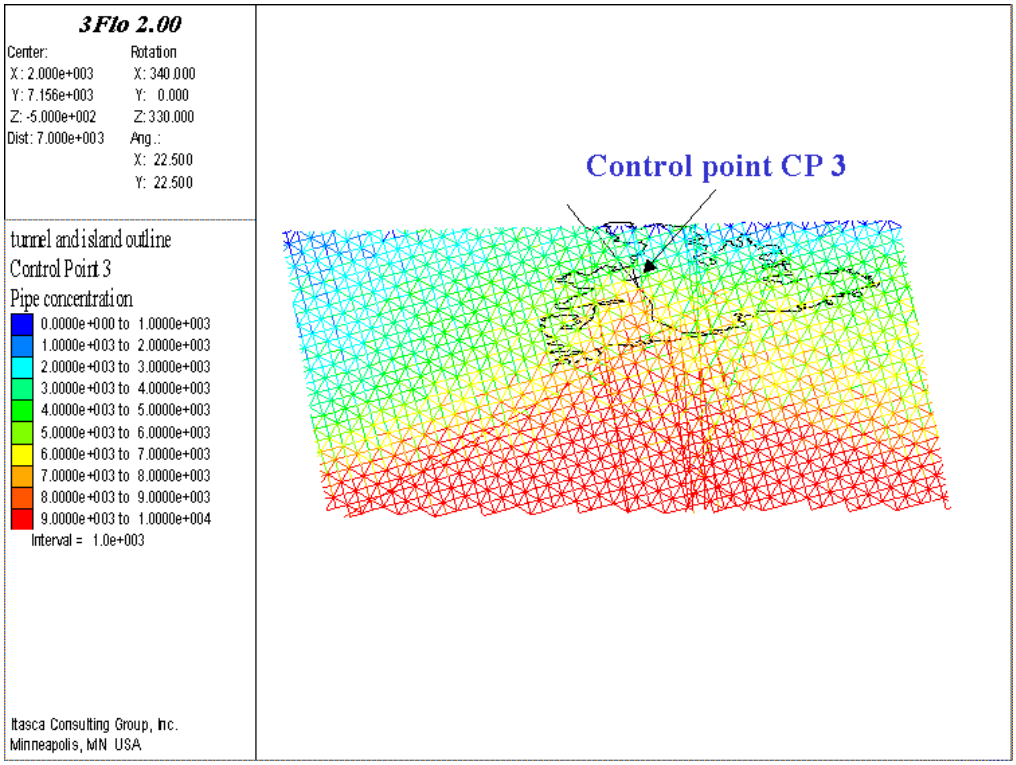

Tunnel at 2021 m

Figure 3-7 (continued): *chlorine concentrations in Zone NE-1, mg/l*

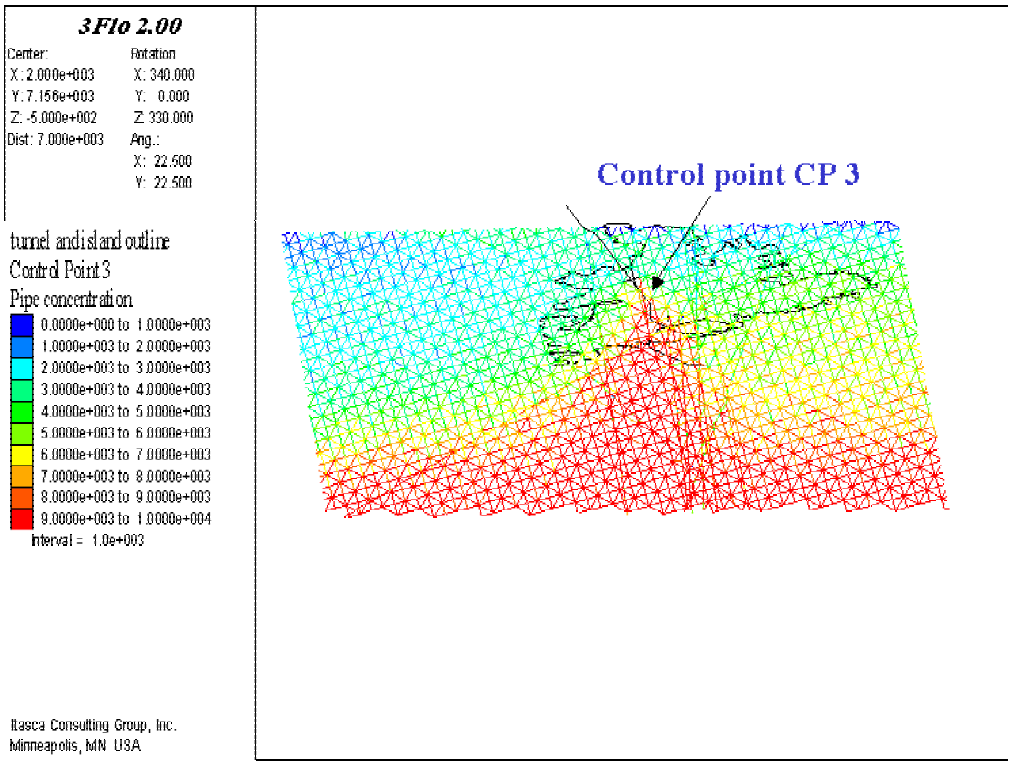

Tunnel at 2790 m

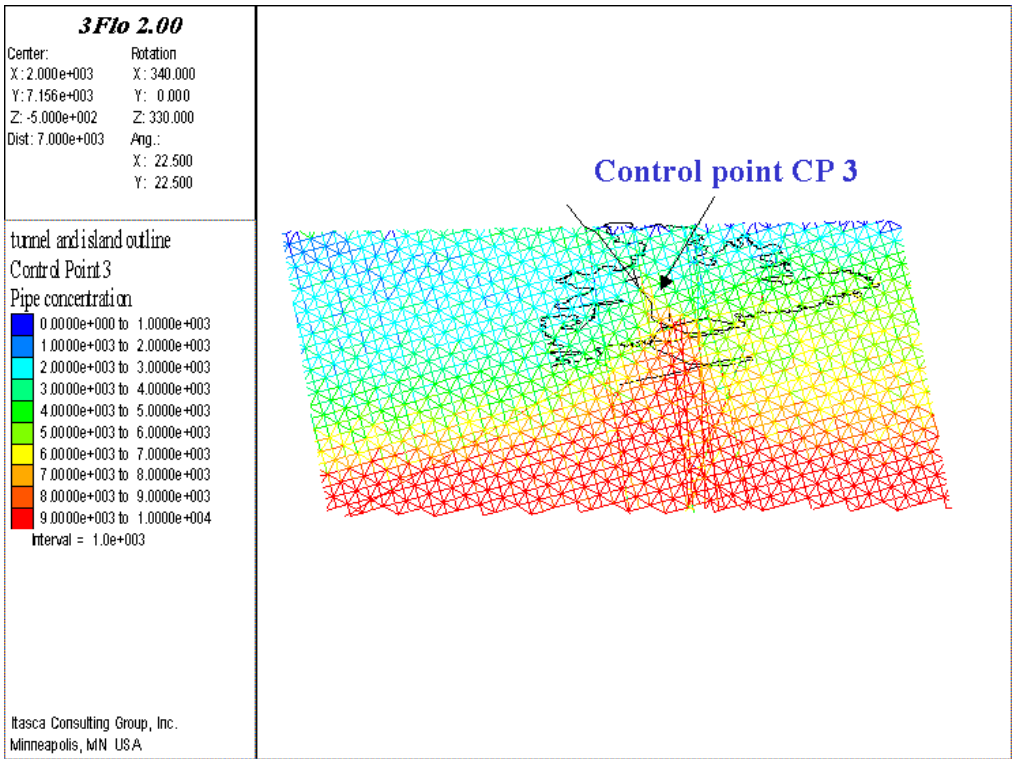

End of simulation

Figure 3-8: *uniform skin fit - Chlorine concentrations*

Time in days after 01/10/1990.

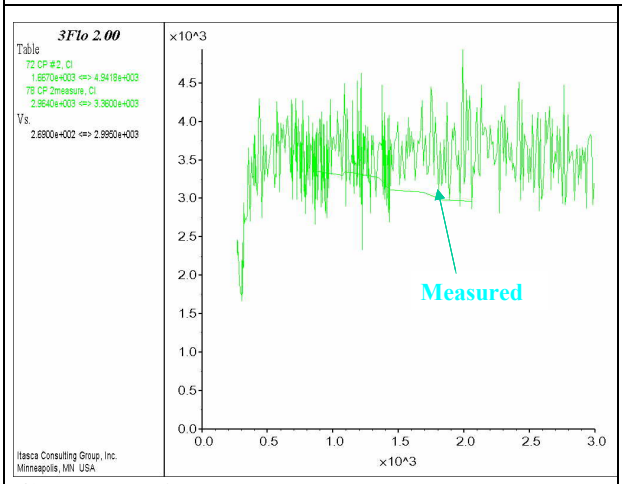

Control Point 2

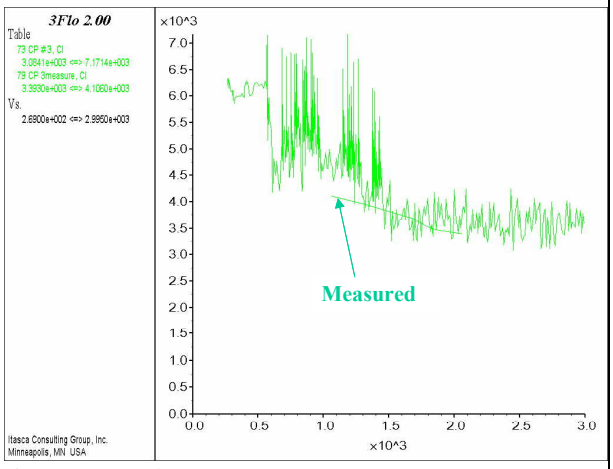

Control Point 3

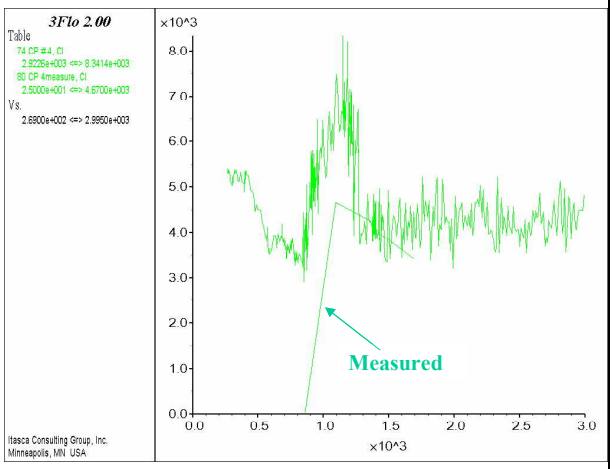

Control Point 4

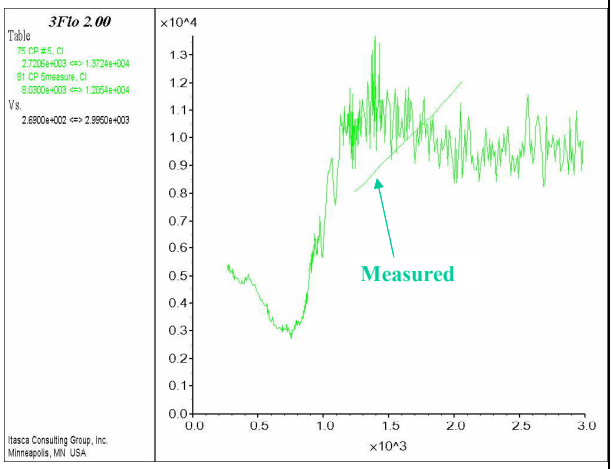

Control Point 5

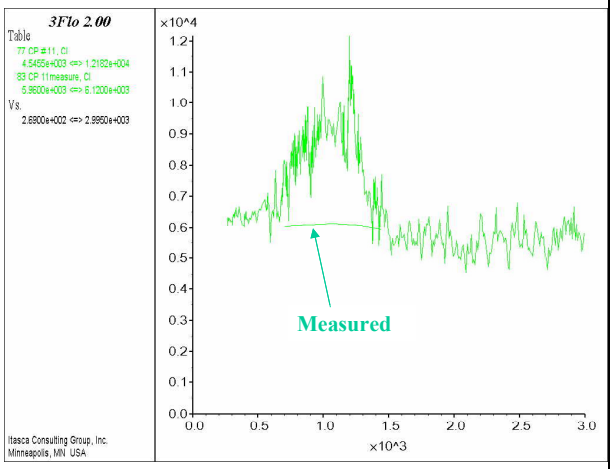

Control Point 11

Figure 3-9: *uniform skin fit – end-member evolution*

Time in days after 01/10/1990.

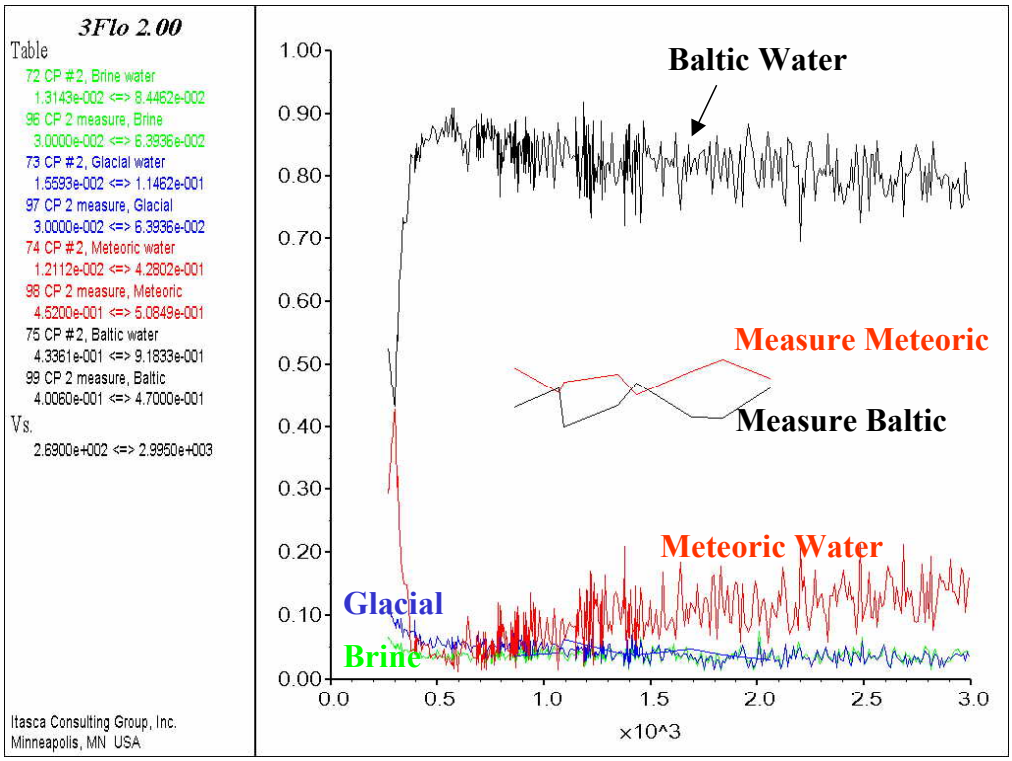

Control Point 2

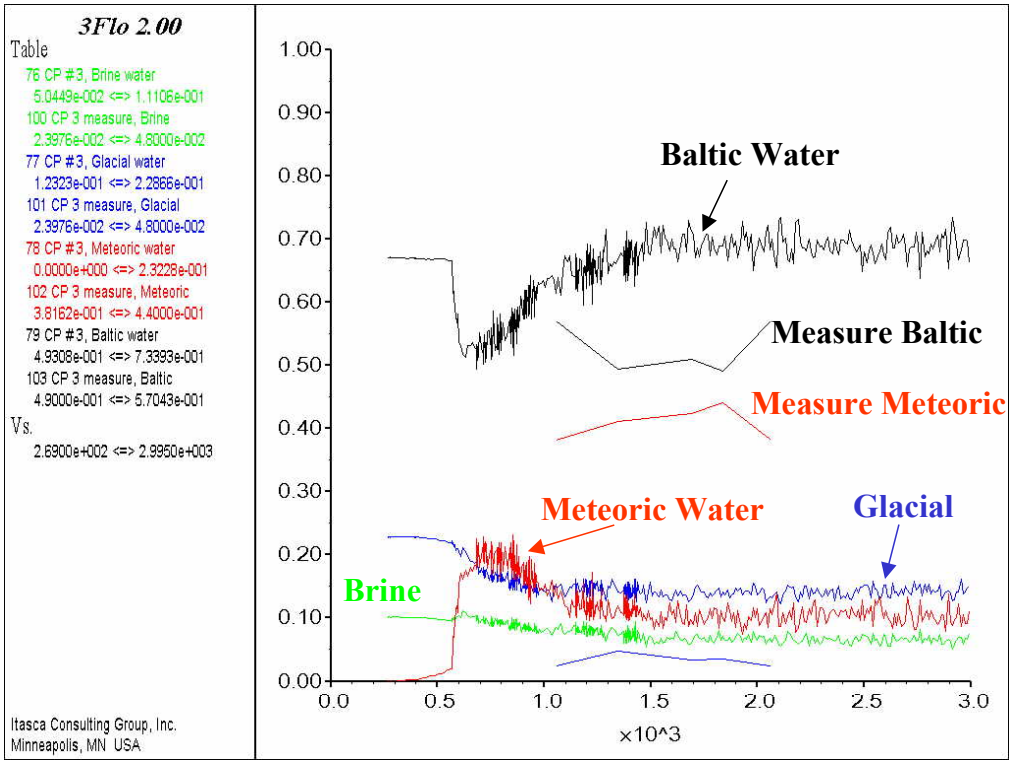

Control Point 3

Figure 3-9 (continued): *uniform skin fit – end-member evolution*

Time in days after 01/10/1990.

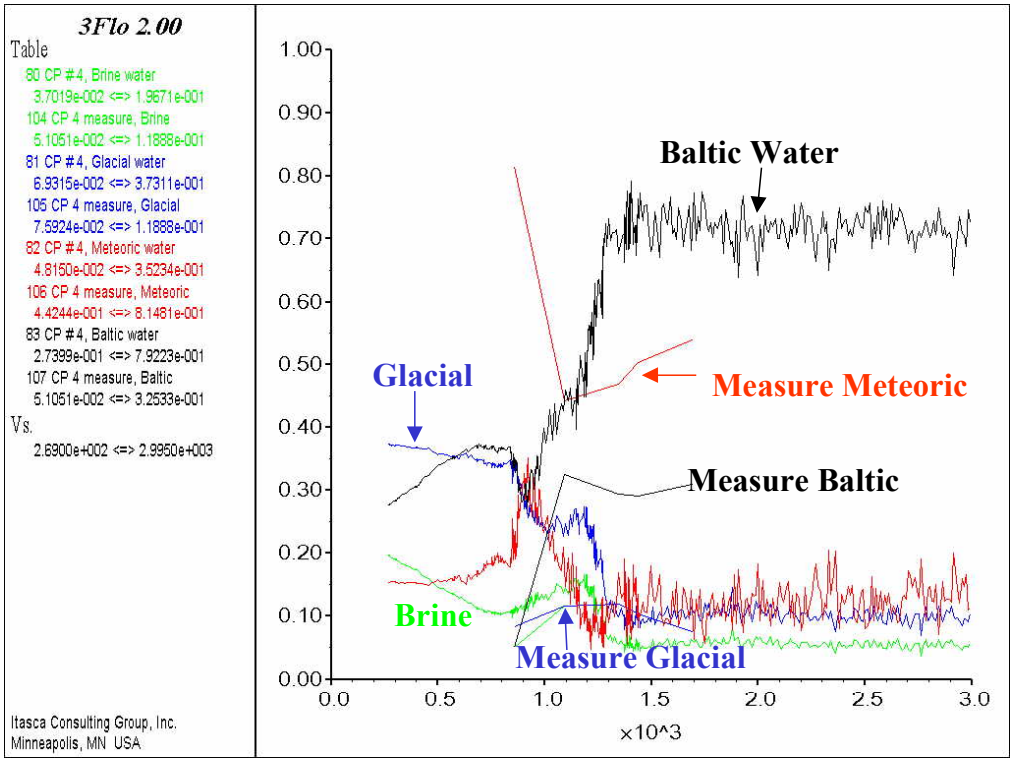

Control Point 4

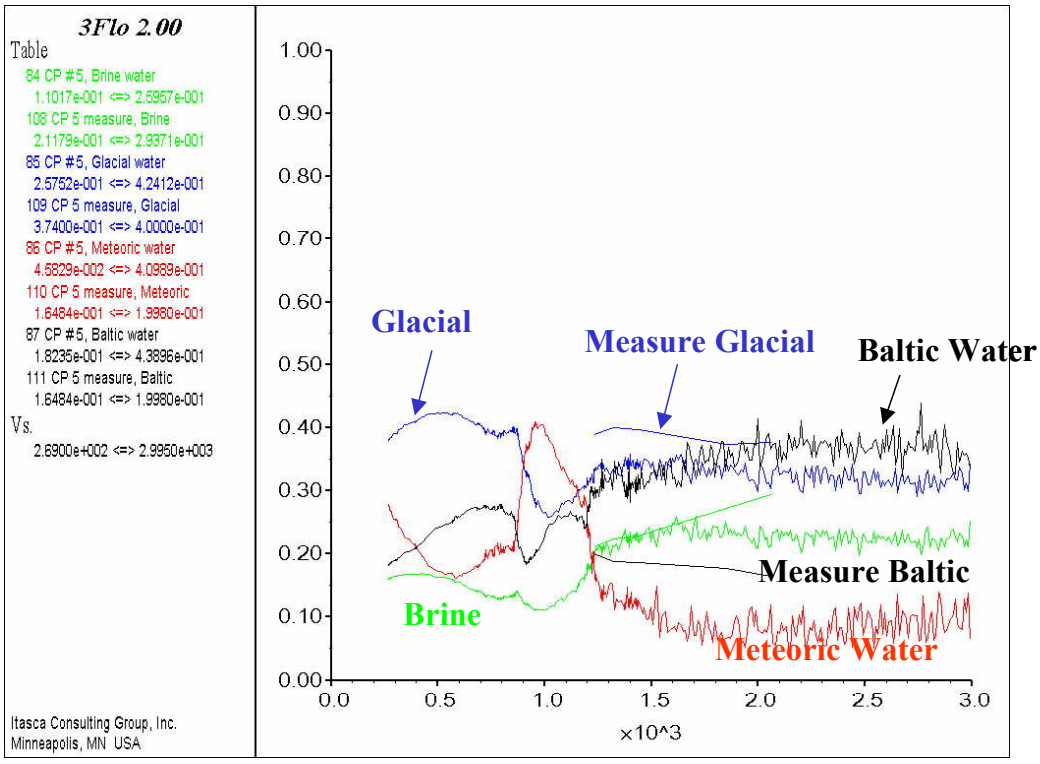

Control Point 5

Figure 3-9 (continued): *uniform skin fit – end-member evolution*

Time in days after 01/10/1990

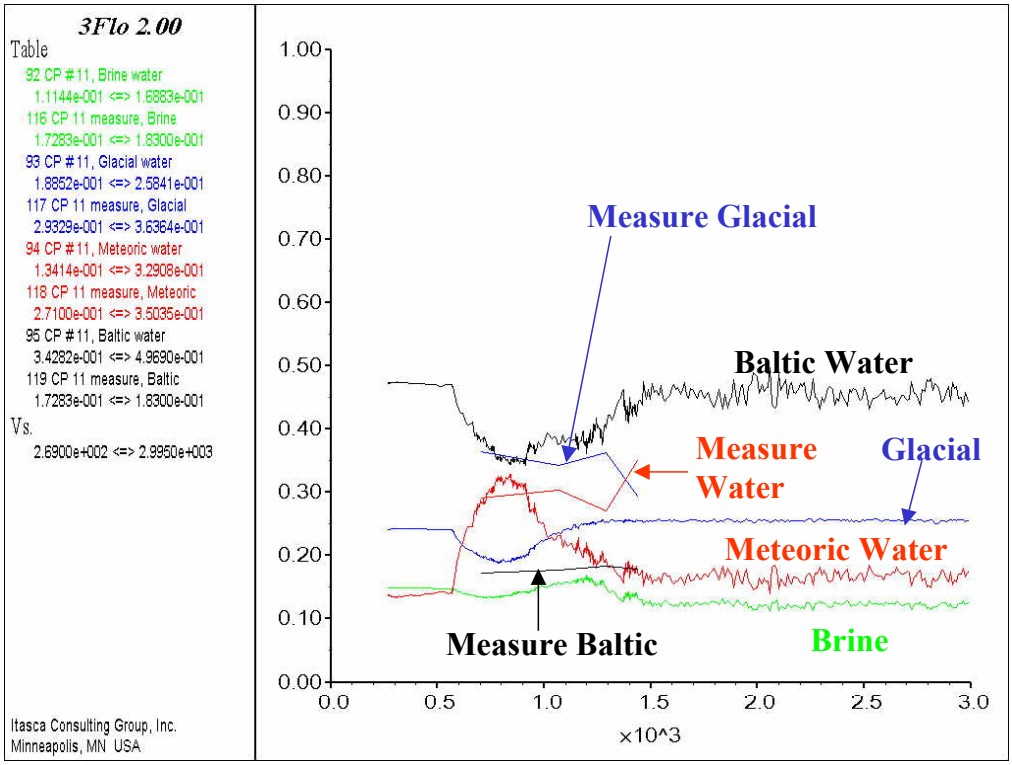

Control Point 11

3.3 Final calibration

Final runs are performed, without touching the fitted HCD transmissivities. Recharge at land nodes is controlled. It is now set to 25 mm/year at the start, with imposed flow at all land nodes as described in paragraph 2.3.2. At each node, the imposed flow is then decreased if the head goes above the topography, and increased if head goes below sea level (up to a four-fold increase from initial value). The resulting recharge varies between 15 and 70 mm/year during the simulation time. Figure **3-10** shows the head response. We can see the influence of the better representation of the recharge on the distribution of the heads in time: while the draw downs in the first 1000 days are not changed significantly, larger draw downs at the end of the run tend to be reduced by a few meters (compare with Figure 3-4). Note however that in HCDs NW-1 and EW-1N (see graph for borehole Kas04, section 0-185 for example), we overestimate the heads at the start of the simulation, and it takes a few hundred days for the procedure to compensate and bring heads down to around zero.

Figure 3-11 and Figure 3-12 illustrate the head field we obtain at the end of the simulation. Comparing with Figure 3-5 and Figure 3-6 from the previous "absolute skin fit", one sees that draw downs below land are reduced, while the heads below sea stay similar to what they were in the previous runs. Overall, the head fits are not changed drastically.

Figure 3-13 to Figure 3-15 show the transport results for chlorine and the four end-members. Lower chlorine levels are obtained below land, as expected. This can be seen for example by comparing the top right of the NE1 concentration plots in Figure 3-13 and Figure 3-7. Clearly, the chlorine levels are reduced in Control Points 4 and 5 (Figure 3-14), whereas other Control Points see less change. End-member ratios (Figure 3-15) show the same behavior, with a much increased influence of meteoric waters, in Control Points 4 and 5 and to a lesser degree in Control Points 2 and 3.

Overall, the response of the model is quite fast: very little happens after the end of the tunnel construction (time 1500 days). We are therefore seeing, for times above 2000 days, the influence of the external (imposed heads and concentrations) and internal (varying imposed fluxes) boundaries of the model. This is an obvious drawback of the modeling: while internal boundary conditions are reasonably well known, since we directly apply the flow values measured at the weirs, concentrations on the outer boundaries of the model (as well as initial concentrations, in fact), are not well known. This means that for a part, the final results depend on somewhat arbitrary parameters.

Figure 3-16 shows the largest transport paths from the Control Points we have considered. Each path is computed upstream from a control Point, by branching systematically to the pipe bringing the largest flow rate, until a boundary is reached. As could be expected, the shallowest Control Points, located under sea, receive mainly water coming from the Baltic sea, while the deeper-sited ones are more influenced by the lateral boundaries. This matches well the end-members evolution (Figure 3-15), with Baltic water prevalence decreasing from Control Point 2 to Control Point 5.

Figure 3-10: *final fit and calibrated head histories*

Black is measured, red is computed. Time in days after 01/10/1990.

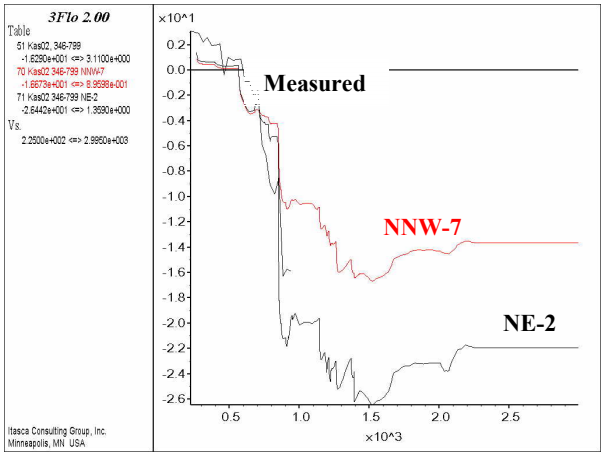

Kas02 section 346-799

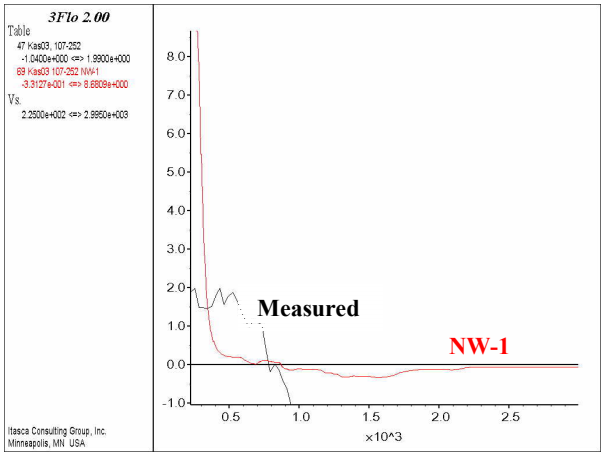

Kas03 section 107-252

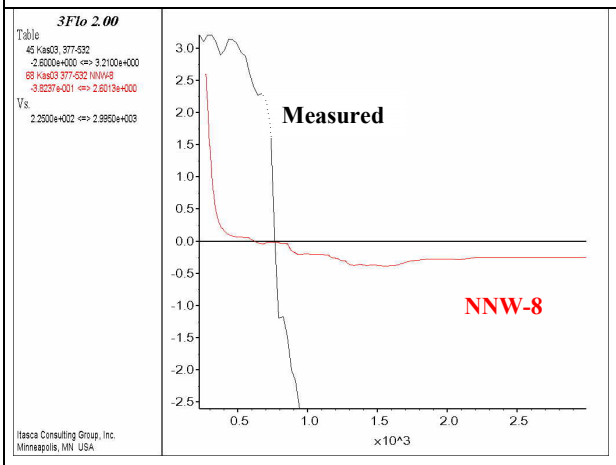

Kas03 section 377-532

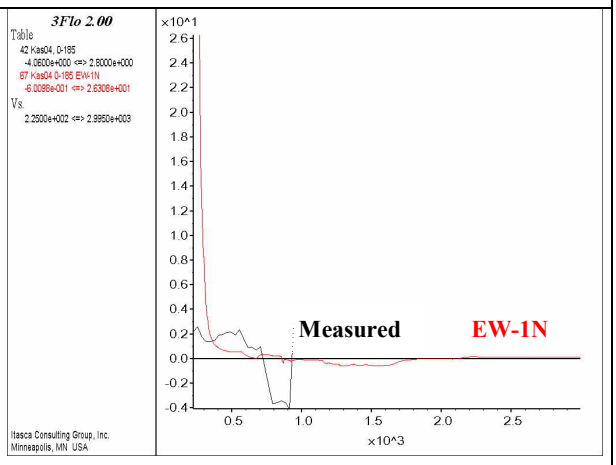

Kas04 section 0-185

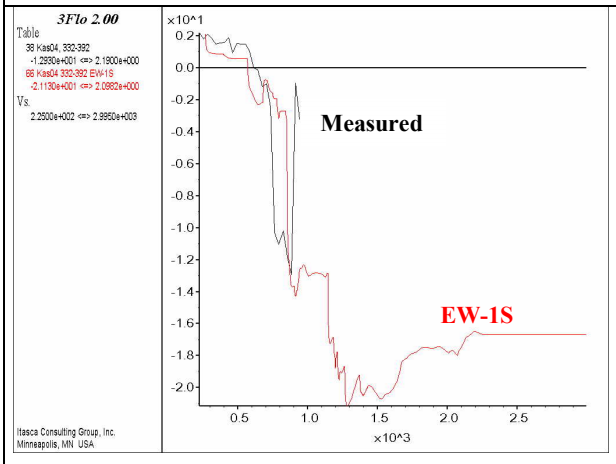

Kas04 section 332-392

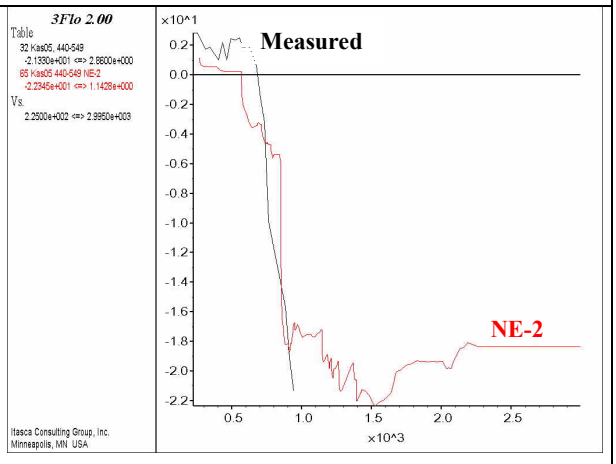

Kas05 section 440-549

Figure 3-10 (continued): *final fit and calibrated head histories*

Black is measured, red is computed. Time in days after 01/10/1990.

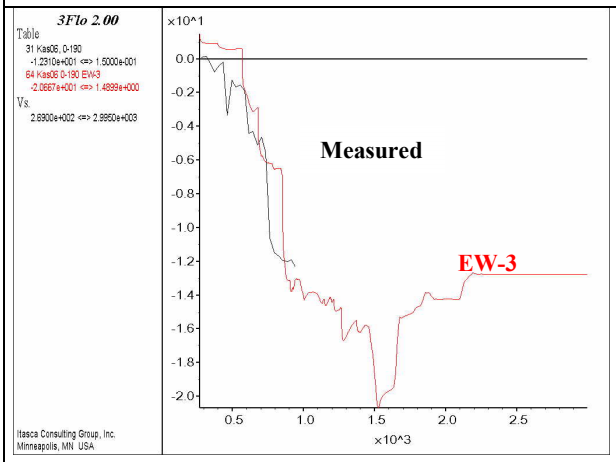

Kas06 section 0-190

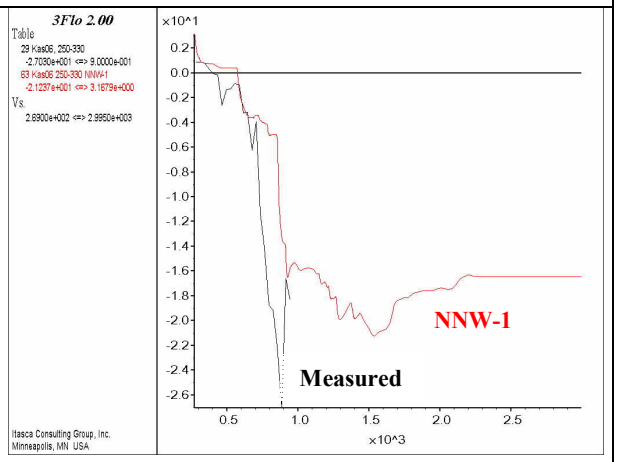

Kas06 section 250-330

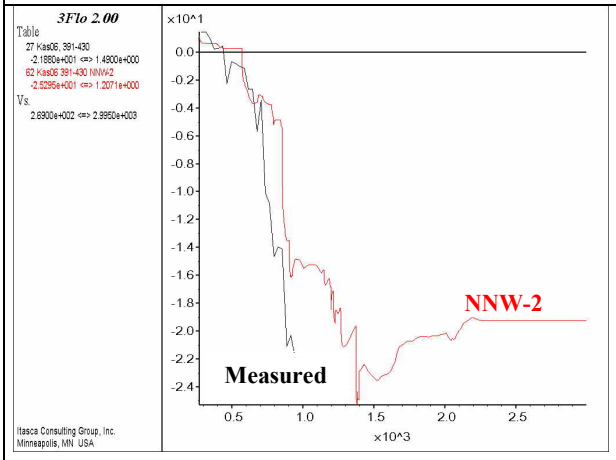

Kas06 section 391-430

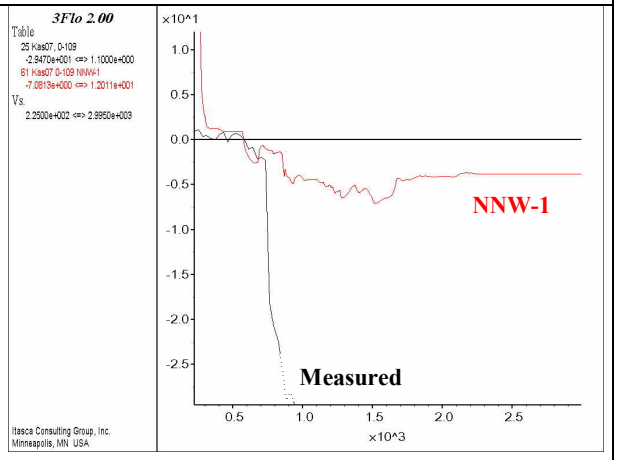

Kas07 section 0-109

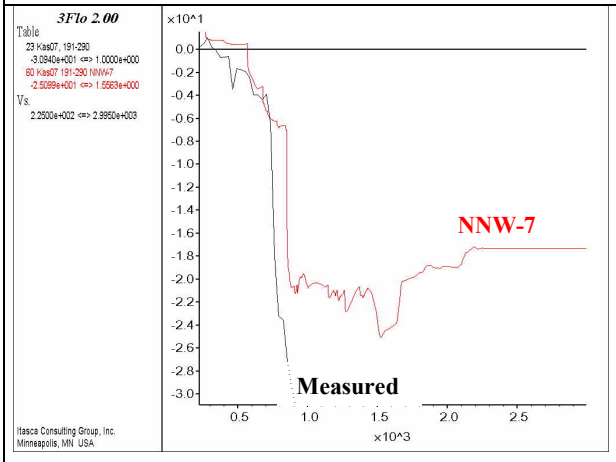

Kas07 section 191-290

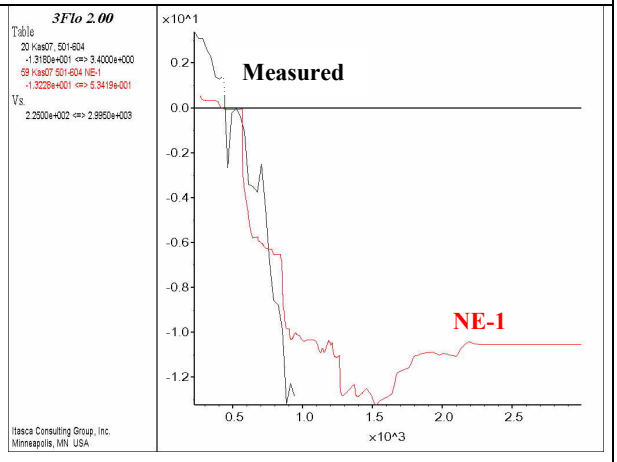

Kas07 section 501-604

Figure 3-10 (continued): *final fit and calibrated head histories*

Black is measured, red is computed. Time in days after 01/10/1990.

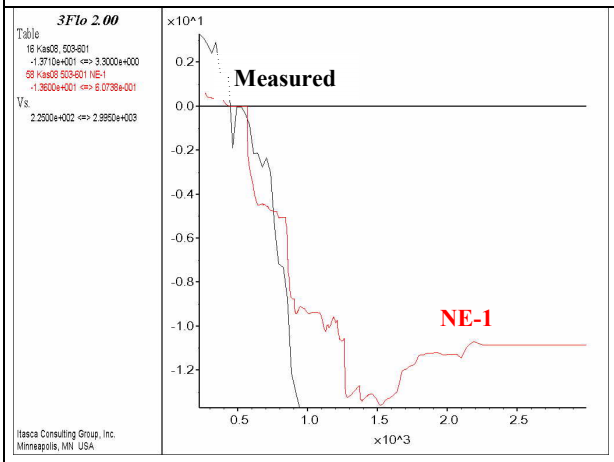

Kas08 section 503-601

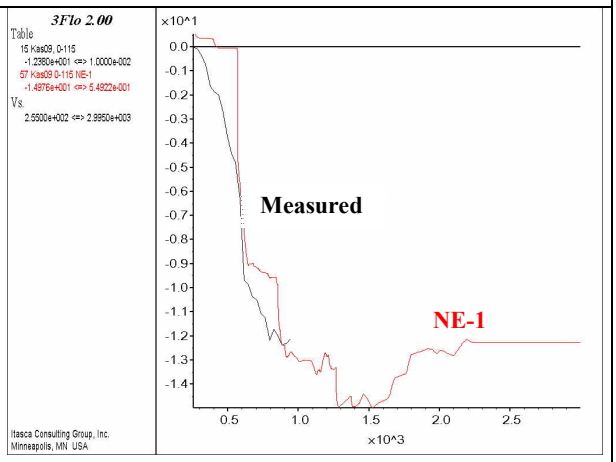

Kas09 section 0-115

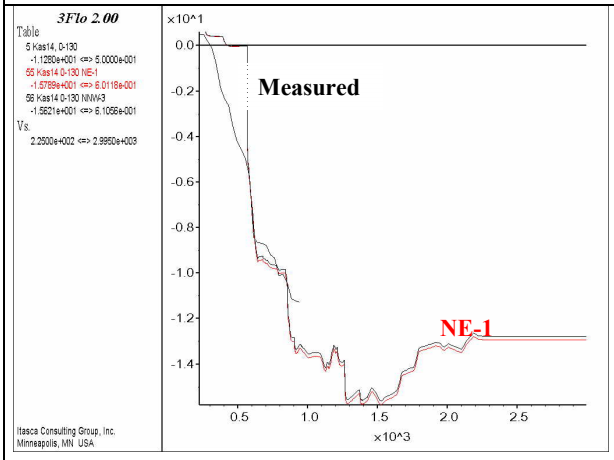

Kas14 section 0-130

Figure 3-11: *hydraulic head at end of simulation - NE and EW HCDs*

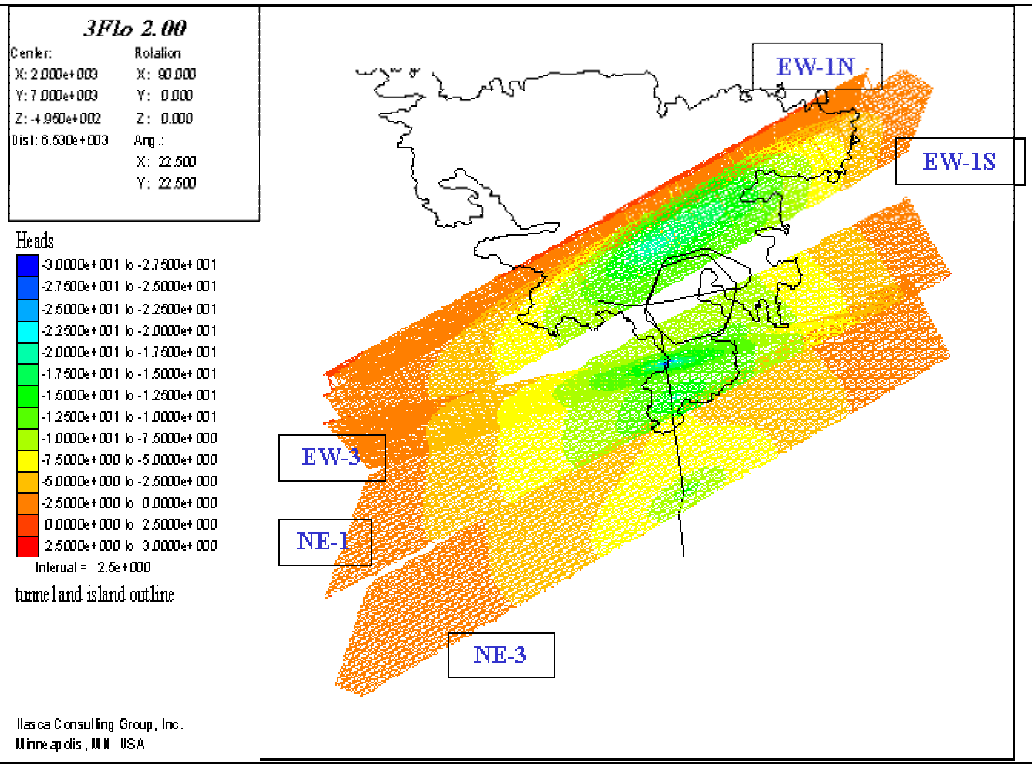

Figure 3-12: *hydraulic head at end of simulation - NE-2 and NNW HCDs*

Figure width : 750 m

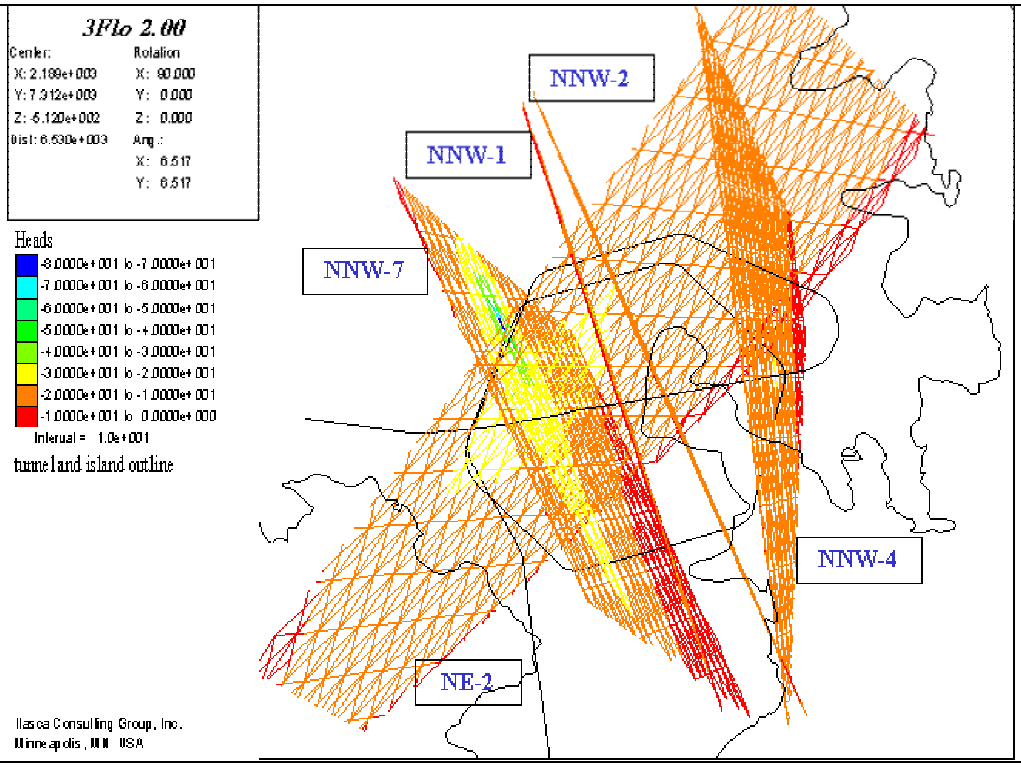

Figure 3-13: *final fit - chlorine concentrations in Zone NE-1*

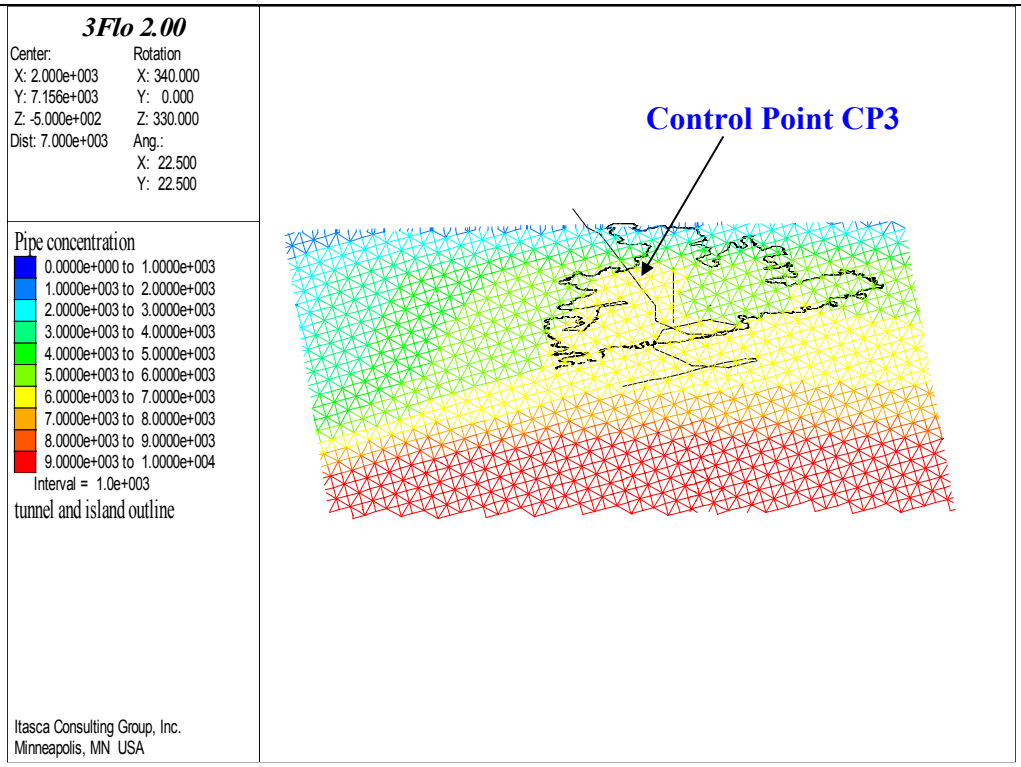

start of simulation

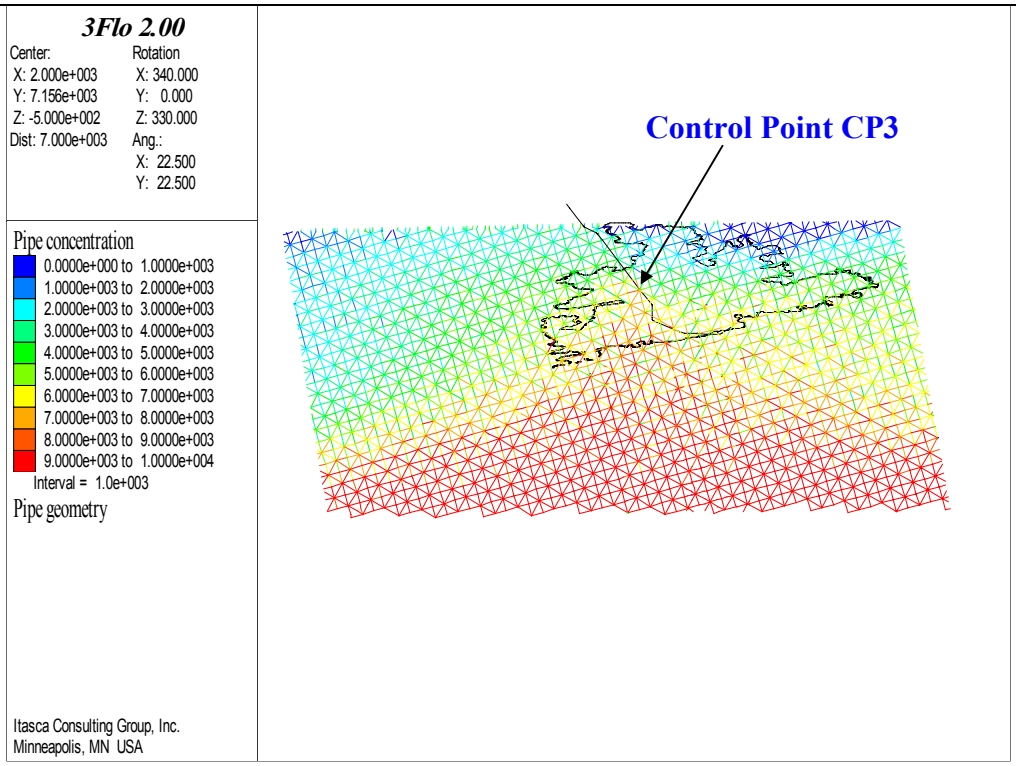

Tunnel at 2021 m

Figure 3-13 (continued): *final fit chlorine concentrations in Zone NE-1*

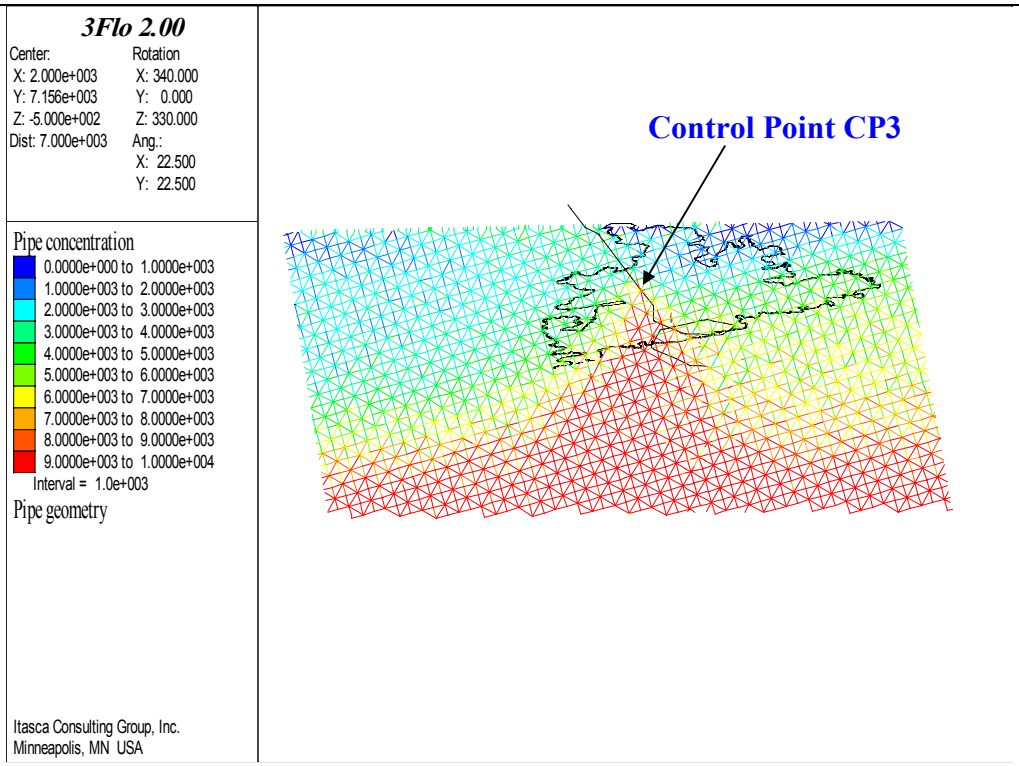

Tunnel at 2790 m

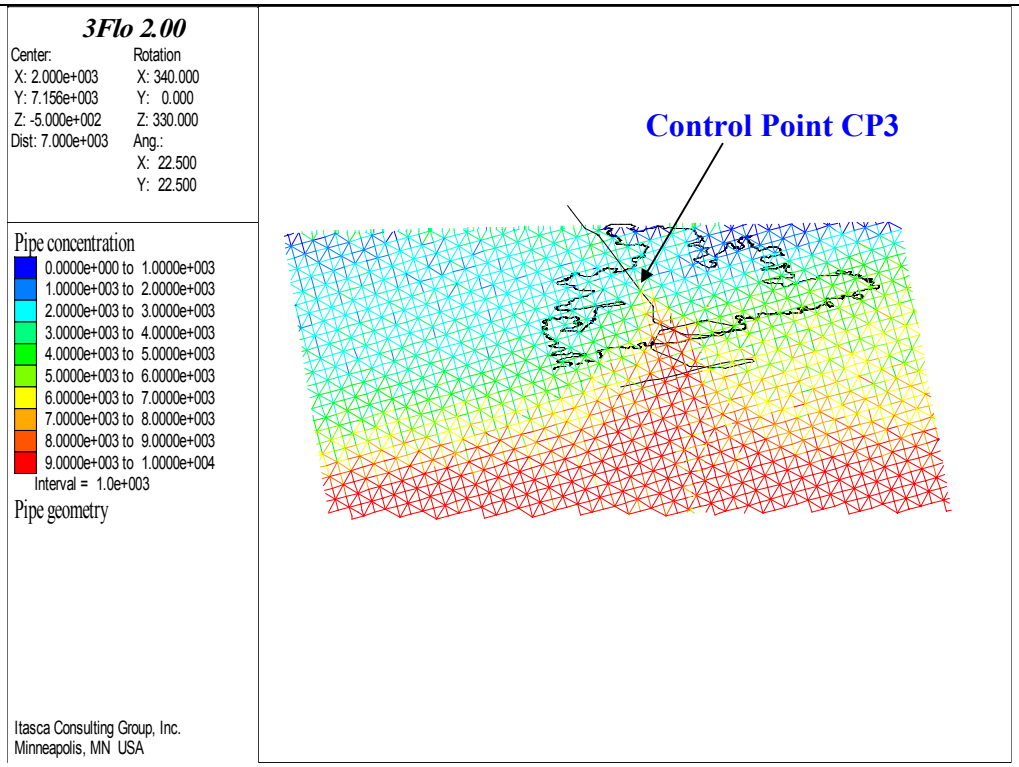

End of simulation

Figure 3-14: *final fit - chlorine concentrations*

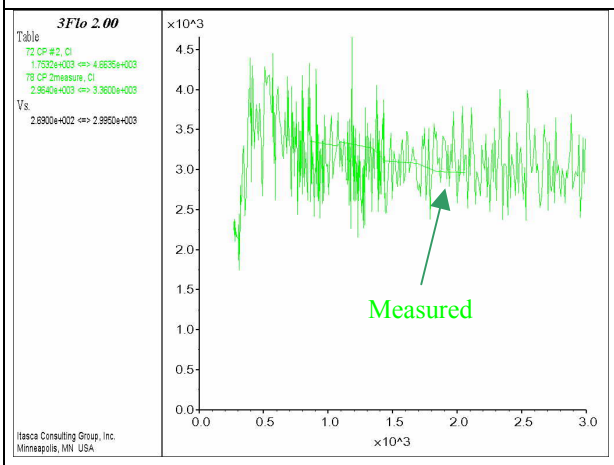

Control Point 2

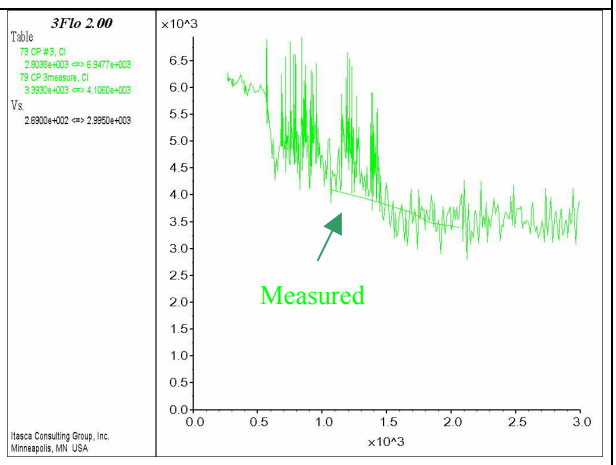

Control Point 3

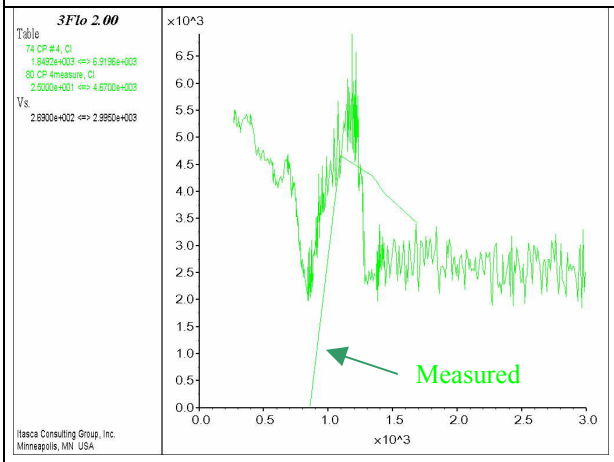

Control Point 4

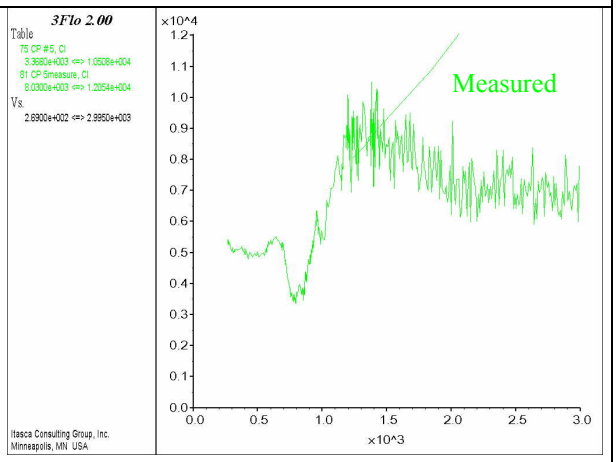

Control Point 5

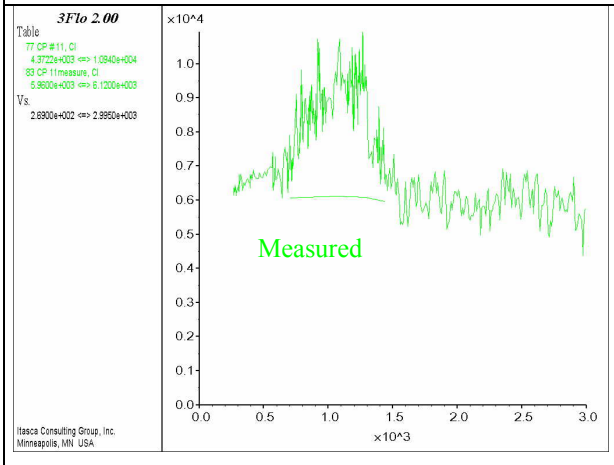

Control Point 11

Figure 3-15: *final fit – end-member evolution*
Time in days after 01/10/1990

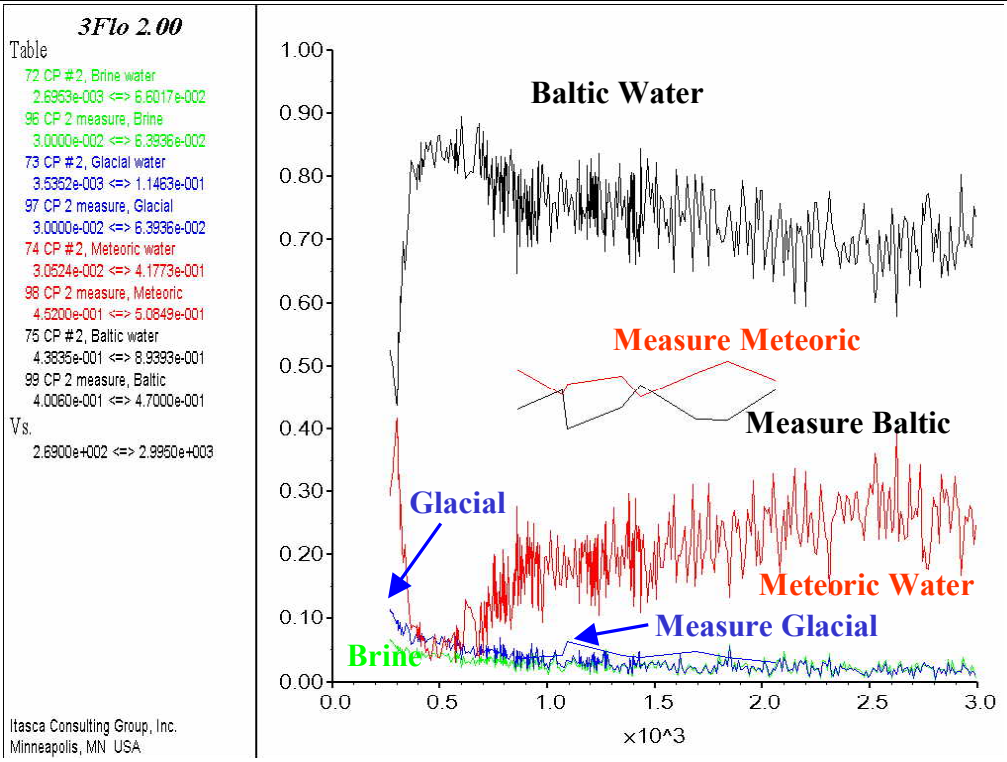

Control Point 2

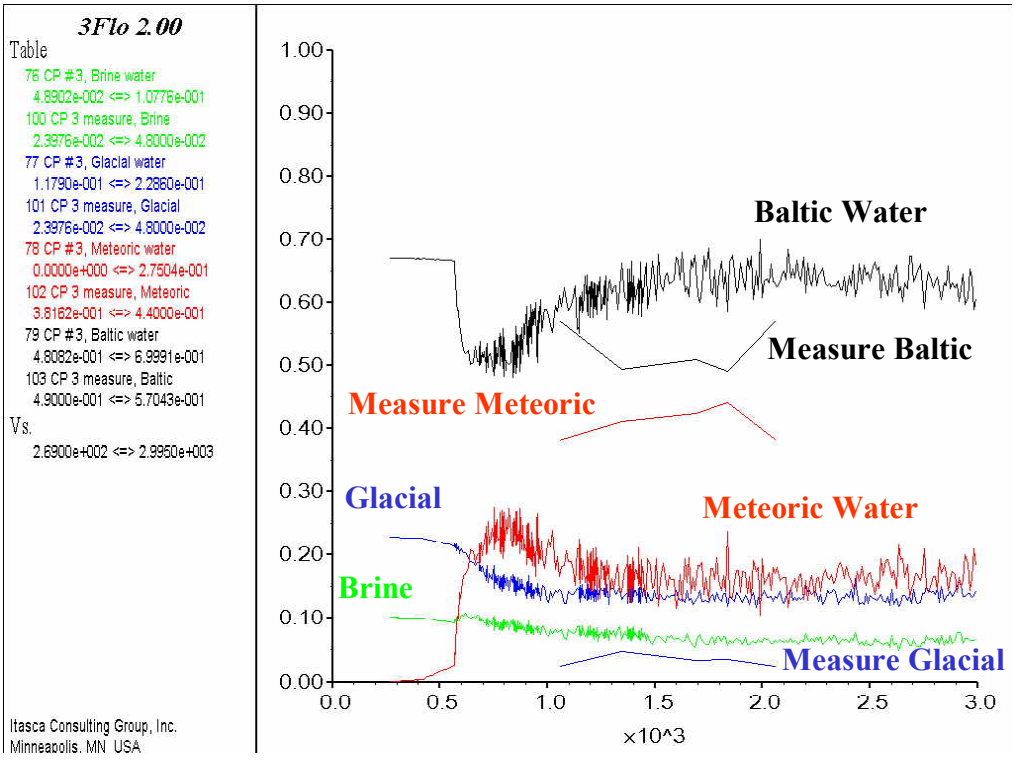

Control Point 3

Figure 3-15 (continued): *final fit – end-member evolution.*
Time in days after 01/10/1990

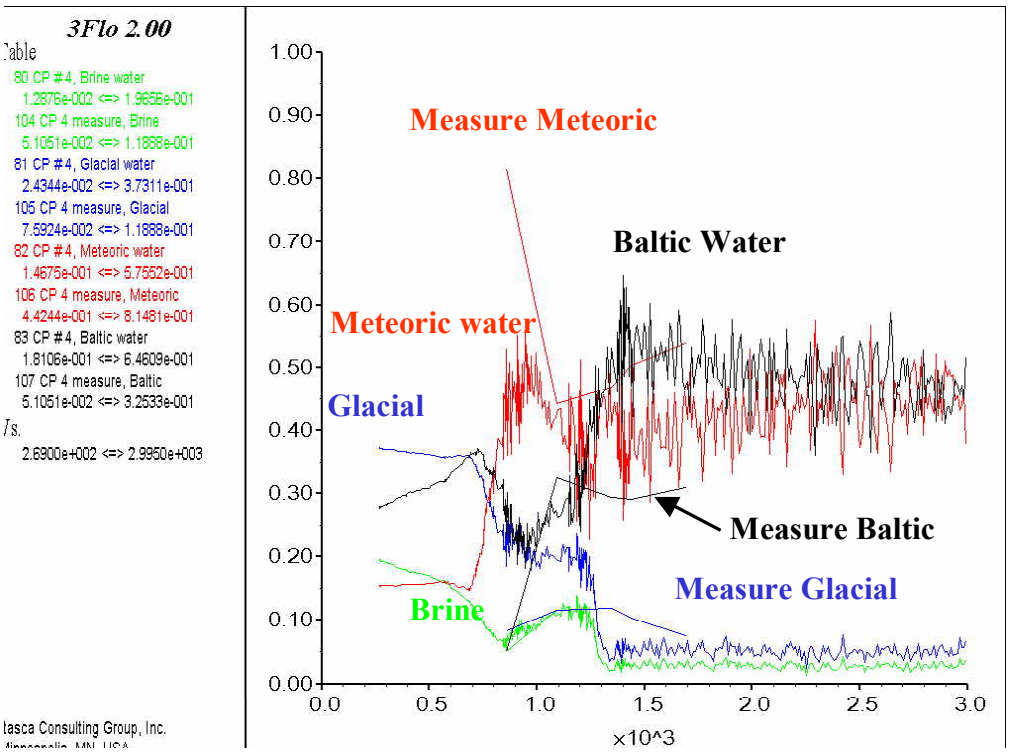

Control Point 4

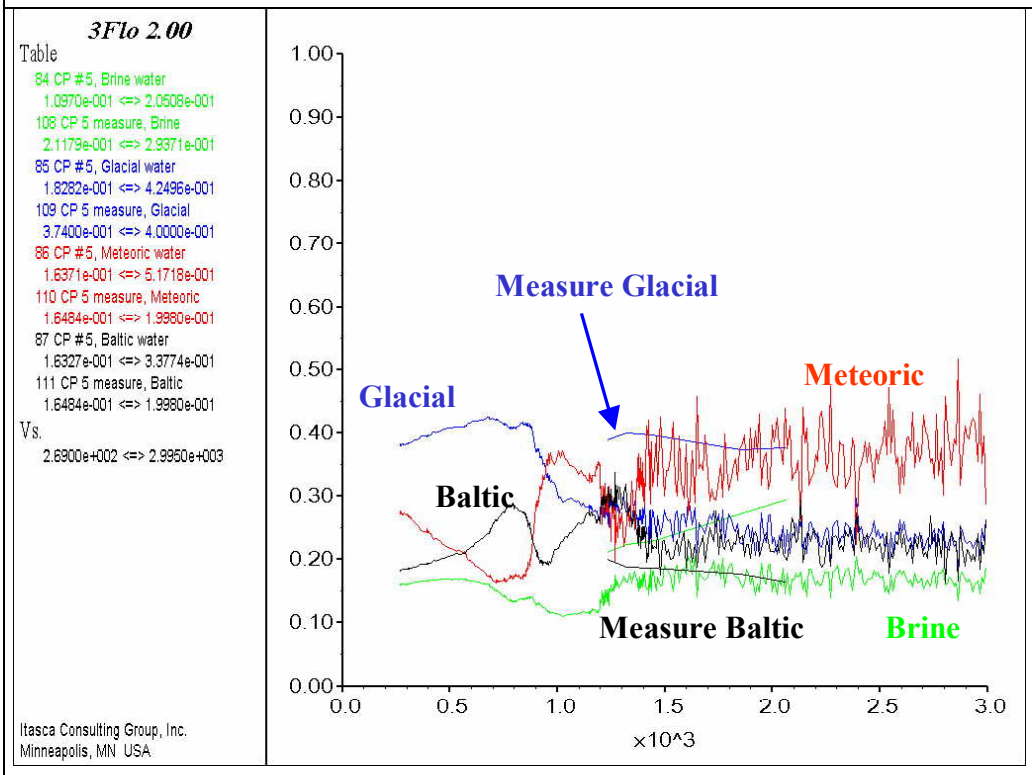

Control Point 5

Figure 3-15 (continued): *final fit – end-member evolution.*
Time in days after 01/10/1990

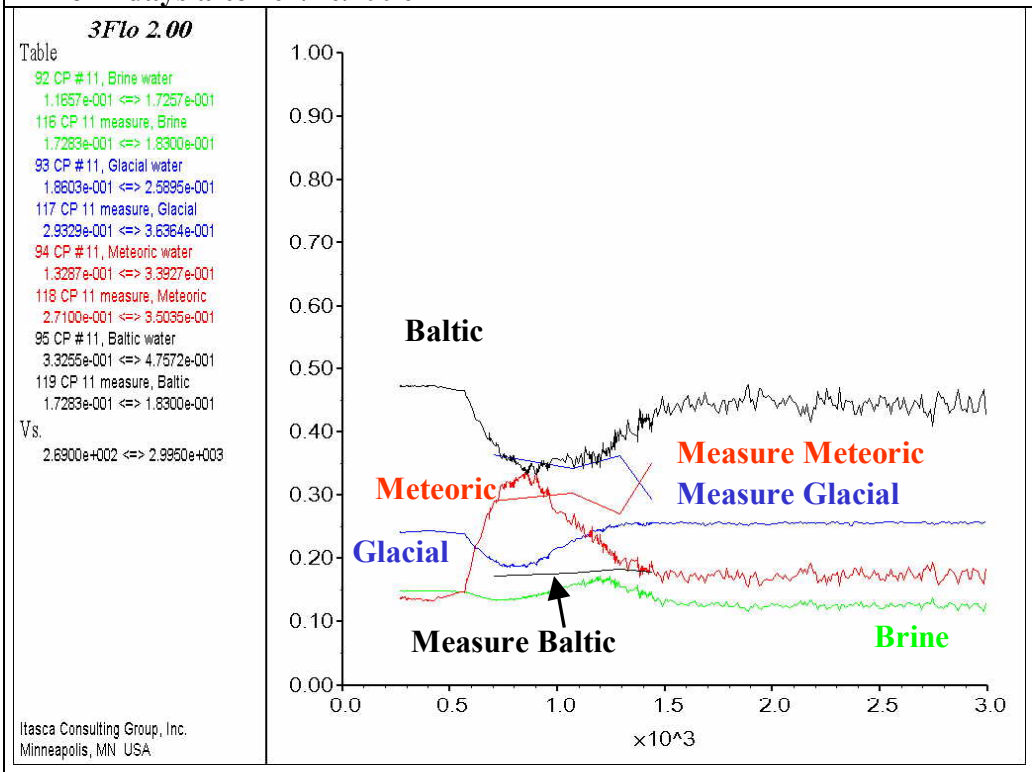

Control Point 11

Figure 3-16: *transport paths*

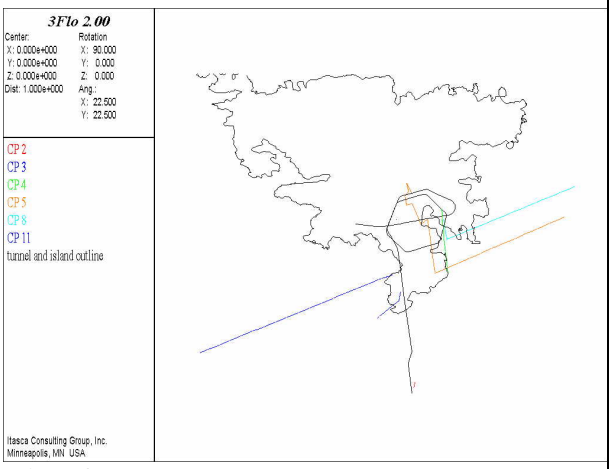

View from top

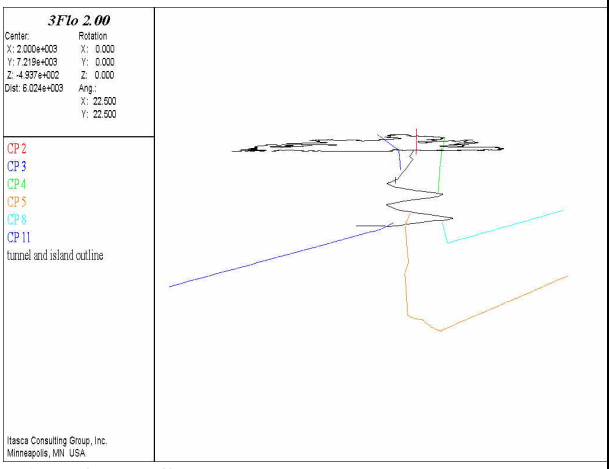

View from South

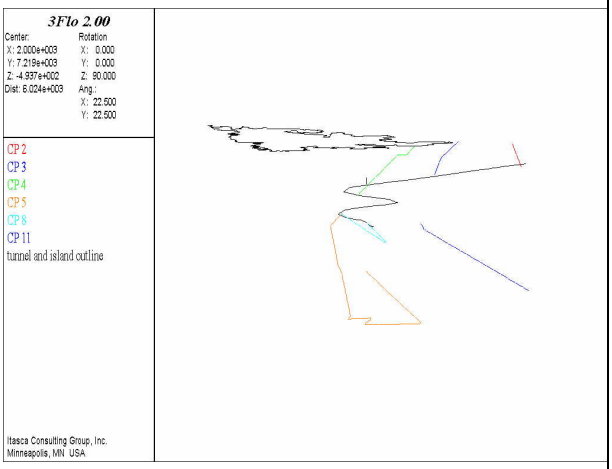

View from East

4 HYDRO-GEOCHEMICAL COUPLED SIMULATIONS

Coupled simulations are performed on a limited region of the model. This work is a preliminary attempt at investigating the fully coupled behavior of a fractured system, using the newly developed chemical speciation module in 3FLO.

4.1 Method and approach

3FLO, the ITASCA flow and transport code, is now fully coupled with a geochemical module resulting in adding variable source or sink terms within the mass transport computations.

The modeling approach assumes thermodynamic equilibrium, that is reactions kinetics are considered being either very fast or very slow with respect to the groundwater residence time.

4.1.1 Description of the speciation module

The code is based on the principal components method, which reduces the system to be solved to *n* independent mole balance equations (Gibb's law) and *n* components. Concentrations of the principal components (e.g. Fe^{3+}, Ca^{2+}, CO_3^{2-}…) are computed after substituting each of the secondary species mass laws into the mole balance equations.

This approach is very widely used in the existing geochemical codes because it decreases dramatically the number of equations to be solved and the number of species to be transported. It also allows easy addition of any supplementary species into the system.

A general geochemical database has been built based on a set of default principal components. All the information needed for the other species (e.g. $FeOH^{2+}$, $CaOH^{+}$, HCO_3^{-}…) are the stoichiometric coefficients and the equilibrium constants corresponding to their formation from the principal components.

For instance, $Fe(SO_4)^{+}$ can be formed by the following reaction:

$$Fe^{3+} + SO_4^{2-} \rightarrow Fe(SO_4)^{+}$$

$Fe(SO_4)^{+}$ concentration is computed from the mass law:

$$[Fe(SO_4)^{+}] = K\,[Fe^{3+}]^{1}\,[SO_4^{2-}]^{1}$$

Consequently, the database information about $Fe(SO_4)^{+}$ only needs to include a coefficient of 1 for both Fe^{3+} and SO_4^{2-} plus the value of the equilibrium constant K.

PH influence is simply addressed by incorporating H^{+} (or OH^{-}) into the set of principal components (and assuming an H_2O activity of 1 at this stage of code development). Treatment of the redox reactions requires both the specification of a redox couple within the components and the Nernst law parameters of the other redox couples of concern.

Solid compounds are introduced by switching with a relevant component. For example, if Ca^{2+} and CO_3^{2-} are the default components, it is possible to simulate calcite ($CaCO_3$) precipitation by substituting either Ca^{2+} or CO_3^{2-} by $CaCO_3$ and assigning a unit activity for $CaCO_3$ (solid phase). Carbonate (CO_3^{2-}) concentration is then computed by the relation:

$$[CO_3^{2-}] = K'\,[Ca^{2+}]^{-1}\,[CaCO_3]^{1} = K'\,[Ca^{2+}]^{-1}$$

The code checks first if an existing solid (therefore a principal component) dissolves. If yes, the solid is removed from the principal component set and exchanged with relevant aqueous specie. If not, 3FLO checks each solid present in the database for precipitation (that is with a saturation index greater than *1*). Any solid fulfilling this condition becomes a principal component by exchange with relevant aqueous specie. The principal components set is adjusted iteratively (automatically) until it includes all of the different compounds allowed to precipitate.

The same approach is used for simulating equilibrium with gas phases. The selected gas is introduced as a principal component and his activity (equivalent to his partial pressure) is assigned for the calculations.

Ionic strength influence is simulated by adjusting the equilibrium constants according to the *Davies law*.

4.1.2 Coupling with transport

The 3FLO transport module uses the Discrete Parcel Random Walk approach.

In this method, the flow equation is solved first, by the finite element method in 3FLO, in order to calculate the velocity field. Geochemical initial concentrations and source terms are modeled by introducing a large number of particles, each particle holding a relevant mass (or number of mole) of the different principal components. In other words, each principal component soluble concentration equals the sum of the different masses (moles) attached to the whole set of particles present in a given pipe.

Each particle moves in the pipe network with the flow velocity (convective transport), its coordinates at time $t + \Delta t$ being:

$$x_i^{t+\Delta t} = x_i^t + V_j^t \Delta t$$

Where V_j^t is the pore velocity vector in the pipe. An additional displacement is imposed to each particle in order to simulate hydrodynamic dispersion. This dispersive displacement is computed by randomly sampling a Gaussian distribution with zero mean and a variance depending on the time step and the dispersion coefficient. 3FLO assumes full mixing at the pipe intersections.

When precipitation / dissolution or adsorption / desorption occur, the total mass of product removed from the bulk solution (or added to it) is transferred from the mobile particles to an immobile fraction (or the reverse) attached to each pipe.

The following process is then performed within every time step.

1. Resolution of the transport equations.
2. Calculation of the new total concentrations for each principal component and for each pipe.
3. Resolution of the geochemical problem for elements, where thermodynamic equilibrium is not met, in order to get new soluble concentrations, which allows an explicit computation of the masses to be attached to the particles.

4.1.3 Reactions of concern

Different processes, activated by the tunnel construction, have been identified at the Äspö site, such as water-rock interactions or mixing of ground waters with different origins.

In order to address the problem of quantifying the geochemical processes and coupling them with the hydrodynamic model, Laaksoharju has described several major reactions (Data Delivery 14):

1. Organic decomposition: $O_2 + CH_2O \rightarrow CO_2 + H_2O$
2. Organic redox reaction: $4Fe\ (III) + CH_2O + H_2O \rightarrow 4Fe^{2+} + 4H^+ + CO_2$
3. Inorganic redox reaction: $HS^- + 2O_2 \rightarrow SO_4^{2-} + H^+$
4. Calcite dissolution/precipitation: $CO_2 + CaCO_3 + H_2O \rightarrow Ca^{2+} + 2HCO_3^-$
5. Ion exchange: $Na_2X(s) + Ca^{2+} \rightarrow CaX(s) + 2Na^+$ (for X being a solid substrate)
6. Sulphate reduction: $SO_4^{2-} + 2(CH_2O) + OH^- \rightarrow HS^- + 2HCO_3^- + H_2O$

In order to be consistent with our objectives, and due to both the complexity of the site data and the time framework, we focused on reactions of type 4 instead of performing a complete coupled model upon the selected zone. We extended this reaction type, that is precipitation / dissolution of carbonates, to magnesium carbonates and to gypsum. We included all the different soluble chemical complexes relevant for this problem using the CHEMVAL database.

4.2 Numerical model

4.2.1 Domain modeled, and flow conditions

Figure 4-1: *initial pH*

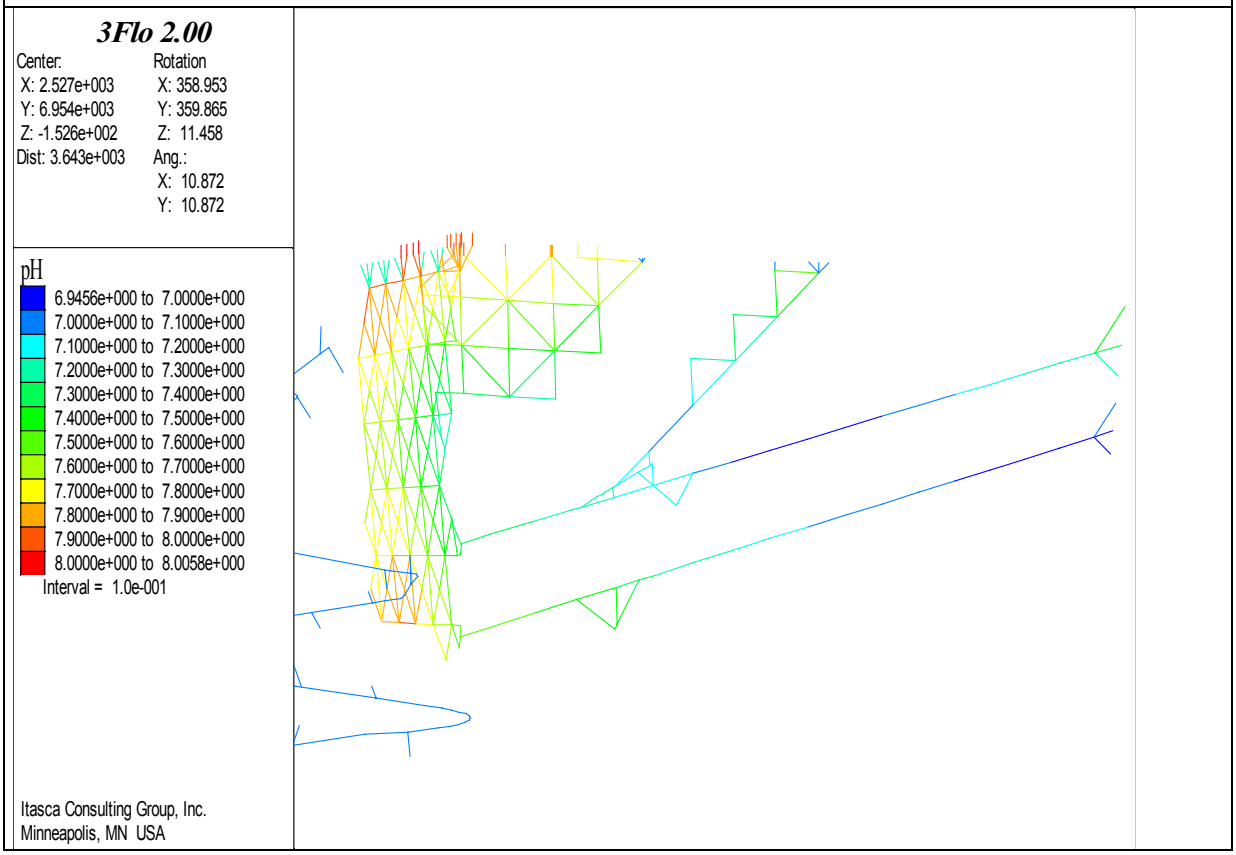

In order to obtain manageable model run times, we restrict this part of the work to a sub-domain in the model displayed on

Figure ***2-3***. Using the steady-stated obtained at the end of the flow and transport simulations, we chose to focus on the main conductors upstream of Control Point number 4. Starting from this control point, we first select all pipes which are situated upstream and from which more than half the flux effectively goes to the control point. Figure 4-8 shows the network we obtain.

We make another simplifying assumption: the flow field is considered in a steady-state corresponding to the end of the previous simulations (tunnel construction finished). Figure 4-9 shows the flow rates provided by this steady-state flow model. The main conductors are displayed in red.

4.2.2 Boundary conditions

Boundary conditions for flow and transport are the same as the ones applied at the end of the simulations (tunnel construction finished). Concentrations at boundary pipes are fixed.

The solutions contained in pipes in contact with the atmosphere (pipes displayed in green on Figure 4-8) are opened to the CO_2 (g) at the partial pressure of 0.0004.

4.2.3 Initial conditions

Based on the previous works performed and on the results of the M3 modeling, we selected: Na^+, Ca^{2+}, CO_3^{2-}, Cl^-, SO_4^{2-}, Mg^{2+}, and K^+ as principal components for the coupled model. Na^+ to SO_4^{2-} are defined in Data Delivery 7 (chapter 3.1), while Mg^{2+}, and K^+ are calculated from the composition and the percentages of the different waters. All these values, which are given in a square grid, are then interpolated on each pipe in the model. Note that for the last two components, we are therefore compounding errors by 1) performing the mixing calculation, and 2) performing the spatial interpolation.

The component H^+ is added in order to account for the solvent (water) reactivity. The initial total concentrations of each chemical principal component are displayed on Figure 4-10 to Figure 4-16.

The total concentrations obtained show an excess of cations, which brings a problem for keeping the solution electro-neutrality. At this point, two techniques can be used for balancing this excess of cations:

1. Adjust the H^+ total concentration (therefore brought to a negative value);
2. Add a "dummy" non-reactive component with a negative electrical charge at a total concentration equaling the excess of cations.

We chose the second solution in order to avoid the very high pH that would result from the first approach. Figure 4-1 shows the resulting initial pH computed by *3FLO*.

Introducing chemistry in our simulations leads to the precipitation of solid $MgCO_3$ (Figure 4-2), according to the following reaction:

$$Mg^{2+} + CO_3^{2-} \rightarrow MgCO_3\,(s) \qquad (1)$$

In reality, such a phenomenon is unlikely. Note that the initial concentrations of Mg computed from mixing portions in the grid data (Data Delivery 7, appendix 12) seem to be quite high with respect to Ca concentrations (see for example direct values of Mg and Ca as measure in a number of boreholes in Data Delivery 7, appendix 9). For example, a higher Ca/Mg ratio would cause $CaCO_3$ precipitation instead of $MgCO_3$.

This precipitation affects soluble concentrations of both principal components Mg and CO_3 (Figure 4-3 and Figure 4-4) and consequently the pH:

$$CO_3^{2-} + H^+ \rightarrow HCO_3^- \qquad (2)$$

These graphs should be compared with their equivalents without geochemistry (Figure 4-15 and Figure 4-16).

Figure 4-2: *initial concentrations of solid $MgCO_3$ (M)*

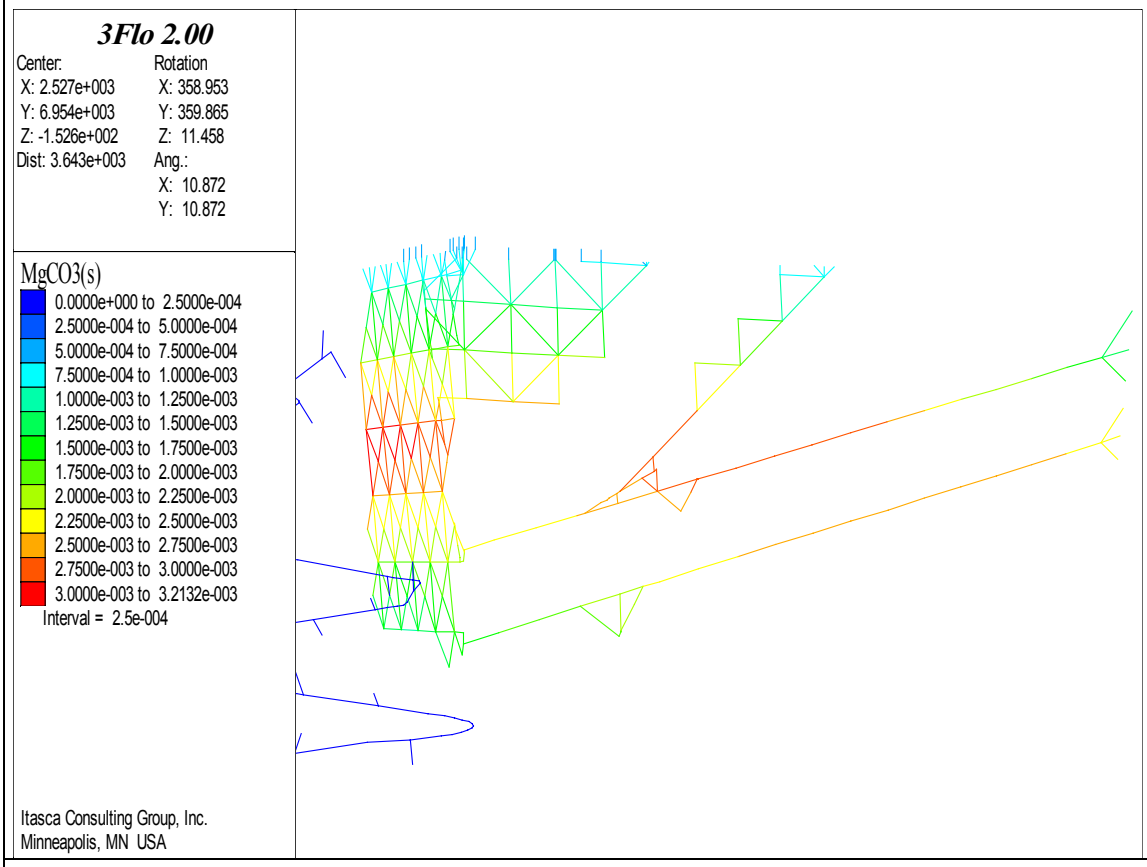

Figure 4-3: *initial magnesium soluble concentrations (M)*

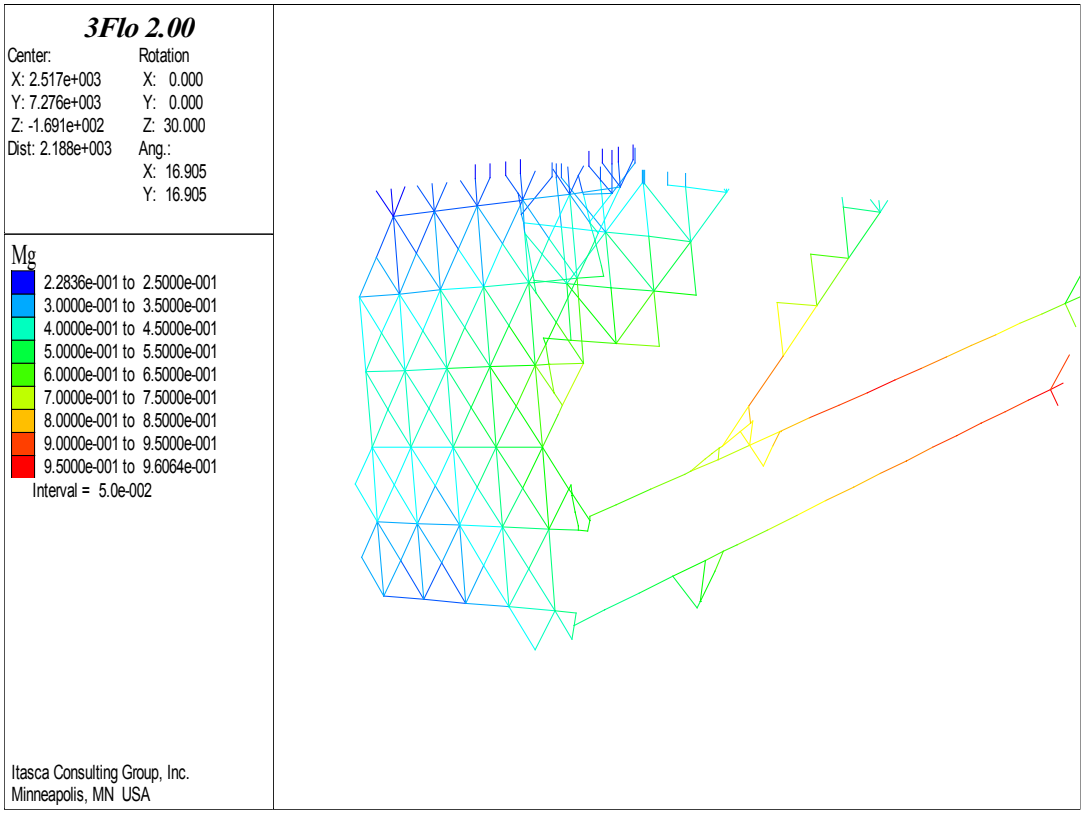

Figure 4-4: *initial total carbonate soluble concentrations (M)*

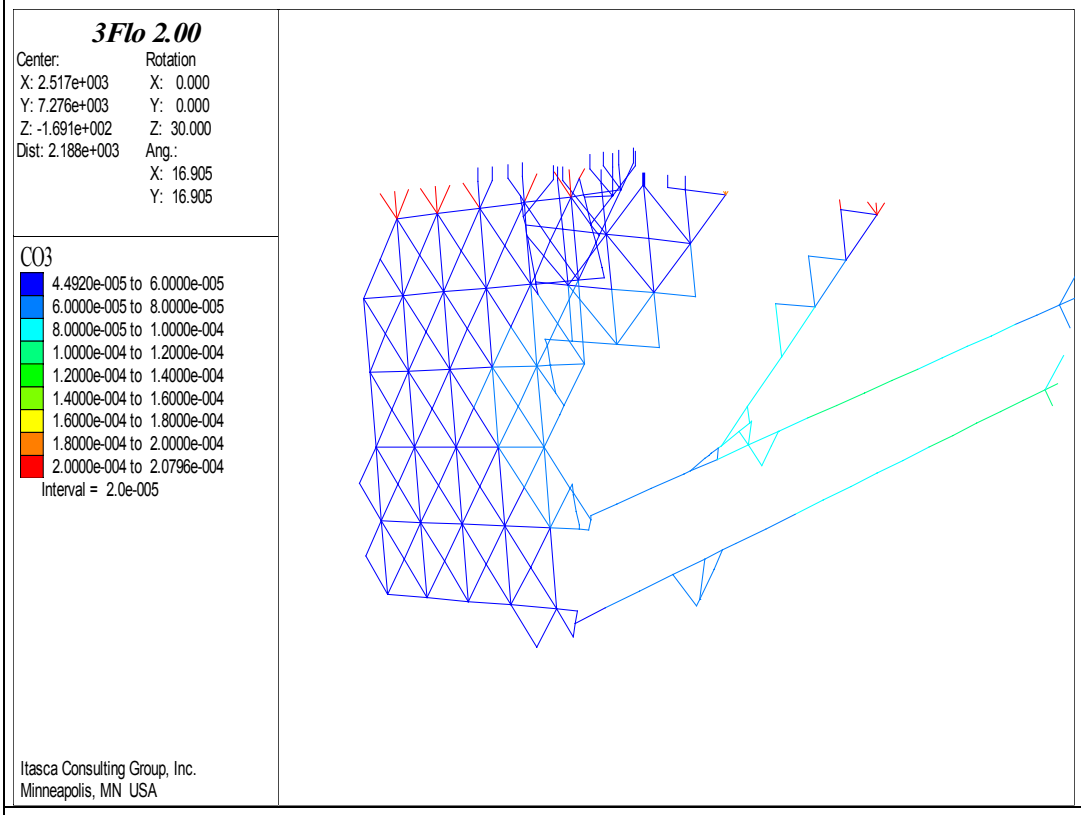

Figure 4-5: *pH after 100 days*

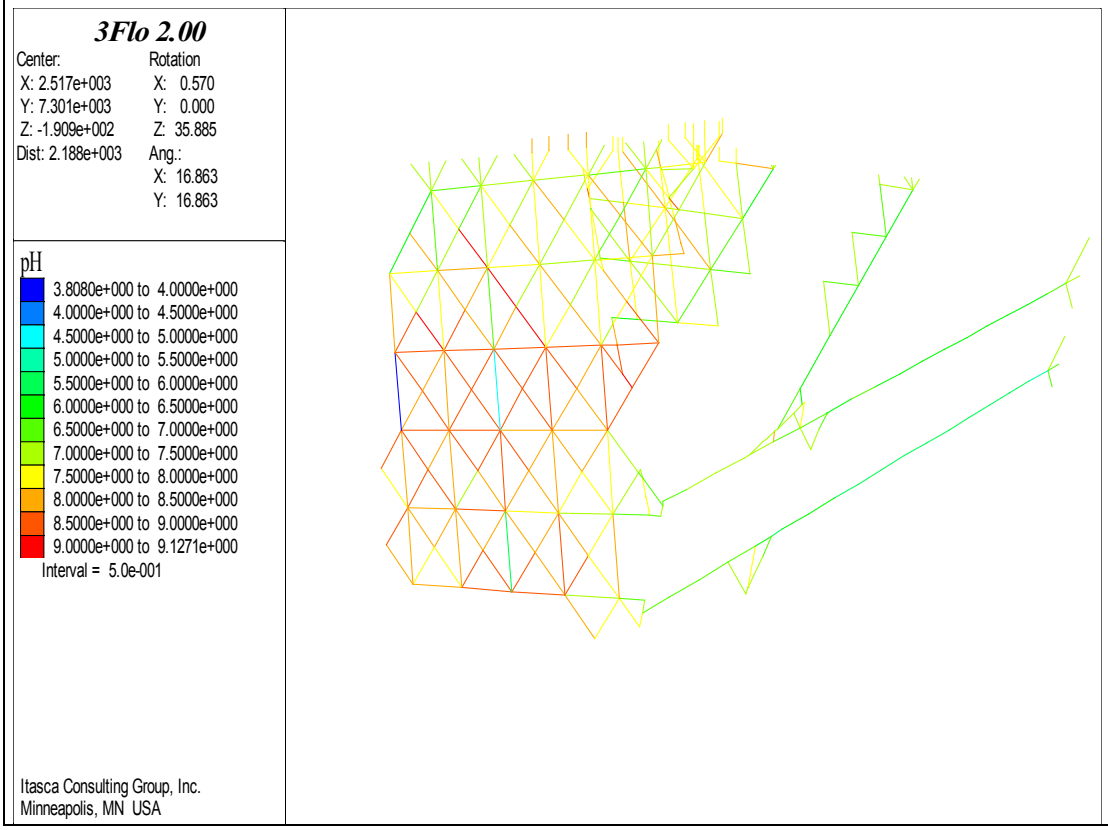

Correlations between CO_3 total concentrations and intensity of $MgCO_3$ precipitation are clear. The large excess of Mg upon the total carbonate concentration causes the latter to be the limiting factor of the $MgCO_3$ precipitation. Soluble inorganic carbon (i.e. sum of concentrations of CO_3 over its different chemical forms) is therefore calculated as constant throughout the modeled domain (Figure 4-4).

Figure 4-6: *sodium distribution (M) after 100 days*

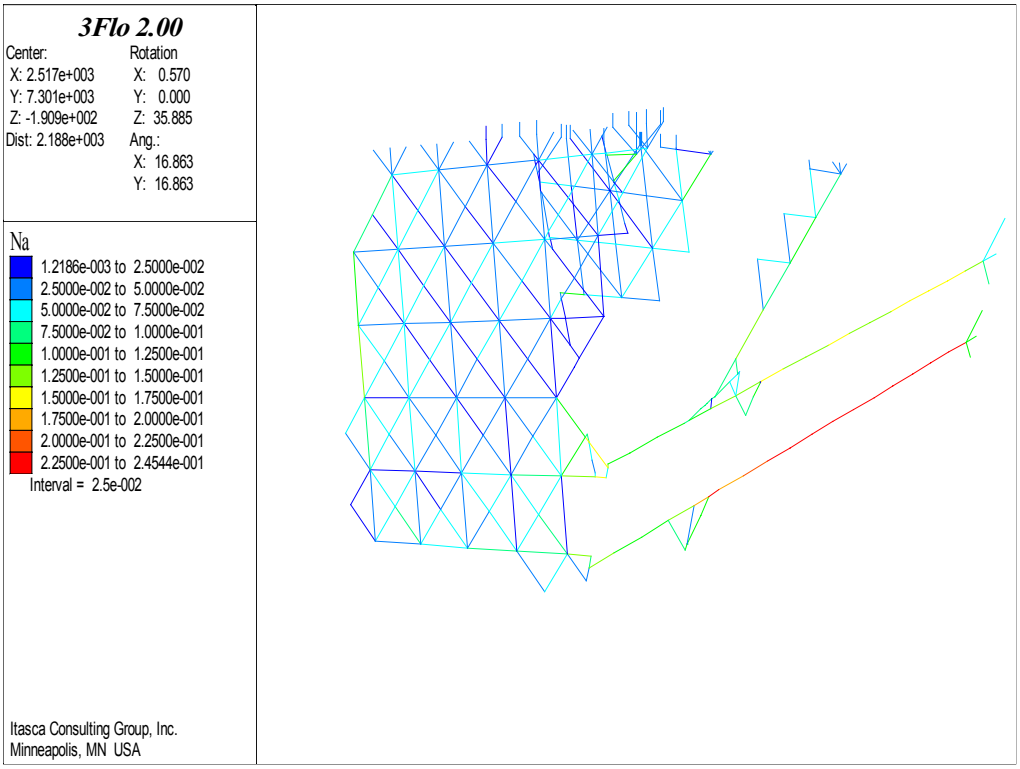

The upper zone (below the sea and the island) shows slightly different results: lower carbon solubility and higher pH. In this area, the groundwater is assumed to be more diluted which is going to increase the apparent constant of reaction (1) and therefore decrease inorganic carbon in solution. This dilution is also going to influence reaction (2) by increasing the apparent constant and consequently the pH.

One can notice the exception of the pipes opened to the atmospheric CO_2 (plotted in green on Figure 4-8) where pH is found to be lower than in the surroundings pipes because of dissolution of gaseous CO_2 (acting as a weak acid). This dissolution is confirmed by the pipes high total inorganic carbon soluble concentration.

We can list the following limits to the extrapolation of the geochemical results:

- There is no guarantee that the initial conditions we derive are at chemical equilibrium;
- The input concentrations are related to the pore water compositions and do not include the matrix. Therefore, there is no matrix dissolution/precipitation or surface effects;
- The ionic species activity coefficients are computed with the Davies law. With respect to the high ionic strength encountered (sea water or brines), the Davies law is out of its range of validity and can locally alter the results;
- Redox phenomena and biodegradation, which could decrease the organic total soluble concentrations (and consequently decrease or cancel any carbonate precipitation), are not taken into account.

Figure 4-7: *initial concentrations (above) and after 100 days (below) of solid $MgCO_3$ (M)*

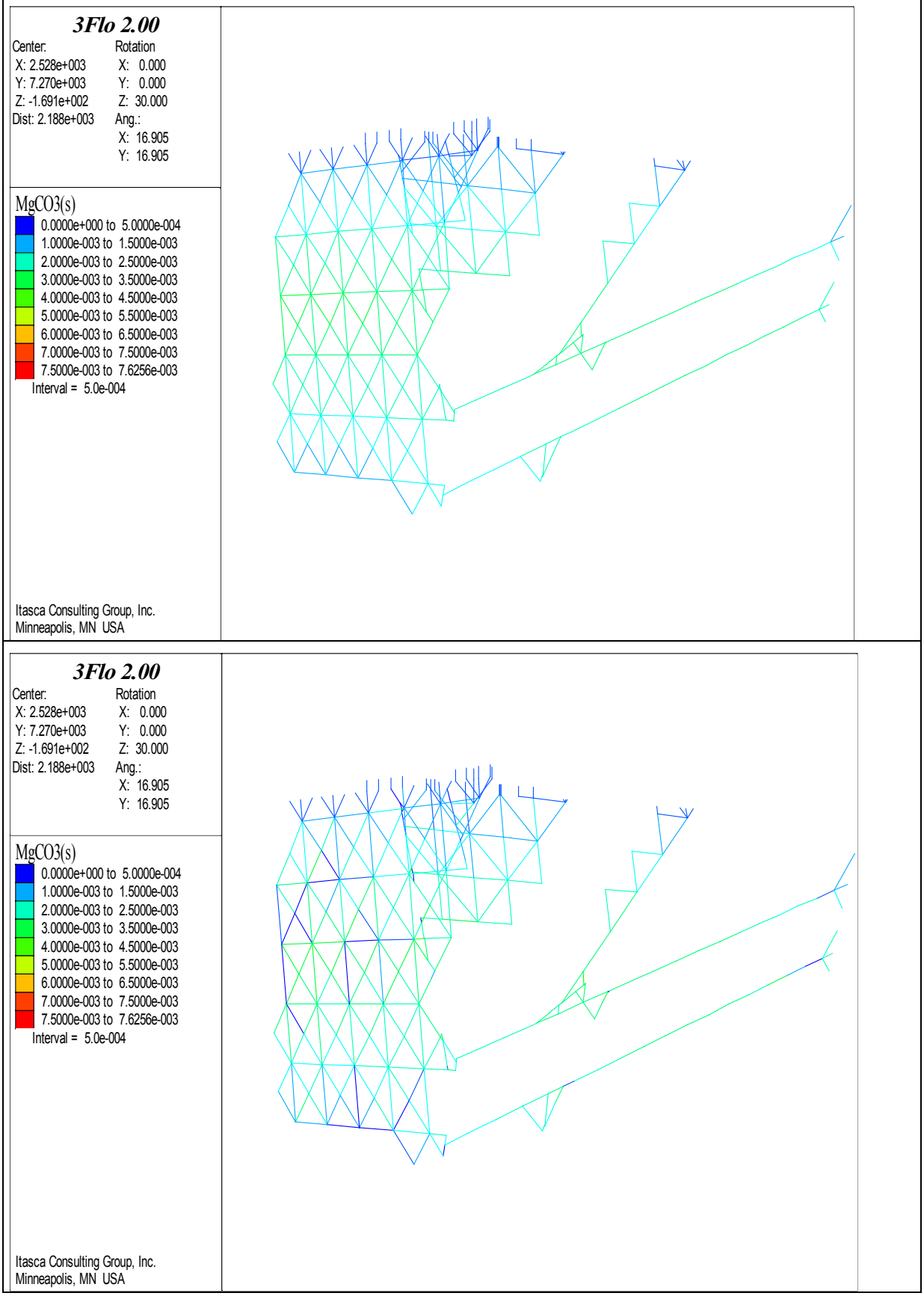

4.3 Simulations performed

The impact of the tunnel construction is simulated by modelling transport within the pipe mesh and at the initial conditions described chapter 2.3.2.

The simulated period extends over 100 days divided into 1,000 constant time steps of 0.1 day each. Up to 300,000 particles have been introduced into the model in order to simulate efficiently hydrodynamic dispersion.

Figure 4-5 shows pH distribution over the domain, which tends to increase in the located zone above the two fractures intersections acting as the model main conductors.

Comparing with sodium concentrations (Figure 4-6) suggests that this increase in pH is due to a dilution of the zone by flushing the initial high concentrations as indicated from Figure 4-17 to Figure 4-22. Dilute water enters into the model from below the island and the sea and progresses towards the tunnel according to the pipe flow rates (see Figure 4-9). Some upward flow of more diluted water (characterized by lower Mg total concentrations) is also expected from the bottom of the main fractured zone.

Figure 4-7 displays the effects of this dilution, which results, as explained in chapter 4.2.3, in both an increase of pH and a decrease of $MgCO_3$ solid concentrations.

A reverse situation can be observed in the main hydraulic conductors where a zone of saline water (with associated low pH) is progressing towards the tunnel. One can observe the subsequent decrease in pH calculated. Note that these low values (pH close to 6) are going in this case to limit the $MgCO_3$ precipitation by degassing CO_2 from the solution.

4.4 Extra figures for chapter 4

Figure 4-8: *spatial discretization*

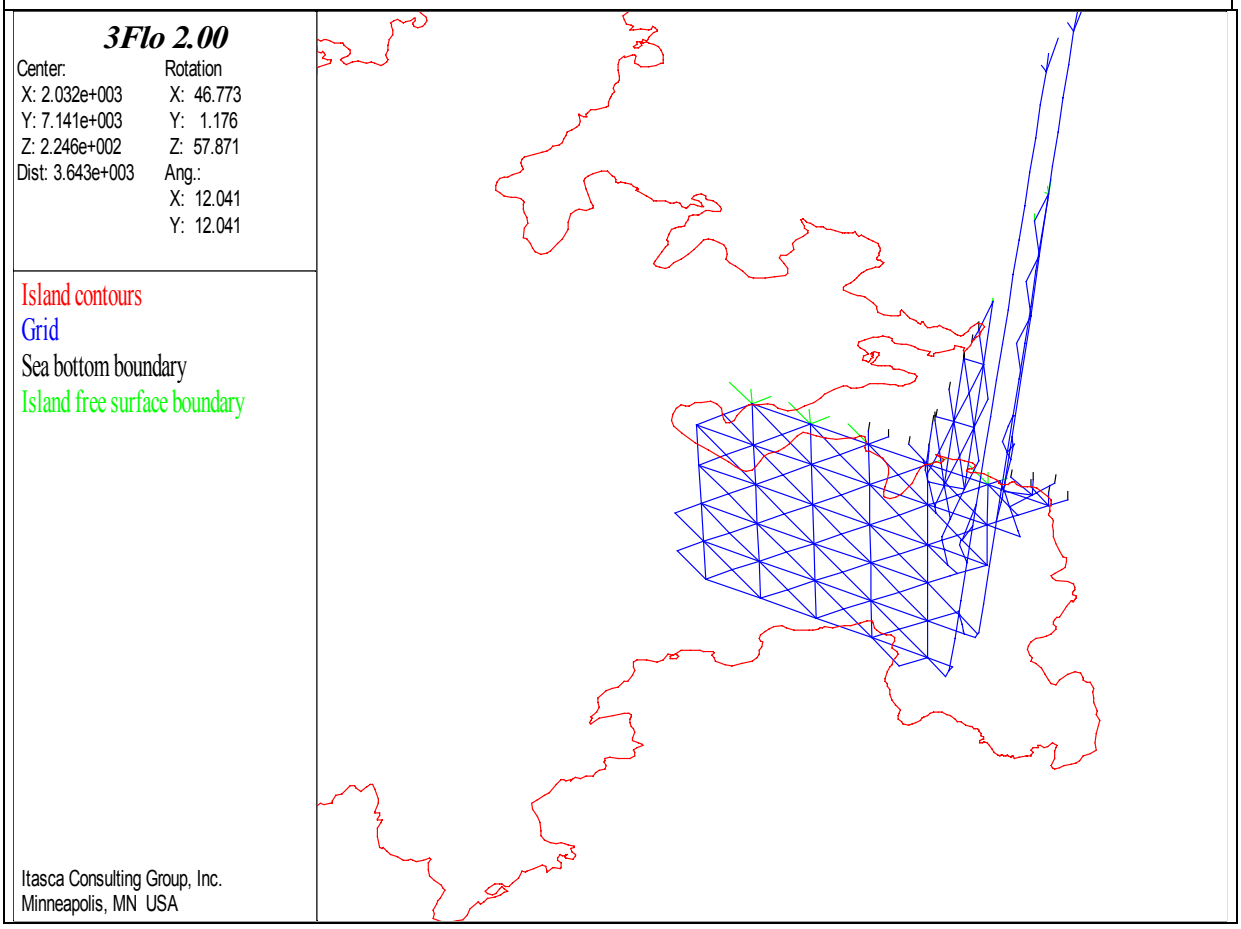

Figure 4-9: *flow rates in the pipe mesh*

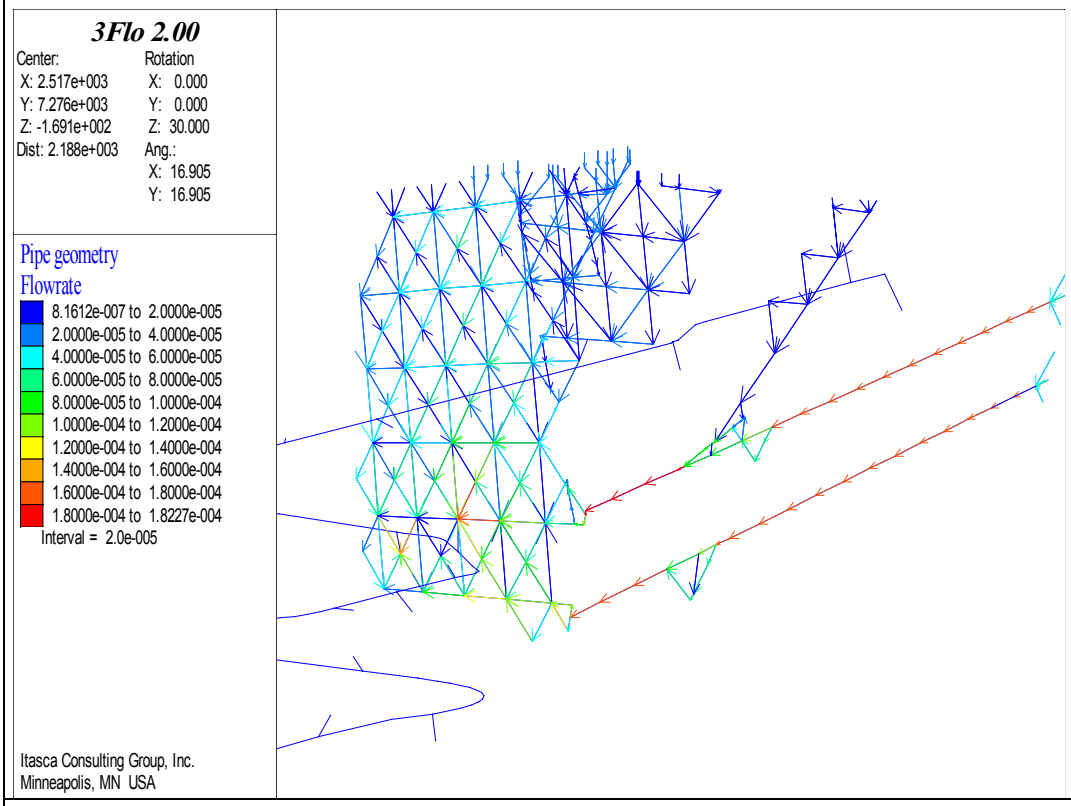

Figure 4-10: *initial sodium concentrations (M)*

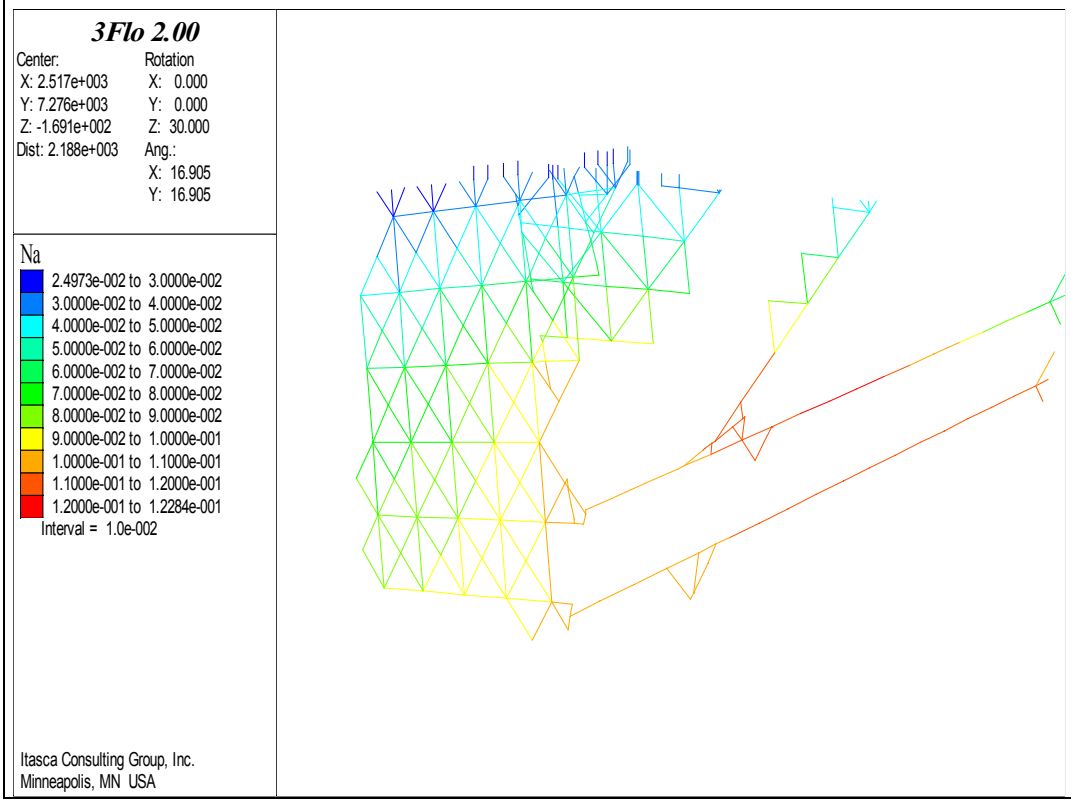

Figure 4-11: *initial calcium concentrations (M)*

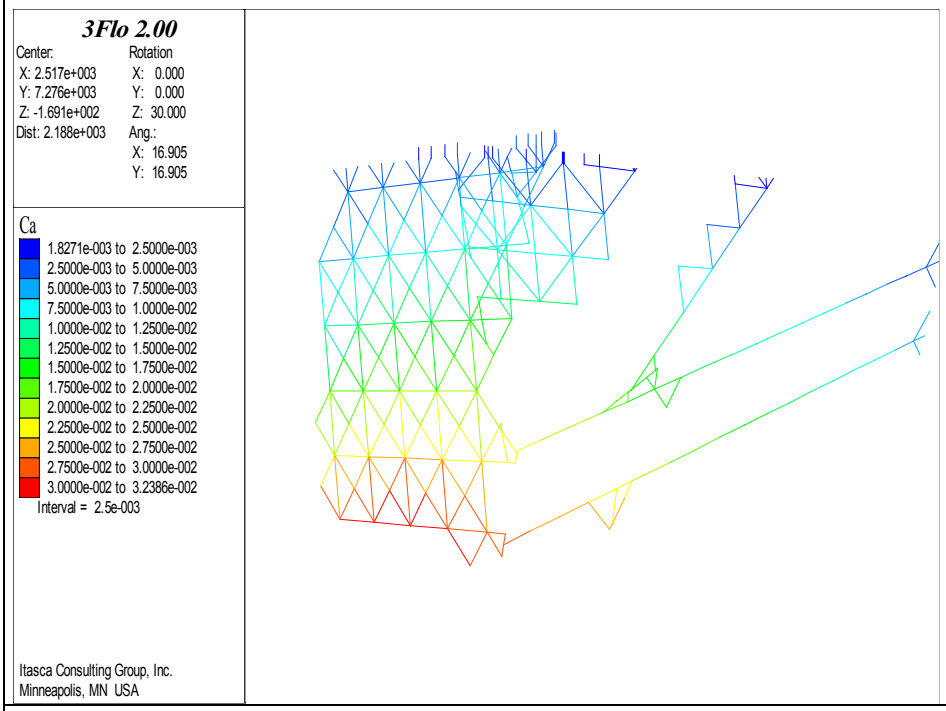

Figure 4-12: *initial chloride concentrations (M)*

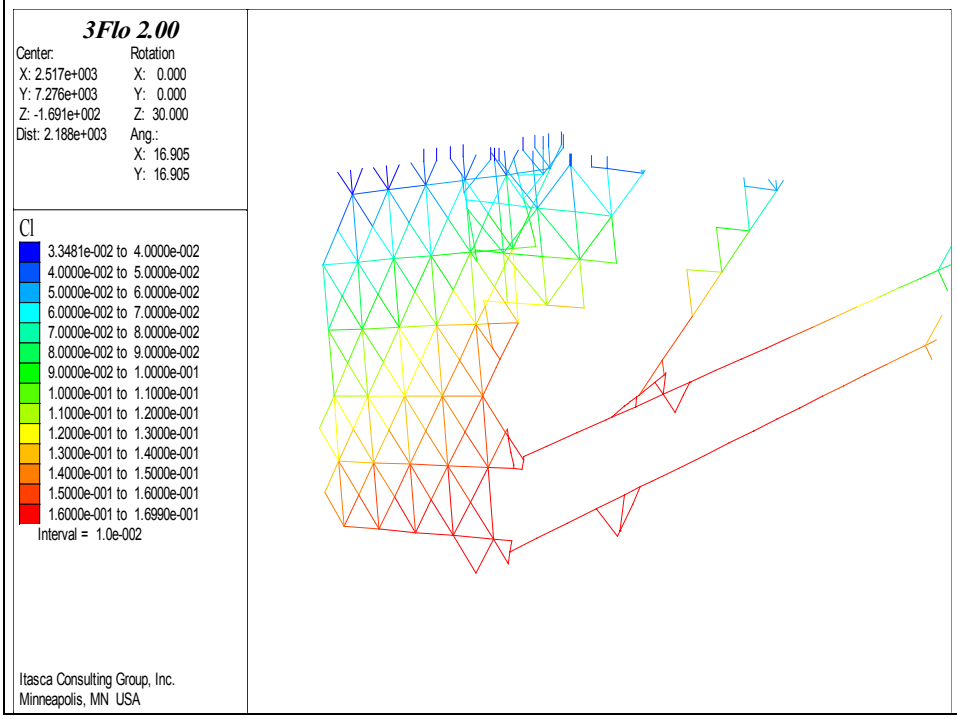

Figure 4-13: *initial sulphate concentrations (M)*

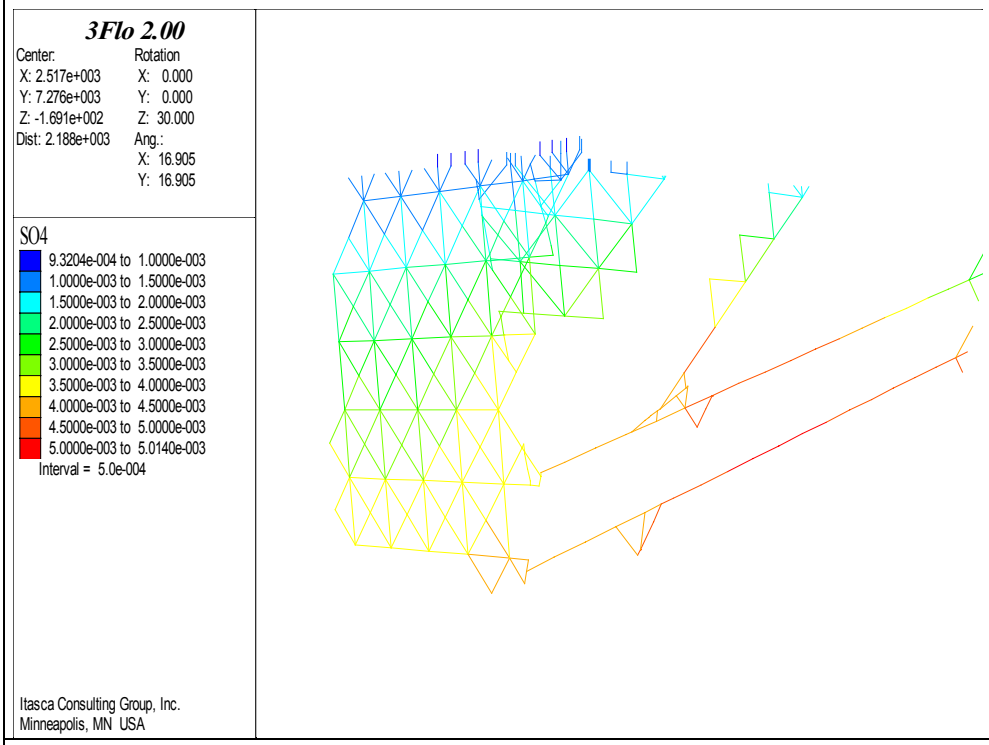

Figure 4-14: *initial potassium concentrations (M)*

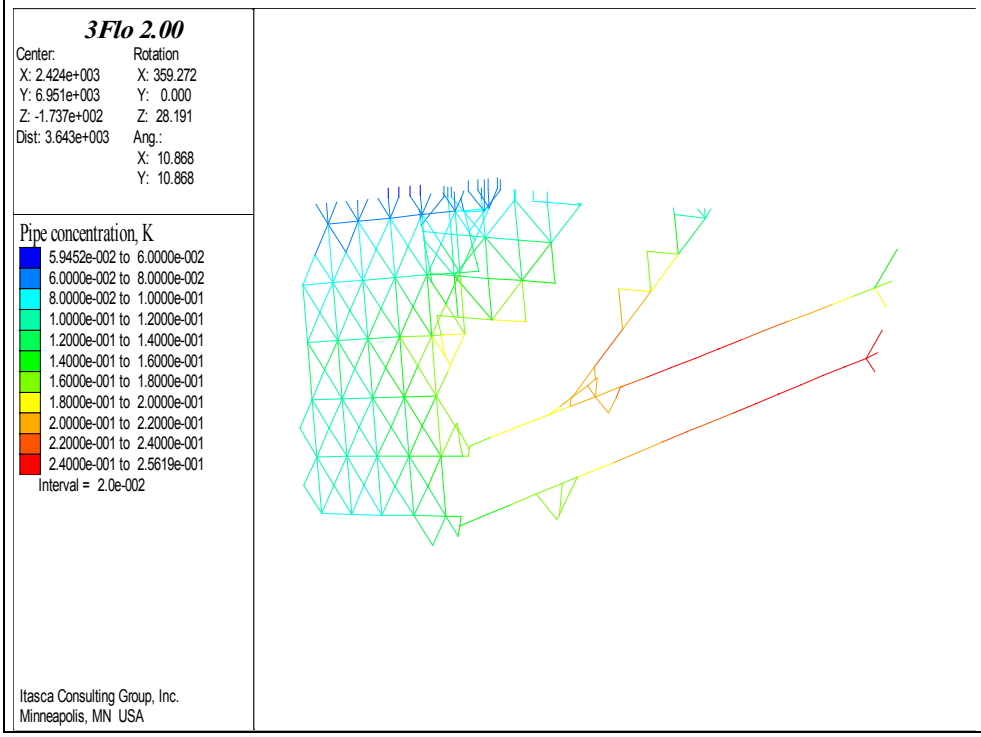

Figure 4-15: *initial magnesium concentrations (M)*

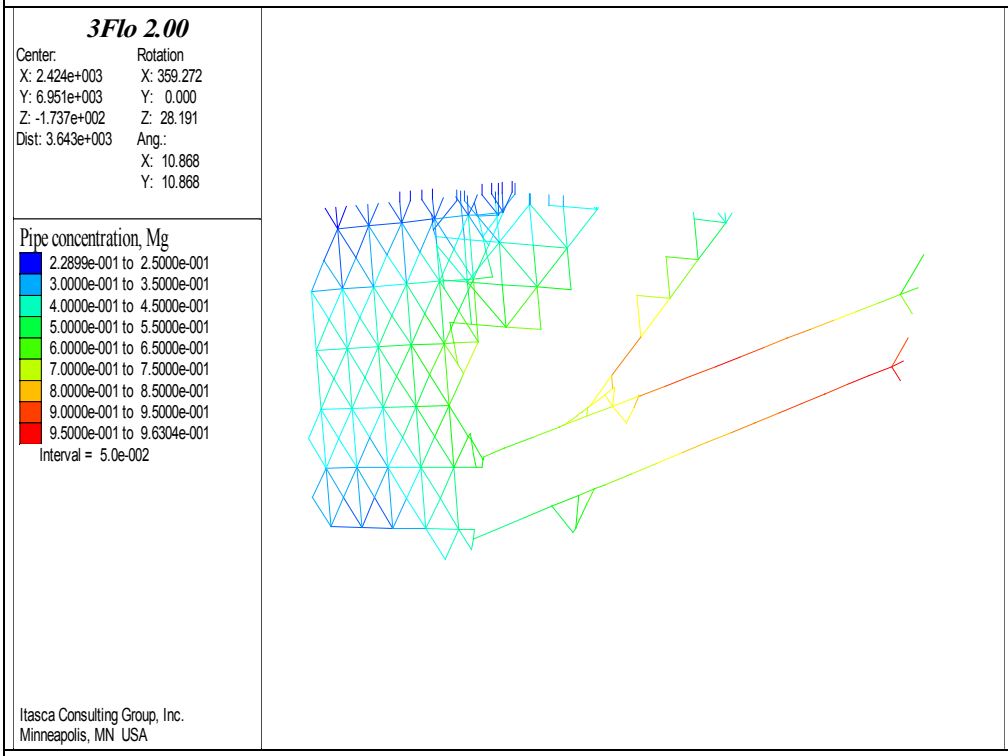

Figure 4-16: *initial total carbonates concentrations (M)*

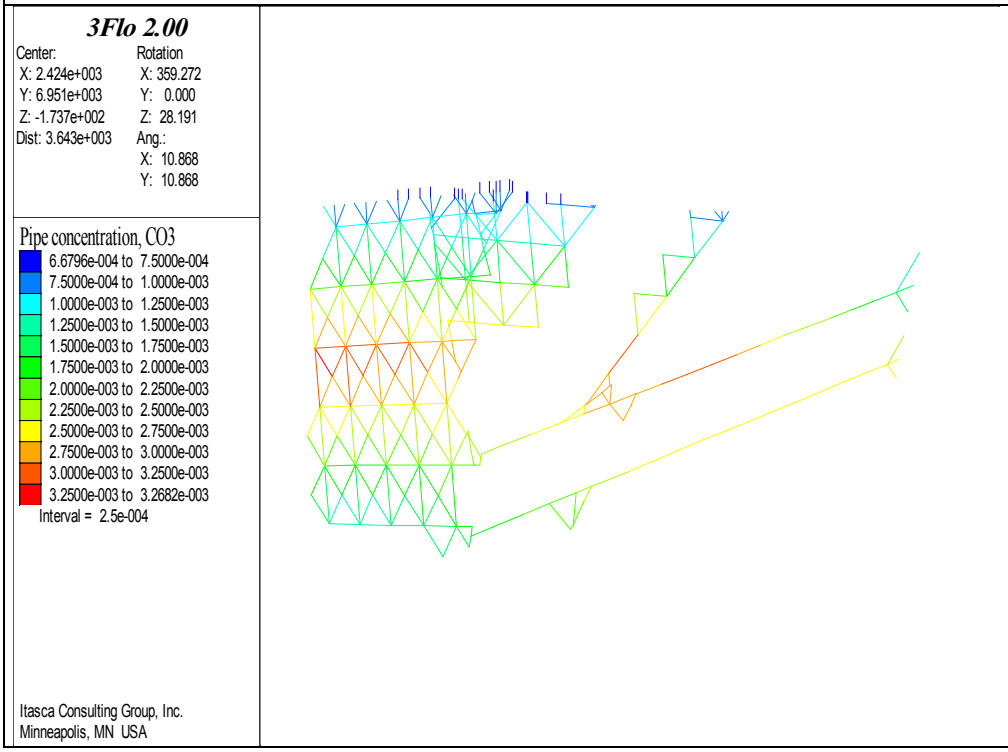

Figure 4-17: *calcium distribution (M) after 100 days*

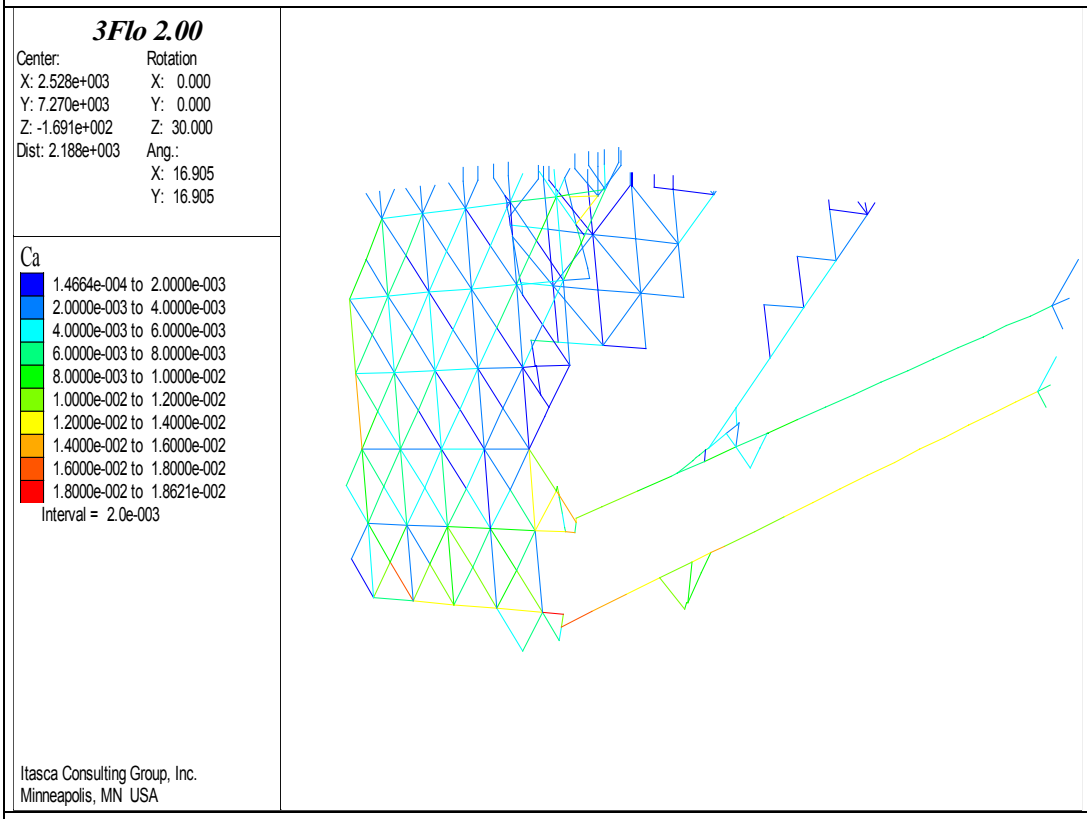

Figure 4-18: *chloride distribution (M) after 100 days*

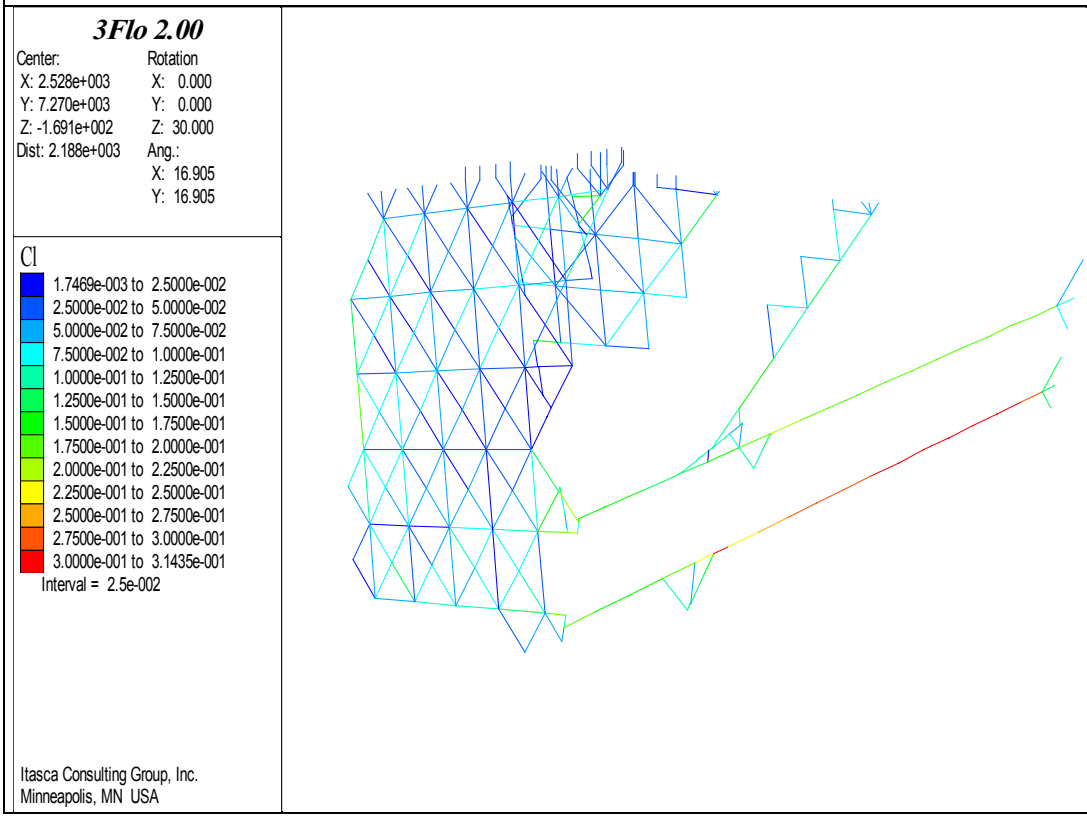

Figure 4-19: *sulphate distribution (M) after 100 days*

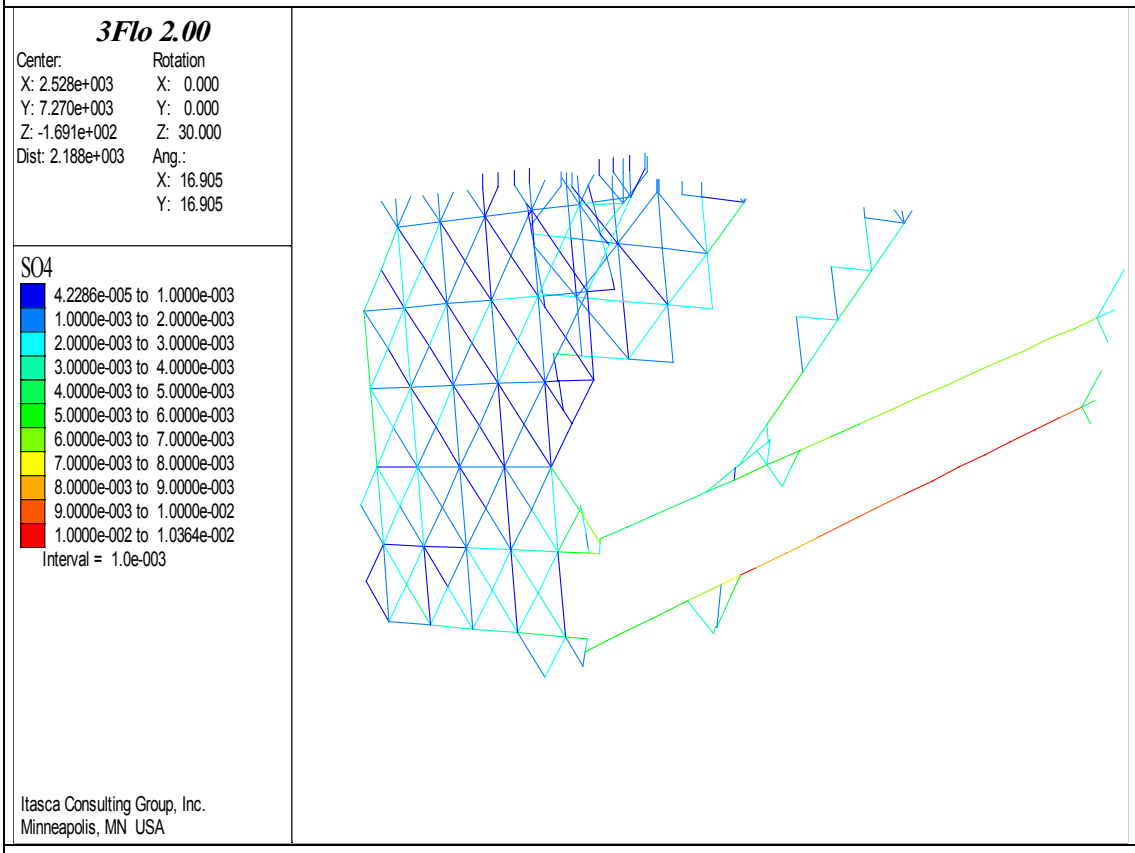

Figure 4-20: *potassium distribution (M) after 100 days*

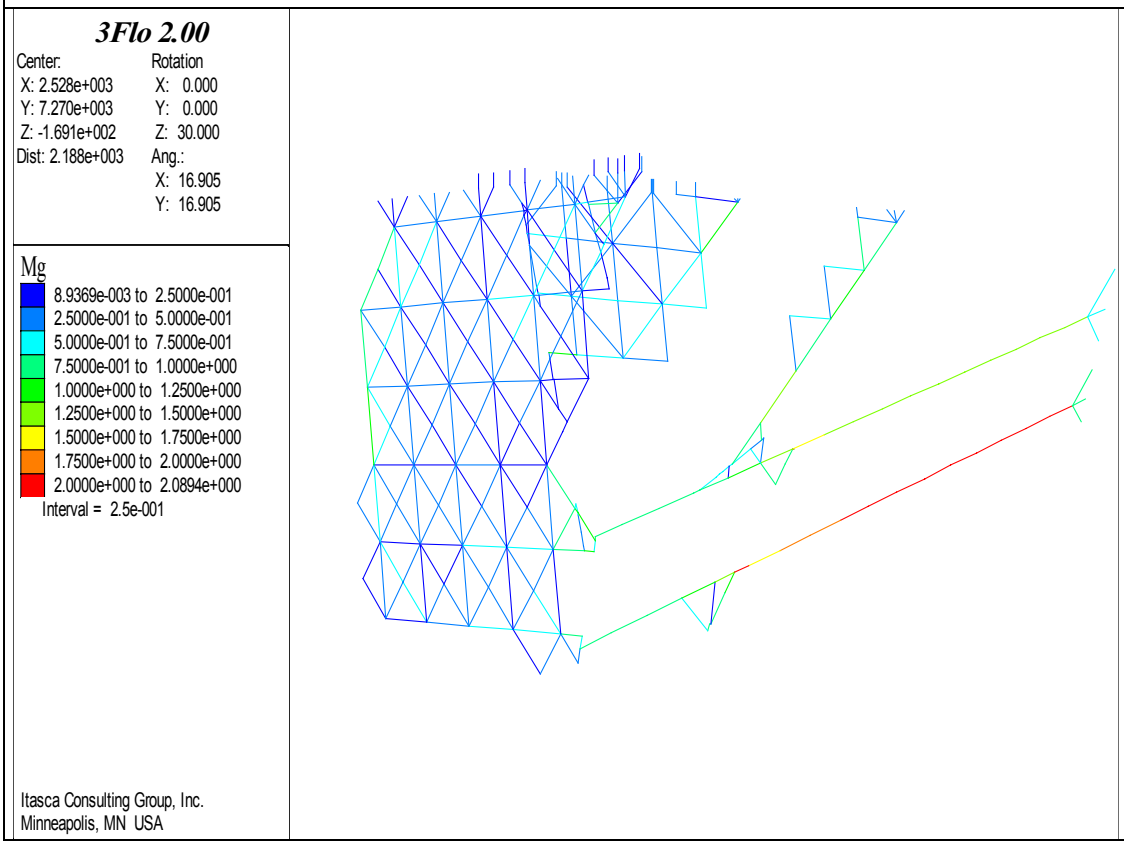

Figure 4-21: *magnesium distribution (M) after 100 days*

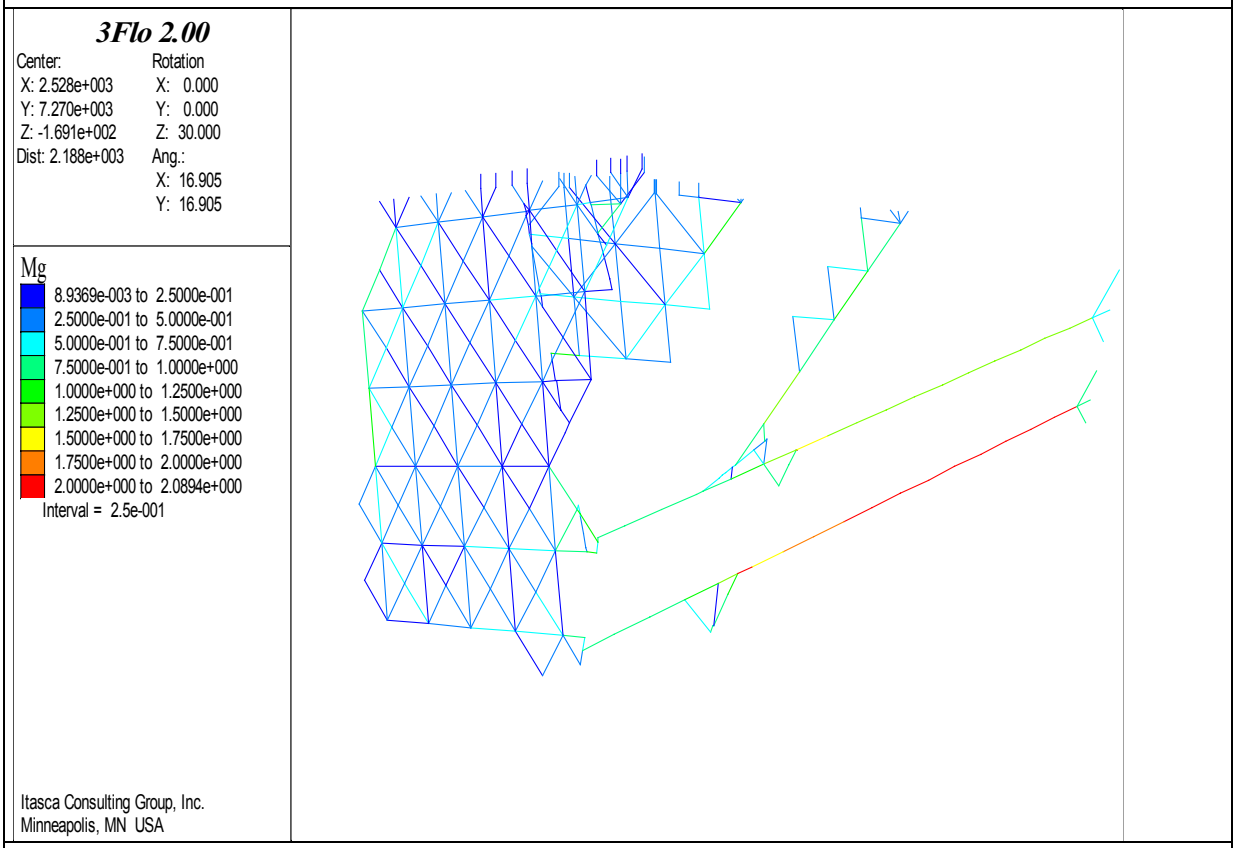

Figure 4-22: *total carbonates distribution (M) after 100 days*

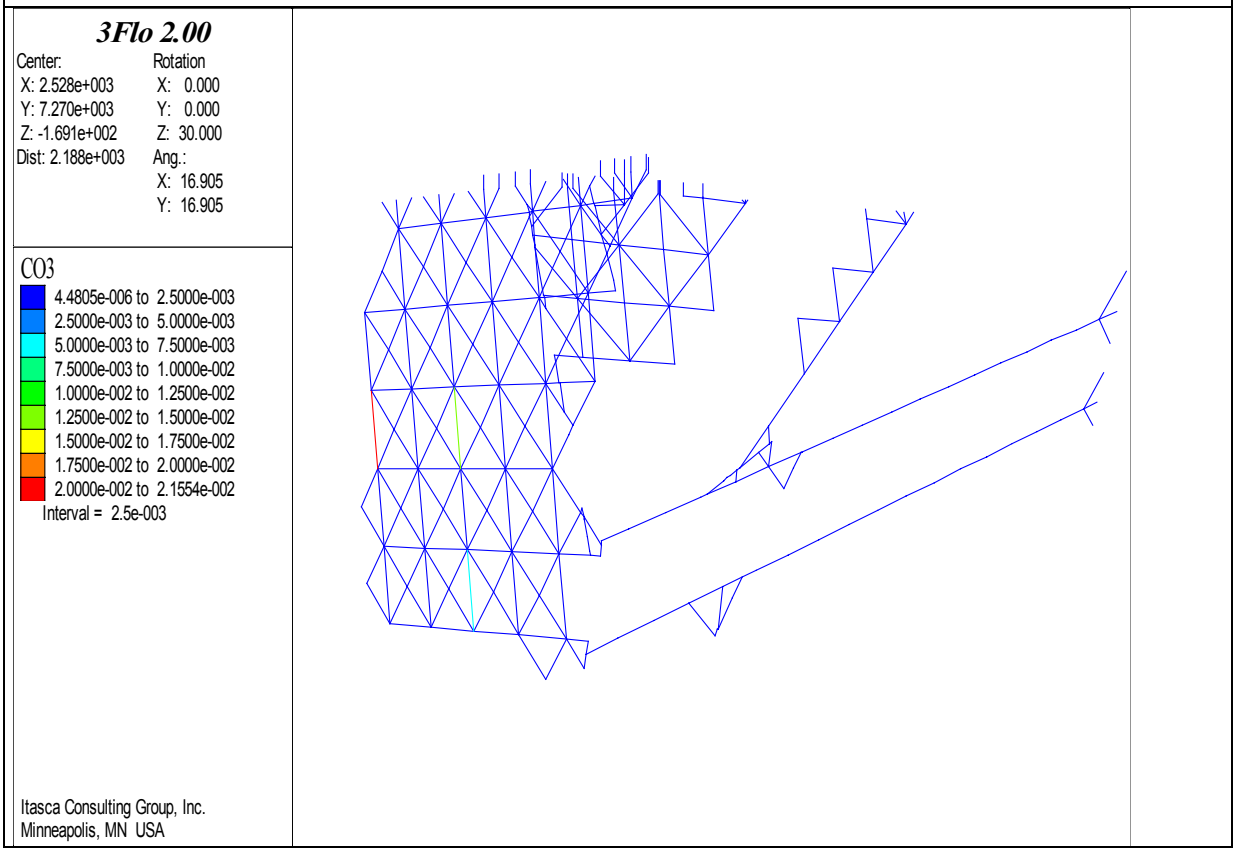

5 CONCLUSION

Flow, then transport, then reactive transport due to the construction of the access drift and the circular tunnel of the Äspö Hard Rock Laboratory were simulated in the framework of the Äspö Task Force on Groundwater Modeling. The model we built is of the Discrete Fracture Network type, allowing for channeling within fracture planes by the use of one-dimensional pipes.

Calibrating the transmissivities of the Hydraulic Conductor Domains to fit piezometric histories in a number of borehole sections proved relatively easy, with relatively minor changes of the HCDs transmissivities needed. The geometrical model is therefore probably well established, with the addition of a communication between the two EW-1 zones. However, when modeling non-reactive transport and comparing to actual measurements, the "flow-only" calibration proved inadequate: the simulations overestimated the amount of Baltic water arriving at the Control Points.

New calibrations, yielding essentially the same quality of fit for heads, but better simulations of chemical end-member arrivals, were then performed. The new calibrations were only moderately different, with most HCD transmissivities unchanged. This shows that the flow-only fit cannot be unique, since various sets of calibration parameters yield what looks like acceptable fits. Clearly, the use of chemical data, by further constraining the model parameters, helped obtaining more realistic simulations.

However, because of the relative scarcity of chemical data, uncertainties remain quite large. Initial chemical compositions are interpolated from a regular grid, itself extrapolated from data points not homogeneously distributed in space. Neither extrapolations nor interpolation take into account the fractured nature of the medium. So in fact there is no guarantee that the initial conditions we derive this way are at chemical equilibrium.

Fully coupled reactive transport was simulated on a part of the model domain only. We did not use the end members provided by the Task Force, but directly dealt with chemical species. For some species, concentrations had to be derived from end member mixing ratios and end member compositions. The simulations performed show some interesting potential features about coupling transport with geochemistry. For example, in the context of the Äspö island, it appears that variable water salinity influences the aqueous solution ionic strength and consequently the "apparent" chemical reaction constants.

Reactive transport results show that, even in zones where geochemistry is considered as simple and of little importance (e.g. in the absence of significant redox or surface reactions), transport of chemical species might in fact be affected by mineral precipitation / dissolution, therefore constraining the hydrogeological modeling.

Table 1: Hydraulic Conductor Domains – Initial geometrical and flow properties

Zone name	Transmissivity T *(m^2/s)*	Thickness th *(m)*	Specific Storage Coefficient	Stops at
EW-1N	1.5e-6	30.	(1)	(3)
EW-1S	2.2e-5	30.	(1)	
EW-3	2.4e-5	15.	(1)	NE-1
EW-7	6.8e-5	10.	(1)	NE-4N
NE-1	3.e-4	30.	2.6e-6	
NE-2	4.1e-7	5.	(1)	EW-1S NE-1 EW-3
NE-3	2.9e-4	50.	(1)	
NE-4N	3.e-5	40.	(1)	
NE-4S	3.e-5	40.	(1)	NE-4N
NW-1	1.7e-7	10.	(1)	EW-1N
NNW-1	1.1e-5	20.	5.e-6	EW-3 EW-1S
NNW-2	5.6e-5	20.	2.e-6	NE-1 EW-1S
NNW-3	2.e-5	20.	(1)	F2 F3
NNW-4	1.5e-4	10.	(1)	NE-1 EW-1S
NNW-5	2.e-6	20.	(1)	NE-4N F1
NNW-6	1.4e-5	20.	(1)	EW-7 NE-4N NE-1
NNW-7	4.8e-6	20.	(1)	EW-3 EW-1S
NNW-8	1.e-5	20.	(1)	EW-1N A1 A2
SFZ11	3.6e-6	20.	(1)	NE-1
SFZ14a	3.6e-6	20.	(1)	SFZ14b
SFZ14b	3.6e-6	20.	(1)	SFZ14a

(1) storage = max(0.00922*T^0.785, 10^{-6}), from TR 97-06

(2) porosity : $n=34.87*(\frac{T}{th})^{0.753}$, from TR 97-06

(3) EW-1N and EW-1S linked together (equivalent perm. = 1/10 of EW-1N)

(4) proportional Baltic skin.

(5) land recharge : constant imposed flux.

(6) initial and boundary compositions : from linear interpolation between regular grid data, values before tunnel construction

Table 2: Hydraulic Conductor Domains – Fitted properties
All properties identical to Table 1, except when mentioned

Zone name	Initial Transmissivity (m^2/s)	Fitted Transmissivity (m^2/s)
EW-3	2.4e-5	3.6e-5
NE-1	3.e-4	4.0e-4
NE-2	4.1e-7	4.1e-5
NNW-1	1.1e-5	1.1e-6
NNW-2	5.6e-5	3.7e-5
NNW-3	2.e-5	2.e-4
(1) uniform Baltic skin (2) land recharge: variable imposed flux		

MODELLING QUESTIONNAIRE FOR TASK 5, Itasca

worked October 1999

This is a Modelling Questionnaire prepared by SKB based on discussions within the Task Force group. It should be answered when reporting Task 5 in order to simplify the evaluation process of the modelling exercise. Preferably, include this response in an appendix to your forthcoming report.

1. SCOPE AND ISSUES

a) What was the purpose for your participation in Task 5?

To gain experience on modelling for a real site, and a first limited approach to coupling of transport and geochemistry.

b) What issues did you wish to address through participation in Task 5?

How can geochemistry help the hydrogeological modelling?
What kind of complexities are added by looking at geochemistry and hydrogeology at the same time?

2. CONCEPTUAL MODEL AND DATA BASE

a) Please describe your models using the tables 1-3 in the appendix.

See tables 1-3

b) To what extent have you used the data sets delivered? Please fill in Table 4 in the appendix.

See table 4

c) Specify more exactly what data in the data sets you actually used? Please fill in "Comments" in Table 4

d) What additional data did you use if any and what assumptions were made to fill in data not provided in the Data Distributions but required by your model? ? Please add in the last part of Table 4.

N/A

e) Which processes are the most significant for the situation at the Äspö site during the simulation period?

The situation is obviously dominated by the drawdown due to the tunnel advance. Transport seems to be dominant over geochemical reactions.

3. MODEL GEOMETRY/STRUCTURAL MODEL

a) How did you geometrically represent the ÄSPÖ site and its features/zones?

The fracture zones were represented as planes, bounded either by the model boundaries or by planar boundaries as specified in the data base. The "matrix" in between was not represented. In each fracture plane, flow and transport occurred along "channel pipes", i.e. a regular grid of one-dimensionnal elements. The grid had channels intersecting each other in four directions, at 45° angles.

b) Which features were considered the most significant for the understanding of flow and transport in the ÄSPÖ site, and why?

Fracture zones are the obvious key element of this flow system. They can explain most of the flow coming to the tunnel.

c) *Motivate selected numerical discretization in relation to used values of correlation length and/or dispersion length.*

Used 50 to 70 m grid cell size, i.e. we consider that mixing and transport tortuosity occur at this scale.

4a. MATERIAL PROPERTIES - HYDROGEOLOGY

a) *How did you represent the material properties in the hydraulic units used to represent the ÄSPÖ SITE?*

The fracture zone conductivity is integrated in the channels, with channel conductivities such that the "macro conductivity" is respected. Channel sections are computed to reproduce the actual volume available for flow, taking fracture zone porosity and width into account.

b) *What is the basis for your assumptions regarding material properties?*

Most properties taken from data provided. One further assumption is the 0.01 skin factor at the bottom of the Baltic. This proved necessary during model fitting to limit the inflow of Baltic water.

c) *Which assumptions were the most significant, and why?*

4b. CHEMICAL REACTIONS - HYDROCHEMISTRY

a) *What chemical reactions did you include?*

None in a first phase. Then, in a second phase, Calcite dissolution/precipitation, plus precipitation/dissolution of carbonates, to magnesium carbonates and to gypsum.

b) *What is the basis for your assumptions regarding the chosen chemical reactions?*

We used only one type of reaction to simplify the fully coupled runs. Our objective here was to perform trial runs, not to be exhaustive.

c) *Which reactions were the most significant, and why?*

N/A

5a. BOUNDARY CONDITIONS FOR HYDROGEOLOGICAL MODEL

a) *What boundary conditions were used in the modelling of the ÄSPÖ site tests?*

See 5b

b) *What was the basis for your assumptions regarding boundary conditions?*

c) *Which assumptions were the most significant, and why?*

5b. BOUNDARY/INITIAL CONDITIONS FOR HYDROCHEMICAL MODEL

a) What boundary conditions were used in the modelling of the ÄSPÖ site tests?

Top surface: constant flux under land, and constant head (with skin factor) under sea.
Vertical faces: constant head
Bottom face: no flux

On all imposed-head boundaries, the value is set to 0.
The imposed constant flux is 25mm per year on all emerged lands. The total influx is distributed equally on all land nodes.

b) What was the basis for your assumptions regarding boundary conditions?

Head boundaries chosen for simplicity. Imposed constant flux calibrated to obtain plausible heads before tunnel construction. Skin factor used to limit influx of Baltic water, based on Control Point observations.

c) Which assumptions were the most significant, and why?

All of them!! In fact, as described in our report, boundary conditions govern most of the response.

6. MODEL CALIBRATION

a) To what extent did you calibrate your model on the provided hydraulic information? (Steady state and transient hydraulic head etc.)

Calibrated by imposing the flowrates in the tunnel and trying to reproduce available drawdown histories in boreholes.

b) To what extent did you calibrate your model on the provided "transport data"? (Breakthrough curves etc.)

Not used

c) To what extent did you calibrate your model on the provided hydrochemical data? (Mixing ratios; density/salinity etc.)

Used them to calibrate skin factor at bottom of Baltic

d) What parameters did you vary?

Transmissivities in fracture zones, skin factor

e) Which parameters were the most significant, and why?

Both were important

f) Compare the calibrated model parameters with the initial data base - comments?

Fracture zone NE2's transmissivity needed a 100-fold increase. This may mean there is another unknown conductor in this area. Otherwise, only NNW1 (divided by 10) and NNW3 (multiplied by 10) had to be modified significantly. Overall, the final model is relatively close to the initial one.

7. SENSITIVITY ANALYSIS

Identify the sensitivity in your model output to:

a) the discretization used

very small (tried with either square or "four directions" grids, with cell sizes from 40 to 80m). Results are almost identical.

b) the transmissivity/hydraulic conductivity (distribution) used

quite high. This was used as the fitting parameter. High influence on flow patterns.

c) transport parameters used

dispersivity not very influential. Dispersion in the model dominated by mixing at intersections.

d) chemical mixing parameters used

full mixing: chemical species are transported, then chemistry is equilibrated in every pipe, at each time step

e) chemical reaction parameters used

From CHEMVAL data base.

8. LESSONS LEARNED

a) Given your experience in implementing and modelling the ÄSPÖ site, what changes do you recommend with regards to:

- Experimental site characterisation?

-

Presentation of characterisation data?

- Performance measures and presentation formats?

b) What additional site-specific data would be required to make a more reliable prediction of the tracer experiments?

c) What conclusions can be made regarding your conceptual model utilised for the exercise?

d) What additional generic research results are required to improve the ability to carry out predictive modelling of transport on the site scale?

9. RESOLUTION OF ISSUES AND UNCERTAINTIES

a) What inferences did you make regarding the descriptive structural-hydraulic model on the site scale for the ÄSPÖ site?

b) What inference did you make regarding the active hydrochemical processes, hydrochemical data provided and the hydrochemical changes calculated?

c) What issues did your model application resolve?

d) What additional issues were raised by the model application?

10. INTEGRATION OF THE HYDOGEOLOGICAL AND HYDROCHEMICAL MODELLING

a) How did you integrate the hydrogeological and hydro chemical work?

In a first phase, simply used mixing ratios to better calibrate the hydrogeological model.
In a second phase, and only on a part of the domain, implemented a full transport/chemistry coupling.

b) How can the integration of the hydrogeological and hydrochemical work be improved?

c) Hydrogeologist: How has the hydrochemistry contributed to your understanding of the hydrogeology around the Äspö site?

Yes, as stated above.

d) Hydrochemist: How has the hydrogeology contributed to your understanding of the hydrochemistry around the Äspö site?

Table 1 Description of model for water flow calculations

TOPIC	Example	Our Model
Type of model	Stochastic continuum model	Discrete fracture model, with channelized flow in fractures
Process description	Darcy´s flow including density driven flow. (Transport equation for salinity is used for calculation of the density)	Darcy's flow, no density effect
Geometric framework and parameters	Model size: 1.8x1.8x1 km^3 . Deterministic features: All deterministic features provided in the data set. Rock outside the deterministic features modelled as stochastic continuum.	Model boundaries, in Aspo coordinates: X = 1000 to 3000 Y = 6000 to 8000 Z = -1000 to 0 Deterministic features: the 21 fracture zones as given in the data set Rock outside fracture zones not modelled
Material properties and hydrological properties	Deterministic features: Transmissivity (T), Storativity(S) Rock outside deterministic features: Hydraulic conductivity(K), Specific storage (Ss)	Transmissivity (T), width (W), storage coefficient (S)
Spatial assignment method	Deterministic features: Constant within each feature (T,S). No changes due to calibration. Rock outside deterministic features: (K,Ss) lognormal distribution with correlation length xx. Mean, standard deviation and correlation based on calibration of the model	Constant for each feature, except at the top boundary under the Baltic, where a "skin factor" of 0.01 is used. Transmissivity started from data set (*Source: HCD-SR97.XLS in Data Delivery 2*), then moved during calibration phase. Specific storage used as given when data available (NE-1, NNW-1, NNW-2, computed from correlation in TR 97-06 for all others
Boundary conditions	Surface: Constant flux. Sea: Constant head Vertical-North: Fixed pressure based on vertical salinity distribution. Vertical-East: Fixed pressure based on vertical salinity distribution. Vertical-South: Fixed pressure based on vertical salinity distribution. Vertical-West: Fixed pressure based on vertical salinity distribution. Bottom: No flux. Linear change by time based regional simulations for undisturbed conditions and with Äspö tunnel present.	Top surface: constant flux under land, and constant head (with skin factor) under sea. Vertical faces: constant head Bottom face: no flux
Numerical tool	PHOENICS	3FLO
Numerical method	Finite volume method	Finite Elements method
Output parameters	Head, flow and salinity field.	Head, flow

Table 2 Description of model for tracer transport calculations

TOPIC	EXAMPLE	Our model
Type of model	Stochastic continuum model	Discrete fracture model, with channelized flow in fractures
Process description	Advection and diffusion, spreading due to spatially variable velocity and molecular diffusion.	Advection and diffusion. Spreading due to both longitudinal dispersion in channels and to complete mixing at channel intersections.
Geometric framework and parameters	Model size: 1.8x1.8x1 km^3 . Deterministic features: All deterministic features provided in the data set. Rock outside the deterministic features modelled as stochastic continuum.	Model boundaries, in Aspo coordinates: X = 1000 to 3000 Y = 6000 to 8000 Z = -1000 to 0 Deterministic features: the 21 fracture zones as given in the data set Rock outside fracture zones not modelled
Material properties	Flow porosity (ne)	Porosity (n), dispersivity (d)
Spatial assignment method	ne based on hydraulic conductivity value (TR 97-06) for each cell in model, including deterministic features and rock outside these features.	n based on hydraulic conductivity value (TR 97-06) for all fractures d constant in model, from TR97-06.
Boundary conditions	Mixing ratios for endmembers as provided as initial conditions in data sets.	End member simulation: mixing ratios as provided in the data base. For the top boundary, use pure Meteoric under land and pure Baltic under sea.
Numerical tool	PHOENICS	3FLO
Numerical method	Particle tracking method or tracking components by solving the advection/diffusion equation for each component	Particle tracking method
Output parameters	Breakthrough curves	Breakthrough curves, and concentration maps.

Table 3 Description of model for chemical reactions calculations

TOPIC	EXAMPLE	Our model
Type of model	xxx	Principal component method.
Process description	Mixing. Reactions: Xx, Yy,Zz,Dd…..	Full mixing in each cell (here each pipe) of the model. Interaction by transport of species using particle tracking method. Reactions modelled: Calcite dissolution/precipitation, plus precipitation/dissolution of carbonates, to magnesium carbonates and to gypsum
Geometric framework and parameters	Modelling reactions within one fracture zone, NE-1.	Coupled transport/chemistry runs in only a part of the domain of interest: main conductors upstream of Control Point number 4.
Reaction parameters	Xx: a=ff, b=gg,… Yy: c=. Zz: d=...	From the Chemval data base
Spatial distribution of reactions assumed	Xx: seafloor sediments Yz: Bedrock below sea, superficial Dd: Bedrock ground surface, superficial Yz: Bedrock below sea, at depth Zz: Bedrock ground surface, at depth Yy, Zz: near tunnel	Initial spatial distribution from initial conditions provided (species concentrations interpolated from grid). Later spatial distribution governed by the transport process.
Boundary/initial conditions for the reactions	Xx: aaa… Yy: bbb…	Initial conditions: see above. Boundary conditions: fixed concentrations according to initial concentrations at boundary pipes. Also, pipes in contact with the atmosphere (island ground surface) are opened to CO_2 (g)
Numerical tool	Phreeque	3FLO
Numerical method	xx	Principal components method. Reduce the system to be solved to *n* independent mole balance equations (Gibb's law) and *n* components. Concentrations of the principal components (e.g. Fe^{3+}, Ca^{2+}, CO_3^{2-}…) are computed after substituting each of the secondary species mass laws into the mole balance equations
Output parameters	xx	Concentrations of dissolved and solid-phase species, pH, in each pipe.

Table 4a Summary of data usage

Data del. No	Data	Importance of data (see notes)	Comment
1	Hydrochemical data 1		
1a	Surface bore holes- undisturbed conditions, Äspö-Laxemar		
1b	Surface bore holes- disturbed conditions (by tunnel excavation), Äspö		
1c	Surface bore holes- undisturbed conditions, Ävrö		
1d	Surface bore holes- sampled during drilling, Äspö		
1e	Data related to the Redox experiment		
1f	Tunnel and tunnel bore holes- disturbed conditions		
2	Hydogeological data 1		
2a1	Annual mean air temperature		
2a2	Annual mean precipitation	**M**	
2a3	Annual mean evapotranspiration	m	
2b1	Tunnel front position by time	**P**	file TASA.XLS, in TUNNFPOS.ZIP,
2b2	Shaft position by time	**P**	
2c1	Geometry of main tunnel	**P**	File TASA.TXT, in Tungeom.zip
2c2	Geometry of shafts	**P**	
2d	Hydrochemistry at weirs (Cloride, pH, Electrical conductivity, period: July 1993- Aug 1993)		
2e	Geometry of the deterministic large hydraulic features (Most of them are fracture zones)	**P**	Main geometrical input. File HCD-SR97.xls

Table 4b Summary of data usage

Data del. No	Data	Importance of data (see notes)	Comment
3	Hydrogeological data 2		
3a	Monthly mean flow rates measured at weirs. Tunnel section 0-2900m, period May 1991 – January 1994		
3b	Piezometric levels for period June 1st 1991 – May 21st 1993. Values with 30 days interval (Task 3 data set)	**P**	Measured piezometric levels used for calibrating the model. File Pietzol0.zip (KAS01.dat, ….KAS14.dat)
3c	Salinity levels in bore hole sections for period -Sept 1993. (Task 3 data set)	**M**	For checking fresh water heads, file pietzol1.zip (SAL_PR01.xls…)
3d	Undisturbed piezometric levels		
3e	Coordinates for bore hole sections	**P**	Borehole sections used for flow fitting, file kas01.zip (KAS01_1.xls … KAS14_1.xls)
3f	Piezometric levels for period July 1st 1990 – January 24st 1994. Daily values.	**M**	Check by comparison to monthly values
4	Hydochemical data 2		Used later release
4a	Chemical components, mixing proportions and deviations for all bore hole sections used in the M3 calculations		
4b	Bore holes with time series, > 3 samples (part of 4a)		
4c	Bore holes sections interpreted to intersect deterministic large hydraulic features (Most of them are fracture zones) (part of 4a)		
4d	Chemical components, mixing proportions and deviations. Grid data based on interpolation. Undisturbed conditions		
4e	Chemical components, mixing proportions and deviations. Grid data based on interpolation. Disturbed conditions (by tunnel excavation)		
4f	Boundary and initial conditions. Chemical components, mixing proportions and deviations (1989). Grid data for vertical boundaries based on interpolation. Undisturbed conditions		
4g	Boundary conditions after tunnel construction (1996) Chemical components, mixing proportions and deviations. Grid data for vertical boundaries based on interpolation. Disturbed conditions (by tunnel excavation)		

Table 4c Summary of data usage

Data del. No	Data	Importance of data (see notes)	Comment
5	Geographic data 1		
5a	Äspö coast line	**M**	For visualisation and checking, file Aspcoast.bna
5b	Topography of Äspö and the nearby surroundings	**P**	For defining "land" and "sea" conditions on top. File Site20_4.grd
6	Hydro tests and tracer tests		
6a	Large scale interference tests (19 tests)		
6b	Long time pump and tracer test, LPT2		
7	Hydochemical data 3, update of data delivery 4 based on new endmembers. Recommended to be used instead of 4.		
7a	Chemical components, mixing proportions and deviations for all bore hole sections used in the M3 calculations	**P**	Composition of the 4 M3 endmembers, file Append9.xls Control point chemistry data, files Append9.xls and Append10.xls
7b	Bore holes with time series, > 3 samples (part of 7a)		
7c	Bore holes sections interpreted to intersect deterministic large hydraulic features (Most of them are fracture zones) (part of 7a)		
7d	Chemical components, mixing proportions and deviations. Grid data based on interpolation. Undisturbed conditions	**P**	Initial concentrations in model, plus fixed concentrations on vertical boundaries, interpolated from values in file Append12.xls
7e	Chemical components, mixing proportions and deviations. Grid data based on interpolation. Disturbed conditions (by tunnel excavation)		
7f	Boundary and initial conditions. Chemical components, mixing proportions and deviations (1989). Grid data for vertical boundaries based on interpolation. Undisturbed conditions		
7g	Boundary conditions after tunnel construction (1996) Chemical components, mixing proportions and deviations. Grid data for vertical boundaries based on interpolation. Disturbed conditions (by tunnel excavation)		

Table 4d Summary of data usage

Data del. No	Data	Importance of data (see notes)	Comment
8	Performance measures and reporting 1		
8a	Performance measures		
8b	Suggested control points. 6 points in tunnel section 0-2900m and 3 point in tunnel section 2900-3600m.		
8c	Suggested flowchart for illustration of modelling		
9	Hydrogeological data 3		
9a	Monthly mean flow rates measured at weirs. Tunnel section 0-3600m, period: May 1991- Dec 1996.	**P**	Weir geometry, file weirf-02.txt Monthly flow rates at weirs, used as a boundary condition, file weirf-02.xls
10	Geographic data 2		
10a	Topography of Äspö and the nearby surroundings (larger area than 5b)		
10b	Co-ordinates for wetlands		
10c	Co-ordinates for lakes		
10d	Co-ordinates for catchments		
10e	Co-ordinates for streams		
10f	Co-ordinate transformation Äspö system- RAK		
11	Boundary and initial conditions		
11a	Pressure before tunnel construction, from the regional SKB model (TR 97-09)		
11b	Salinity before tunnel construction, from the regional SKB model (TR 97-09)		
11c	Pressure after tunnel construction, from the regional SKB model (TR 97-09)		
11d	Salinity after tunnel construction, from the regional SKB model (TR 97-09)		

Table 4e Summary of data usage

Data del. No	Data	Importance of data (see notes)	Comment
12	Performance measures and reporting 2		
12a	Suggested control points. 6 points in tunnel section 0-2900m and 3 point in tunnel section 2900-3600m (same as 8b) and 2 outside the tunnel.		
13	Transport parameters compiled		
13a	LPT2 tracer tests		
13b	Tracer test during passage of fracture zone NE-1		
13c	Redox tracer tests		
13d	TRUE-1 tracer tests		
14	Hydrochemical data 4		
14a	Groundwater reactions to consider within TASK5 modelling (Description of how M3 calculates the contribution of reactions and identifying dominating reactions based on the M3 calculations.		
15	Co-ordinates for the test sections defining the control points	**P**	Control points geometry, file Cpoints4.xls
16	Co-ordinates for bore holes drilled from the tunnel		

Table 4f Summary of data usage

Data del. No	Data	Importance of data (see notes)	Comment
17	Hydogeological data - prediction period		
17a	Hydrochemistry at weirs (Cloride, pH, Electrical conductivity, period: July 1993- Dec 1995)		
17b	Piezometric levels for period July 1st 1990 – Dec 1996. Daily values.		
18	Hydochemical data - prediction period.		
18a	Chemical components, mixing proportions and deviations for all bore hole sections used in the M3 calculations. Data for tunnel section 2900-3600m.		
18b	Bore holes with time series, > 3 samples (part of 18a)		
18c	Bore holes sections interpreted to intersect deterministic large hydraulic features (Most of them are fracture zones) (part of 18a)		
	Other data (part of data to Task 1, 3 and 4)		
	Fracture orientation, fracture spacing and trace length – tunnel data		
	Fracture orientation, fracture spacing– mapping of cores		
	Fracture orientation, fracture spacing and trace length – mapping of outcrops		

P = data of great importance for quantitative estimation of model parameters
p = data of less importance for quantitative estimation of model parameters
M = data of great importance used qualitatively for setting up model
m = data of less importance used qualitatively for setting up model
X = data useful as general background information
- = data not used